ASSESSMENT OF SOLAR RADIATION DATA USED IN ANALYSES OF SOLAR ENERGY SYSTEMS

by
Gayathri Vijayakumar

A thesis submitted in partial fulfillment
of the requirements for the degree of

Master of Science
(Mechanical Engineering)

at the
UNIVERSITY OF WISCONSIN-MADISON
2004

Abstract

Solar radiation data is essential to conducting performance analyses of solar energy systems. In the US, the National Solar Radiation data base has archived 30 years of hourly data for 239 US cities. Since the computational effort required to simulate systems for 30 years is excessive, it is more convenient to use typical meteorological year (TMY) data in performance analyses. TMY data provide hourly solar radiation and meteorological data representative of one 'typical' year for the same 239 locations in the database.

Simulation studies have generally used these hourly values, although solar radiation can exhibit wide variations during an hour. Variations in solar radiation during an hour could result in inaccurate performance estimates for some types of solar systems, such as photovoltaic systems, that respond quickly and non-linearly to solar radiation.

Short-term radiation data is not as readily available as hourly data. One year of 1-minute data for one US location and one year of 3-minute data for eight US locations were made available for this research. The impact of using short-term radiation data in performance analyses instead of hourly data and the accuracy of using statistically formulated TMY data instead of the actual long-term data was investigated.

In addition, the behaviors of both data sets were studied in terms of diffuse fraction and frequency distributions. Correlations and distribution curves have been previously developed and comparisons of real data to these correlations were made to determine their accuracy. To quantify impacts, calculation of radiation on tilted surfaces using known models were made for both TMY data and short-term radiation data sets, and utilizability analyses were made to quantify the impact on performance analyses in a system-independent manner.

Acknowledgements

I would like to thank the National Science Foundation for funding this research project since without their funding I wouldn't be writing a solar related thesis.

A great big thank you goes to Michael Kummert, our Transys engineer and general computer wizard. No amount of chocolate chip cookies can accurately express how much I valued his help and MATLAB expertise. This research could not have been finished without his guidance and advice on how to manipulate hundreds of thousands of rows of data without killing my little DELL.

Of course, I owe thanks to my parents. Their determination and perseverance to succeed in life and to provide the best for their children has always been an inspiration. They've supported me in every decision I have ever made and never pushed me to do something I didn't want. They also didn't let me give up on myself when engineering became a challenge I didn't think I could handle.

And the final and biggest thanks are reserved for my advisers. Thanks to Tim for meeting me on a cold Sunday my first semester to convince me that I didn't need to quit engineering because I failed my first thermodynamics exam. Thanks to Dr. Beckman for developing a solar-related project for me when I just couldn't get excited about my first project. Thanks to Dr. Klein for all the EES help, for teaching me about 'data' and for your belief in my capabilities as an engineer. I hope that when I become a teacher I can instill the same self-confidence in my own students as you have done for me. And thank you both for your contribution to solar energy research. Although it won't be research related, I hope one day that I too will make a contribution and at least convince more people to utilize the renewable energy technology that your research has helped to develop.

Table of Contents

Abstract ii

Acknowledgements iii

List of Figures vi

List of Tables xi

Chapter 1
Introduction 1

1.1 Available Data 1
1.1.1. Hourly Data 1
1.1.2. Minute Data 3

1.2 Assessment Techniques 4
1.2.1 Hourly Data 5
1.2.2 Minute Data 5

Chapter 2
Typical Meteorological Year Data 7

2.1 Analysis of Data 7
2.1.1 Monthly Average Daily Radiation 8
2.1.2 Distribution of Daily Solar Radiation 10
2.1.3 Diffuse Fraction 14
2.1.4 Data Sources 20
2.2 Radiation on a Tilted Surface 22
2.3 Utilizability 25
2.4 Assessment of Data 29

Chapter 3
3-Minute Radiation 31

3.1 Analysis of Data 31
3.1.1 Diffuse Fraction 31
3.1.2 Distribution of Short-term Solar Radiation 39
3.2 Radiation on a Tilted Surface 44
3.3 Utilizability 49

Chapter 4
1-Minute Radiation **56**

4.1 Analysis of Data 56
4.1.1 Diffuse Fraction 57
4.1.2 Distribution of Short-term Solar Radiation 62
4.2 Radiation on a Tilted Surface 63
4.3 Utilizability 66
4.4 Assessment of Short-term Radiation Data 69

Chapter 5
Conclusions **70**

Appendix A: TMY2 Data **73**

Appendix B: 3-Minute Radiation Data **77**

Appendix C: 1-Minute Radiation Data **85**

Appendix D: Computer Programs **87**

References **88**

List of Figures **Page**

Chapter 1

1.1 Map showing the 239 National Weather Service stations for which TMY2's were derived. 2

1.2 ISIS network stations in the US. 4

Chapter 2

2.1 Generalized daily distribution of K_T as a function of $\bar{K}_T$ using equation from Bendt et al. [1981]. 11

2.2 Distribution of K_T in Madison, WI based on TMY2 data for December and compared with Bendt et al. [1981] generalized distribution. 12

2.3 Distribution of K_T in Albuquerque, NM based on TMY2 data for March and compared with Bendt et al. [1981] generalized distribution. 13

2.4 Distribution of K_T in Atlanta, GA based on TMY2 data for December and compared with Bendt et al. [1981] generalized distribution. 14

2.5 Diffuse fraction versus hourly clearness index for Madison, WI. 15

2.6 Diffuse fraction versus hourly clearness index for Madison, WI.

2.7 Diffuse radiation exceeding total for hours other than sunset and sunrise. 17

2.8 Comparison of TMY2 values of total horizontal radiation to the sum of the components of beam and diffuse on a horizontal surface for Madison, WI. 18

2.9 Seattle diffuse fraction; I and I_d modeled from observed sky cover. 19

2.10 Seattle diffuse fraction; I is measured post-1976 with a calibration correction and I_d is derived from I and I_{bn}. 21

2.11 Hourly radiation on a tilted surface calculated using TMY2 beam and diffuse data, compared to using TMY2 total radiation data and Erbs' diffuse fraction, using Liu and Jordan method. 23

2.12 Hourly radiation on a tilted surface calculated using TMY2 beam and diffuse data, compared to using TMY2 total radiation data and Erbs' diffuse fraction, using HDKR method. 25

2.13 Average daily utilizability for December for critical levels ranging from 0 to 4 MJ/m^2. 26

2.14 Average daily utilizability for March for critical levels ranging from 0 to 4 MJ/m^2. 27

2.15 Average daily utilizability for July for critical levels ranging from 0 to 4 MJ/m^2. 27

2.16 Average daily utilizability for January for critical levels ranging from 0 to 4 MJ/m^2. 28

Chapter 3

3.1 Three minute diffuse fraction as a function of clearness index for December 2002, in Madison, WI. 32

3.2 Diffuse fraction as a function of clearness index for a clear April day in Oak Ridge, TN. 34

3.3 Comparison of diffuse fraction correlations to ISIS data, for January 26, 2003. 35

3.4 Comparison of diffuse fraction correlations to ISIS data for July 18, 2003. 36

3.5 The dependence of diffuse fraction on air mass for June 2002, Hanford, CA. 37

3.6 Diffuse fraction as a function of air mass for clear January and July days in Seattle, Albuquerque, and Madison. 38

3.7 Diffuse fraction as a function of air mass for clear September days in eight ISIS stations. 39

3.8 Frequency distribution of 3-minute clearness indices in Sterling, VA, grouped by hourly average. 41

3.9 Frequency distribution of hourly clearness indices in Sterling, VA, grouped by daily average. 42

3.10 Frequency distribution of 3-minute clearness indices in Albuquerque, NM, grouped by hourly average and air mass, *m*. 43

3.11 Comparison of 4 methods of calculating hourly tilted radiation for a clear March day in Madison, WI. 47

3.12 Comparison of 4 methods of calculating hourly tilted radiation for a cloudy March day in Madison, WI. 47

3.13a Comparing 4 methods of calculating monthly average daily tilted radiation from 3-minute data in Madison, WI. Note expanded scale. 48

3.13b Comparing 4 methods of calculating monthly average daily tilted radiation from 3-minute data in Seattle, WA. 49

3.14 Graphical representation of utilizability. 50

3.15 Graphical representation of utilizability with a raised critical level. 50

3.16 Comparison of average daily beam normal utilizability for January in Seattle for calculated and actual short-term data. 52

3.17 Comparison of average daily beam normal utilizability for January in Seattle for actual and correlated short-term data. 53

3.18 Comparison of average daily beam normal utilizability for January in Seattle for actual short-term data and hourly correlated data. 54

3.19 Comparison of average daily beam normal utilizability for January in Hanford for short-term data and hourly data. 55

Chapter 4

4.1 ISIS instruments in Madison, WI. 56

4.2 One minute diffuse fraction as a function of clearness index for August 2003, in Madison, WI. 57

4.3 Hourly diffuse fraction as a function of clearness index for August 2003, in Madison, WI. 58

4.4 ISIS data for consecutive April days, representative of a cloudy, partly cloudy, and clear day. 59

4.5 One-minute diffuse fraction as a function of one-minute clearness indices for the three consecutive days in April shown in Figure 4.4. 60

4.6 One-minute diffuse fraction as a function of one-minute clearness indices for a cloudy April day. Note expanded scale. 61

4.7 One-minute diffuse fraction as a function of one-minute clearness indices for a clear April day. 61

4.8 Frequency distribution of 1-minute clearness indices in December in Madison, WI. 62

4.9 Hourly comparison of ISIS beam normal data to estimated beam normal data using Erbs' correlation for the month of April. 64

4.10 Hourly comparison of ISIS beam normal data to estimated beam normal data using Erbs' correlation for a clear day in April. 66

4.11 Comparison of average daily beam normal utilizability for September in Madison for actual 1-minute data and hourly correlated data. 67

4.12 Distribution of 3-minute solar radiation. 68

4.13 Comparison of average daily beam normal utilizability for September in Madison for 1-minute data and hourly data. 69

List of Tables **Page**

Chapter 2

Table 2.1: Monthly Average Daily Clearness Index $\overline{K}_T$ 9

Table 2.2: RMSE Between Correlations and TMY2 Data 16

Chapter 4

Table 4.1: Monthly Average Daily Tilted Radiation $\overline{H}_T$ 63

CHAPTER 1. Introduction

1.1 Available Data

Analyses to predict long-term performance of solar energy systems rely on the availability of solar radiation data. These data generally include measurements of global horizontal irradiance, diffuse irradiance, and direct (beam normal) irradiance in W/m^2. In the United States, hourly data are most commonly used in these analyses and are readily available for 239 US locations for 30 years. These data can be actual measured values, but are most often interpolated or calculated using other meteorological data. Variations in solar radiation data exist within an hour and measurements of 1-minute, 3-minute, and 5-minute data have been made. These measurements exist for only a few locations and for only a few years. They are not traditionally used in performance analyses but research continues to validate the use of these short-term data in analyses rather than hourly data.

1.1.1 Hourly Data

The US National Solar Radiation Data Base (NSRDB) contains hourly solar radiation data for 239 National Weather Service Stations. This database currently spans 30 years, from 1961 to 1990 and replaces the outdated SOLMET/ERSATZ database, which had fewer locations and only contained data between 1952 and 1975. Because the computational effort required to simulate solar energy systems for 30 years is excessive, it is convenient for simulation purposes to use data that represents one year of 'typical' meteorological conditions. The National Renewable Energy Laboratory (NREL) initially used the SOLMET data to derive typical meteorological year (TMY) data sets, and later used the NSRDB to derive TMY2 data sets.

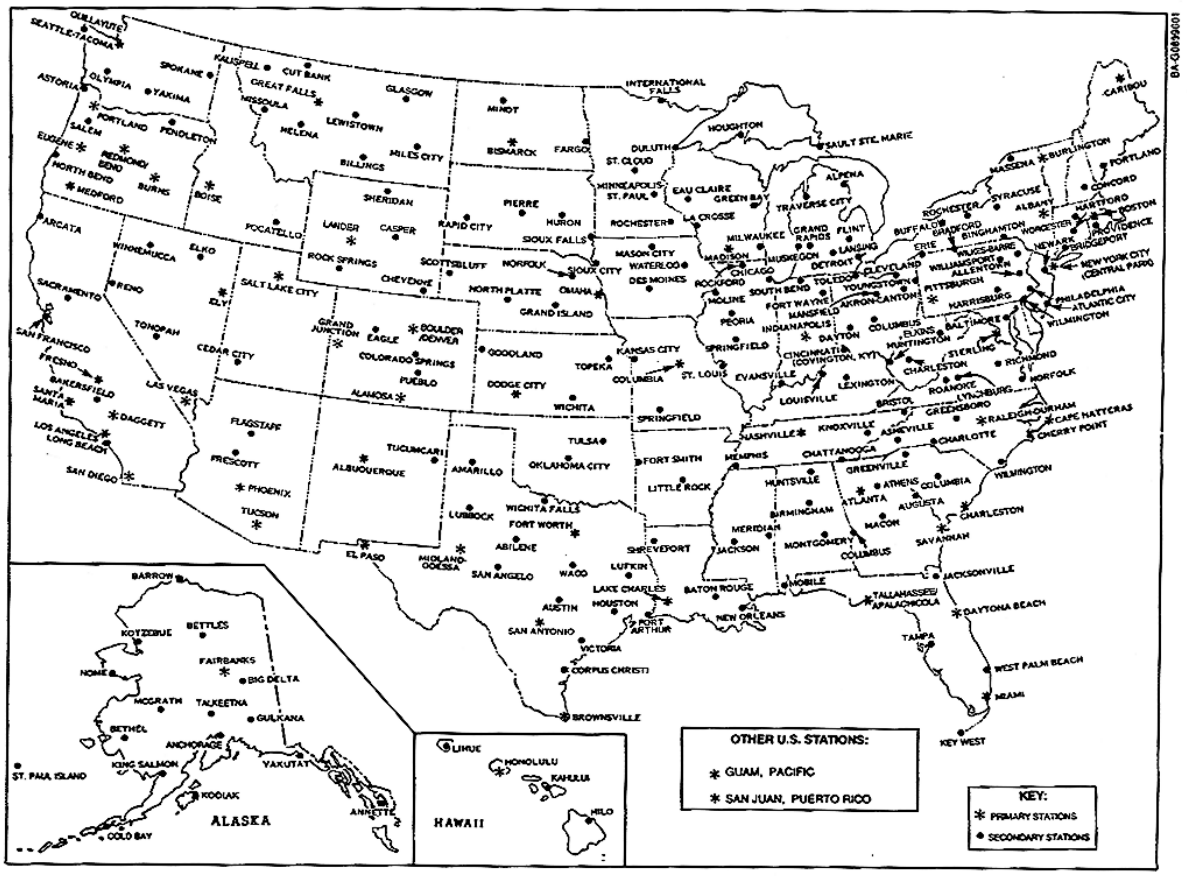

Fig. 1.1: Map showing the 239 National Weather Service stations for which TMY2's were derived.

TMY2 data represent conditions judged to be typical over a long period of time and exist for the 239 locations in the original NSRDB (Fig 1.1). These data provide a statistically formulated set of hourly values of solar radiation and other meteorological data for a one-year period that can be used in simulation studies and performance comparisons of solar energy systems. The 12 ‘typical’ months selected for each station were chosen based on five elements: global horizontal radiation, direct normal radiation, dry bulb temperature, dew point temperature, and wind speed. The months were selected from individual years based

on their ability to match long-term distributions and averages and were then concatenated to form a complete year using a modified version of the empirical approach developed by Sandia National Laboratories for the original TMY data sets. The User's Manual for TMY2's, published by NREL [1995], provides further details on their formulation.

1.1.2 Minute Data

The Surface Radiation Research Branch is home to both the SURFRAD network and the Integrated Surface Irradiance Study (ISIS) network. ISIS is responsible for monitoring surface radiation in the United States and provides measurements of solar radiation data on a 1-minute basis for Madison, WI, and on a 3-minute basis for Albuquerque, NM, Bismarck, ND, Hanford, CA, Oak Ridge, TN, Madison, WI, Seattle, WA, Salt Lake City, UT, and Sterling, VA [2003].

Fig. 1.2: ISIS network stations in the US.

1.2 Assessment Techniques

Both data sets needed to be assessed in regard to their ability to be effectively used in performance analyses and to determine the validity of existing correlations. For both hourly and minute data, relationships between available radiation data were investigated and compared to existing correlations. Radiation data were analyzed to determine diffuse fraction characteristics as functions of clearness index and to determine frequency distributions. The concept of utilizability was used to assess the data in performance analyses of solar energy systems.

1.2.1 Hourly Data

TMY2 data were selected for analysis to verify that months chosen to represent the typical meteorological year, for a given location, were chosen appropriately. Inconsistencies in the data appeared early in the analysis which warranted further investigation into how these discrepancies would impact the accuracy of performance analyses that commonly utilized this data.

1.2.2 Minute Data

Short-term variations in solar radiation data have not been investigated to the same extent that hourly radiation has. Recognizing this shortcoming, Skartveit and Olseth [1992] used hourly averages to produce "realistic time series of short-term global or beam irradiance" analogous to previous research on "probability density distributions of daily and hourly global irradiation [that were] parameterized in terms of the monthly mean value". Their research was based on one year of 5-minute global and beam radiation data from Atlanta, San Antonio and Geneva. More recently, Tovar, Olmo, and Alados-Arboledas [1998] "analyzed the probability density distributions of 1-minute values of global irradiance, conditioned to the optical air mass" and proposed a function to generate short-term radiation data. They extended this research the following year to analyze and model 1-minute probability density distributions of beam normal and diffuse irradiance, conditioned to the optical air mass [1999]. Another way to demonstrate the variability in solar radiation data is through cumulative frequency distributions. Research on the comparison of cumulative frequency distributions for short-term radiation data to hourly data has been done by Suehrcke [1988] and Gansler [1995], but with very limited data sets. Still another way is to

analyze short-term diffuse fraction relationships. Existing diffuse fraction correlations were developed based on hourly data as were methods used to calculate the radiation that strikes a tilted surface. Gonzalez and Calbo [1999] have shown in their research that the variability of global irradiation within an hour, in addition to solar altitude and hourly clearness index, influence hourly diffuse fraction correlations. Their research was based on 5-minute data in Catalonia. If existing hourly correlations and distributions cannot be used accurately with short-term data, new correlations will need to be developed for widespread use.

Although it is clear that solar radiation can exhibit wide variations within an hour, simulation studies of solar energy systems have traditionally used hourly values to estimate the long-term annual performance of the system. This simplification has been made because short-term radiation data simply do not exist for an extended periods of time or for a great number of locations, like the TMY2 data. However, some types of solar systems, (i.e. photovoltaic and daylighting) respond quickly and non-linearly to variations in solar radiation within an hour. A study performed by Walkenhorst, Luther, Reinhart and Timmer [2002], showed how the short-term variations in daylight can affect simulation-based predictions of the annual daylight availability for a building. The results of their investigation showed that annual artificial lighting demand predictions were being underestimated by up to 27% when based on hourly data rather than 1-minute data generated using the Skartveit-Olseth model.

System specific simulation studies are showing that variability within an hour can significantly impact performance estimates compared to using hourly data. The purpose of this research is to analyze the available short-term data and to quantify the impact of variability on performance estimates in a system-independent manner.

CHAPTER 2. Typical Meteorological Year Data

TMY2 data were analyzed to determine how accurately the data represent long-term averages and the impact inconsistencies in the data have on performance estimates. Of the 239 National Weather Stations in the NSRDB, only 56 "primary" stations provide actual solar measurements. None of these stations provide actual solar measurements for the entire 30 year time period of the database. The 183 remaining "secondary" stations have no recorded radiation measurements. The User's Manual for TMY2's states that more than 90% of the solar radiation data used to create the TMY2 data are "modeled" data as opposed to "measured" data. The source of each data value is identified in the TMY2 data sets indicating whether the datum is measured, derived from other available solar radiation data, or modeled from available or interpolated meteorological elements.

TMY2 data are provided by NREL as integrals of instantaneous values for the previous 60 minutes in units of Wh/m^2. The database includes integrated hourly values of extraterrestrial global horizontal radiation (I_o), total horizontal radiation (I), diffuse horizontal radiation (I_d), and beam normal radiation (I_{bn}). Any time dependent geometry factors that needed to be evaluated were calculated at the midpoint of the hour and applied to the hourly integrated value.

2.1 Analysis of Data

TMY2 data for six primary stations, Seattle, WA, Madison, WI, Atlanta, GA, Miami, FL, Boston, MA and Albuquerque, NM, were selected for the analysis. These locations were selected to represent locations of low, average and high levels of solar radiation across the nation.

TMY2 solar radiation data for these locations have been processed and established relationships that govern solar radiation have been applied to quantify any inconsistencies in the data.

2.1.1 Monthly Average Daily Radiation

The monthly average daily total radiation, $\overline{H}$, can be calculated by summing the hourly measurements of solar radiation on a horizontal surface (*I*) for monthly periods and evaluating the daily average. The ratio of this amount to the monthly average daily extraterrestrial radiation is the monthly average clearness index, $\overline{K}_T$.

$$\overline{K}_T = \frac{\overline{H}}{\overline{H}_o} \tag{2.1}$$

Monthly clearness indices based on TMY2 data were compared to long-term average (LTA) values calculated from 30 years of data in the NSRDB [1992]. The results of this comparison appear in Table 2.1.

TABLE 2.1a: MONTHLY AVERAGE DAILY CLEARNESS INDEX $\overline{K}_T$ *

Month	Madison		Seattle		Albuquerque	
	TMY2	LTA	TMY2	LTA	TMY2	LTA
January	0.47	0.49	0.30	0.32	0.61	0.62
February	0.52	0.52	0.36	0.36	0.63	0.63
March	0.48	0.50	0.42	0.42	0.64	0.64
April	0.47	0.50	0.44	0.45	0.68	0.68
May	0.54	0.52	0.50	0.49	0.71	0.69
June	0.55	0.54	0.52	0.50	0.70	0.70
July	0.55	0.55	0.55	0.54	0.68	0.66
August	0.56	0.54	0.51	0.53	0.66	0.66
September	0.49	0.50	0.50	0.49	0.64	0.65
October	0.48	0.47	0.39	0.41	0.66	0.65
November	0.42	0.41	0.33	0.33	0.64	0.62
December	0.47	0.43	0.28	0.30	0.61	0.61

*Long-term average (LTA) clearness index calculated from daily statistical files from NSRDB[1992].

TABLE 2.1b: MONTHLY AVERAGE DAILY CLEARNESS INDEX $\overline{K}_T$ *

Month	Atlanta		Miami		Boston	
	TMY2	LTA	TMY2	LTA	TMY2	LTA
January	0.48	0.48	0.52	0.53	0.47	0.47
February	0.51	0.50	0.56	0.54	0.51	0.50
March	0.52	0.53	0.55	0.55	0.51	0.50
April	0.59	0.56	0.59	0.57	0.48	0.49
May	0.57	0.55	0.54	0.54	0.51	0.51
June	0.56	0.56	0.51	0.49	0.52	0.52
July	0.56	0.54	0.53	0.52	0.53	0.53
August	0.55	0.54	0.53	0.52	0.54	0.53
September	0.52	0.53	0.50	0.50	0.52	0.51
October	0.57	0.55	0.52	0.52	0.51	0.49
November	0.52	0.50	0.50	0.52	0.43	0.43
December	0.48	0.47	0.53	0.52	0.45	0.43

*Long-term average (LTA) clearness index calculated from daily statistical files from NSRDB[1992].

From this analysis, there appears to be good agreement between the monthly clearness indices from the TMY2 and long-term average data sets. Months statistically chosen to be

typical accurately represent the long-term average value for monthly average daily total solar radiation.

2.1.2 Distribution of Daily Solar Radiation

The frequency distribution, i.e., the relative number of cloudy, average and sunny days that together form the monthly average, is important in determining the performance of solar energy systems. The distribution can be represented in a non-dimensional manner in terms of the fractional time of occurrence of the daily clearness index, K_T, the ratio of the total radiation to the extraterrestrial radiation for a particular day. Liu and Jordan [1960] showed that cumulative distributions representing the long-term average distribution of clearness index values are a unique function of $\overline{K}_T$. Generalized distribution curves were developed by Liu and Jordan and equations representing these curves were developed by Bendt et al. [1981] based on 20 years of data from 90 North American locations (Fig. 2.1).

Recent research has shown that these curves may not be entirely accurate when applied to tropical climates. Theilacker [1980] showed that data from Miami, FL, was not described accurately by the Bendt et al. curves and Saunier et al.[1987] showed that these curves overestimated clearness indices in tropical climates. Modifications of these distribution curves have been proposed by Saunier et al.[1987], Feuillard et al. [1989], and Babu and Satyamurty [2001]. The Bendt et al. functions are used throughout this research for the purpose of comparison only. Data from locations, such as Seattle and Miami, with higher atmospheric water vapor content may be better described by recently modified distributions, but for the sake of consistency, the Bendt et al. curves were used for all locations.

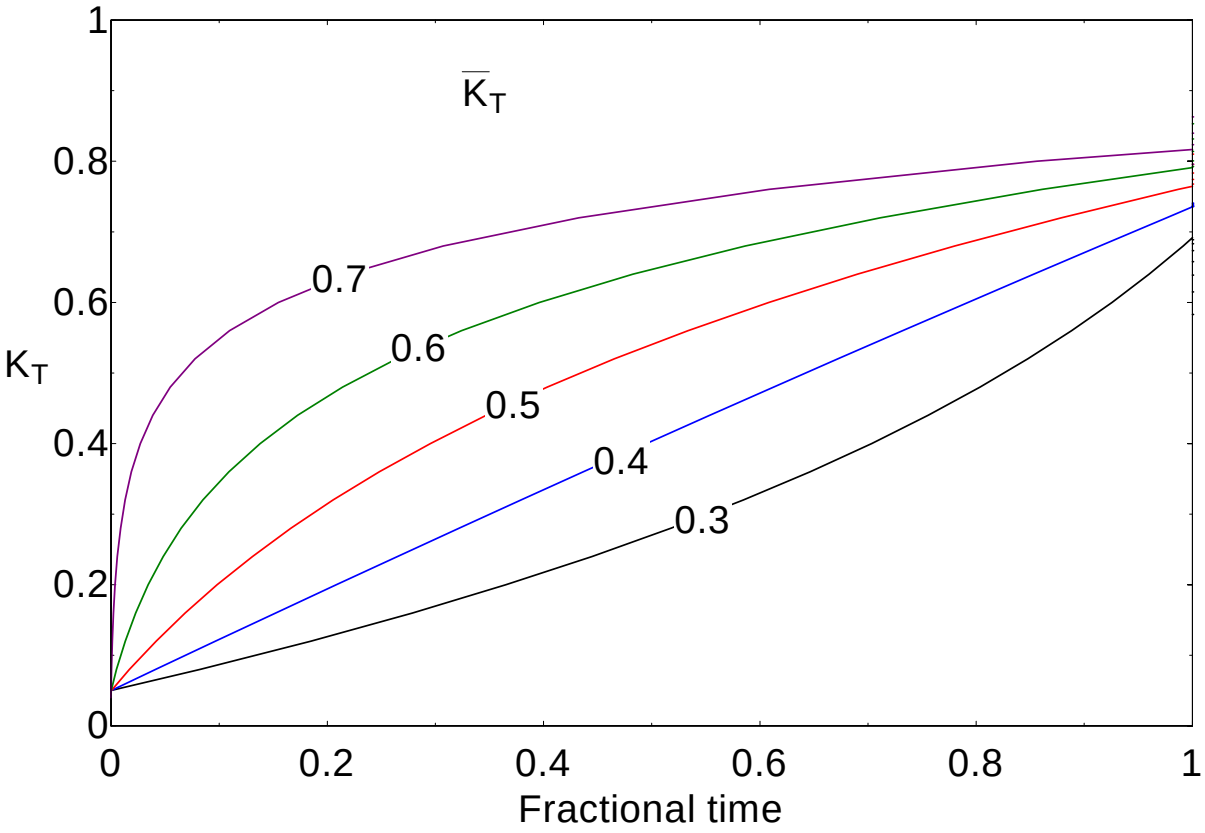

Fig. 2.1: Generalized daily distribution of K_T as a function of $\overline{K}_T$ using equation from Bendt et al. [1981].

Using the TMY2 data, frequency distribution curves were generated for each month and city and compared to the generalized distribution predicted by Bendt et al. [1981]. Two representative distributions are shown in Figures 2.2 and 2.3. Figure 2.2 represents a month of poor correlation to Bendt et al. distributions and Figure 2.3 represents a month of excellent correlation. A standard deviation to represent the difference between the TMY2 and Bendt distributions can be defined as:

$$SD = \sqrt{\frac{\sum_{N} (K_{T,TMY2} - K_{T,Bendt})^2}{N}} \tag{2.2}$$

where *N* is the number of days in a month. Values of SD less than 0.03 indicate excellent agreement between the TMY2 data and the long-term Bendt et al. distributions, as seen in Figure 2.3.

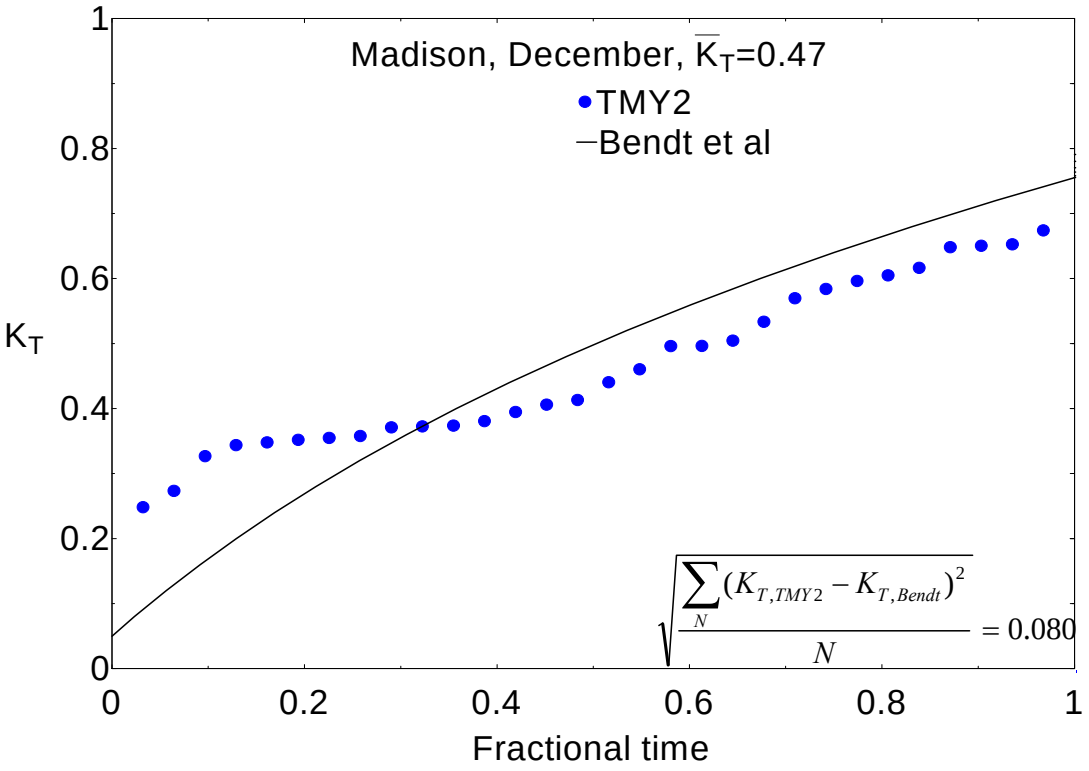

Fig. 2.2: Distribution of K_T in Madison, WI based on TMY2 data for December and compared with Bendt et al. [1981] generalized distribution.

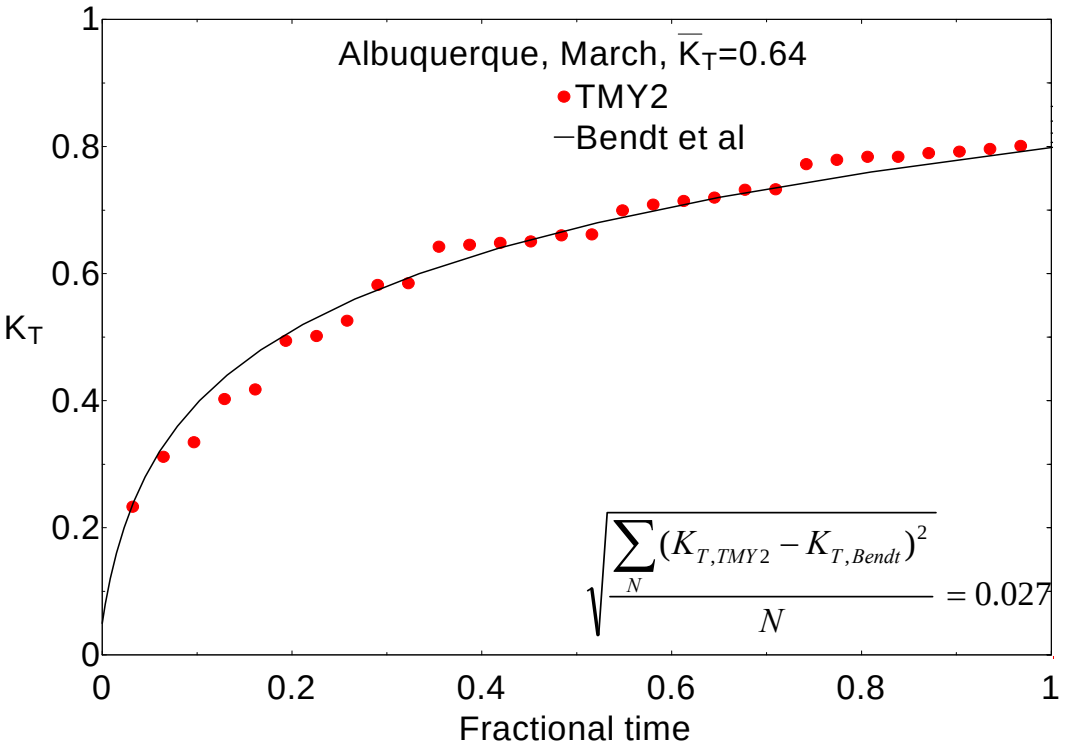

Fig. 2.3: Distribution of K_T in Albuquerque, NM based on TMY2 data for March and compared with Bendt et al. [1981] generalized distribution.

The true long-term distributions were also calculated from the 30 year database and compared to Bendt et al. and TMY2 distributions, as shown for Atlanta in Figure 2.4. Plots for the other locations and months can be found in Appendix A. A conclusion of these analyses based on six locations is that the TMY2 data represent the true long-term average distribution of days reasonably well. The Bendt et al. correlation tends to overpredict the clearness of the really clear days (K_T>0.6) and predict cloudier days (K_T<0.2) than actually occur over the long-term.

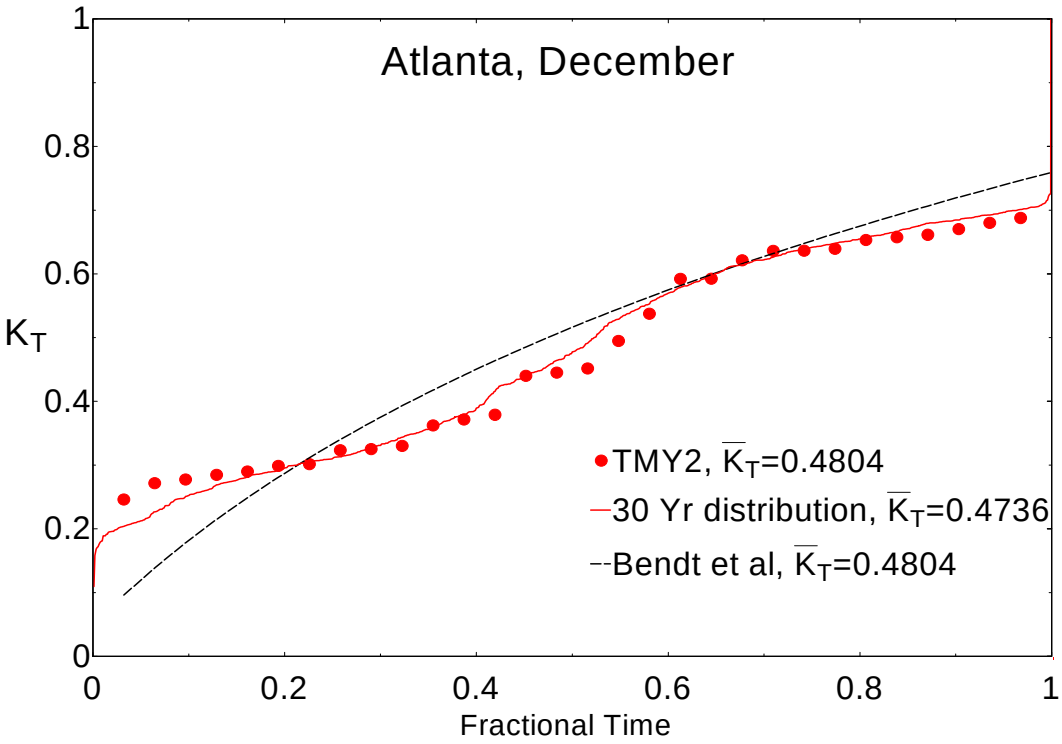

Fig. 2.4: Distribution of K_T in Atlanta, GA based on TMY2 data for December and compared with Bendt et al. [1981] generalized distribution.

2.1.3 Diffuse Fraction

Solar energy systems utilize beam and diffuse radiation differently so that it is generally necessary to know the individual contributions in addition to their total. Also, the estimation of radiation on a tilted surface requires knowledge of the beam and diffuse components. The ratio of the diffuse radiation to total radiation on a horizontal surface is known as the diffuse fraction. Figure 2.5 shows TMY2 data for Madison, WI plotted in the form of the hourly diffuse fraction versus hourly clearness index, k_T, i.e., the ratio of the total

hourly radiation to the hourly extraterrestrial radiation on a horizontal surface.

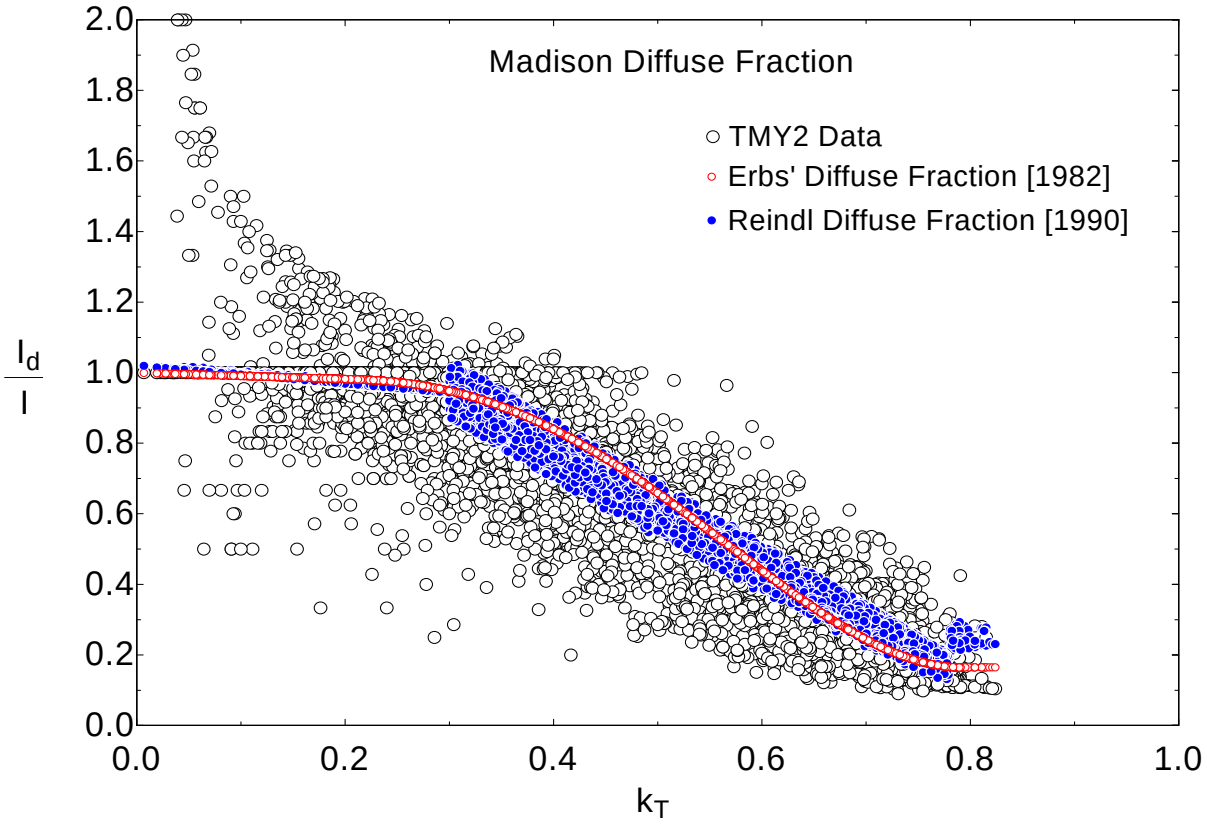

Fig. 2.5: Diffuse fraction versus hourly clearness index for Madison, WI.

Shown in Figure 2.5 are two diffuse fraction correlations. Erbs' [1982] correlation is a function of k_T and Reindl's [1990] correlation is a function of k_T and solar altitude, the angle between the horizontal and the line to the sun. The root mean square errors were calculated for each city and month in the study and are shown in Table 2.2.

TABLE 2.2a: RMSE BETWEEN CORRELATIONS AND TMY2 DATA

Month	Madison		Seattle		Albuquerque	
	Erbs	Reindl	Erbs	Reindl	Erbs	Reindl
January	0.1018	0.0935	0.0910	0.0825	0.1377	0.1237
February	0.1168	0.1052	0.0936	0.0834	0.1095	0.1059
March	0.1088	0.1018	0.0969	0.0868	0.1167	0.1101
April	0.1128	0.1025	0.0830	0.0710	0.1166	0.1079
May	0.1001	0.0835	0.1080	0.0979	0.1150	0.1034
June	0.1167	0.1013	0.0982	0.0866	0.1371	0.1287
July	0.1026	0.0889	0.1370	0.1278	0.0855	0.0741
August	0.1068	0.0933	0.1259	0.1110	0.0995	0.0842
September	0.1320	0.1229	0.1469	0.1355	0.1416	0.1293
October	0.1016	0.0882	0.0997	0.0906	0.1249	0.1068
November	0.1200	0.1072	0.0768	0.0650	0.1086	0.0920
December	0.1080	0.1082	0.0841	0.0748	0.1069	0.0829

TABLE 2.2b: RMSE BETWEEN CORRELATIONS AND TMY2 DATA

Month	Atlanta		Miami		Boston	
	Erbs	Reindl	Erbs	Reindl	Erbs	Reindl
January	0.1102	0.0972	0.1138	0.0951	0.1095	0.0890
February	0.1211	0.1070	0.1251	0.1097	0.1042	0.0992
March	0.0934	0.0838	0.1116	0.0988	0.0948	0.0828
April	0.1010	0.0857	0.1045	0.0919	0.0926	0.0802
May	0.0900	0.0715	0.1084	0.0973	0.0886	0.0769
June	0.0909	0.0722	0.0889	0.0767	0.0842	0.0669
July	0.0967	0.0825	0.0954	0.0810	0.0956	0.0805
August	0.0941	0.0833	0.0991	0.0839	0.0972	0.0823
September	0.0870	0.0694	0.0850	0.0747	0.0971	0.0835
October	0.1040	0.0868	0.0860	0.0727	0.1009	0.0810
November	0.0984	0.0805	0.1118	0.0976	0.0990	0.0845
December	0.1124	0.0963	0.0979	0.0807	0.1211	0.1107

Because the Reindl correlation accounts for a greater spread of data associated with solar altitude, Reindl's correlation results in a lower root mean square error for over 90% of months studied in this analysis.

For comparison, Figure 2.6 shows TMY2 data for Madison, WI, the Erbs correlation, and another correlation developed by Reindl [1990] where diffuse fraction is dependent on

k_T, solar altitude, ambient temperature and relative humidity. This correlation accounts for a slightly greater spread in data, however this additional data may not always be available. With very little data available, the Erbs correlation can be used to estimate diffuse fraction and the validity of its simplicity is explored later in this chapter.

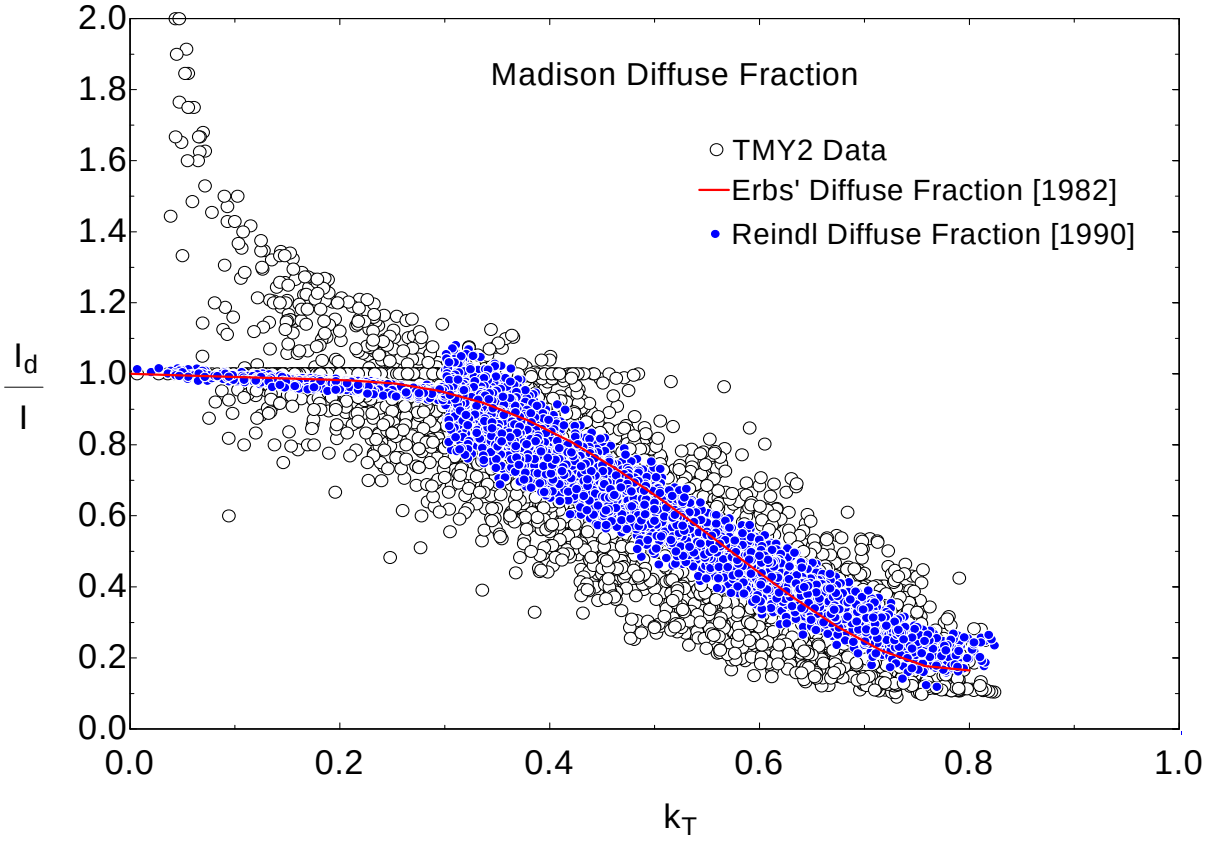

Fig. 2.6: Diffuse fraction versus hourly clearness index for Madison, WI.

A surprising result illustrated in Fig. 2.5 and Fig 2.6 is the inconsistency in the TMY2 data that leads to the horizontal diffuse radiation significantly exceeding the total horizontal radiation. Measured values of the ratio can be expected to be greater than one at times of low total radiation, such as near sunrise or sunset, because of instrument uncertainties. However, inspection of the data shows that the diffuse fraction ratio exceeds one at other times as well, as indicated in Figure 2.7.

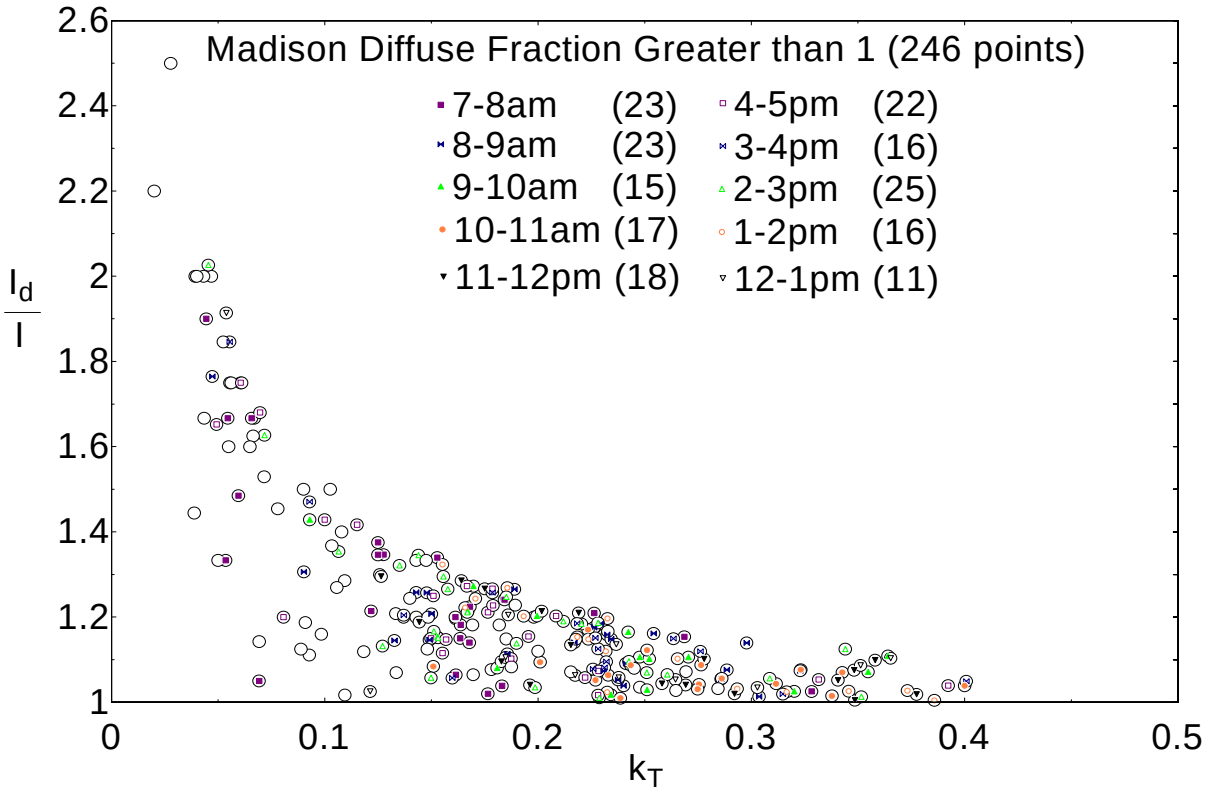

Fig. 2.7: Diffuse radiation exceeding total for hours that do not contain sunset or sunrise.

Over 57% of the data for which the diffuse fraction was greater than one occurred during hours that do not include the time of sunrise or sunset. Similar results were observed in the TMY2 data for the other locations.

Figure 2.8 compares the total horizontal radiation reported by the TMY2 database with the sum of the beam (I_{bn}) and diffuse (I_d) radiation on a horizontal surface that can be determined using Equation 2.3,

$$I = I_d + I_{bn} \cos \theta_z \qquad (2.3)$$

where the zenith angle, θ_z, is the angle between the vertical and the line to the sun calculated at the midpoint of the hour. One would expect that there would be no difference between these values. Figure 2.8 shows that some inconsistencies exist. If total, beam normal, and diffuse radiation are independently measured, differences can be expected due to instrument errors; however, these differences occur for modeled data as well.

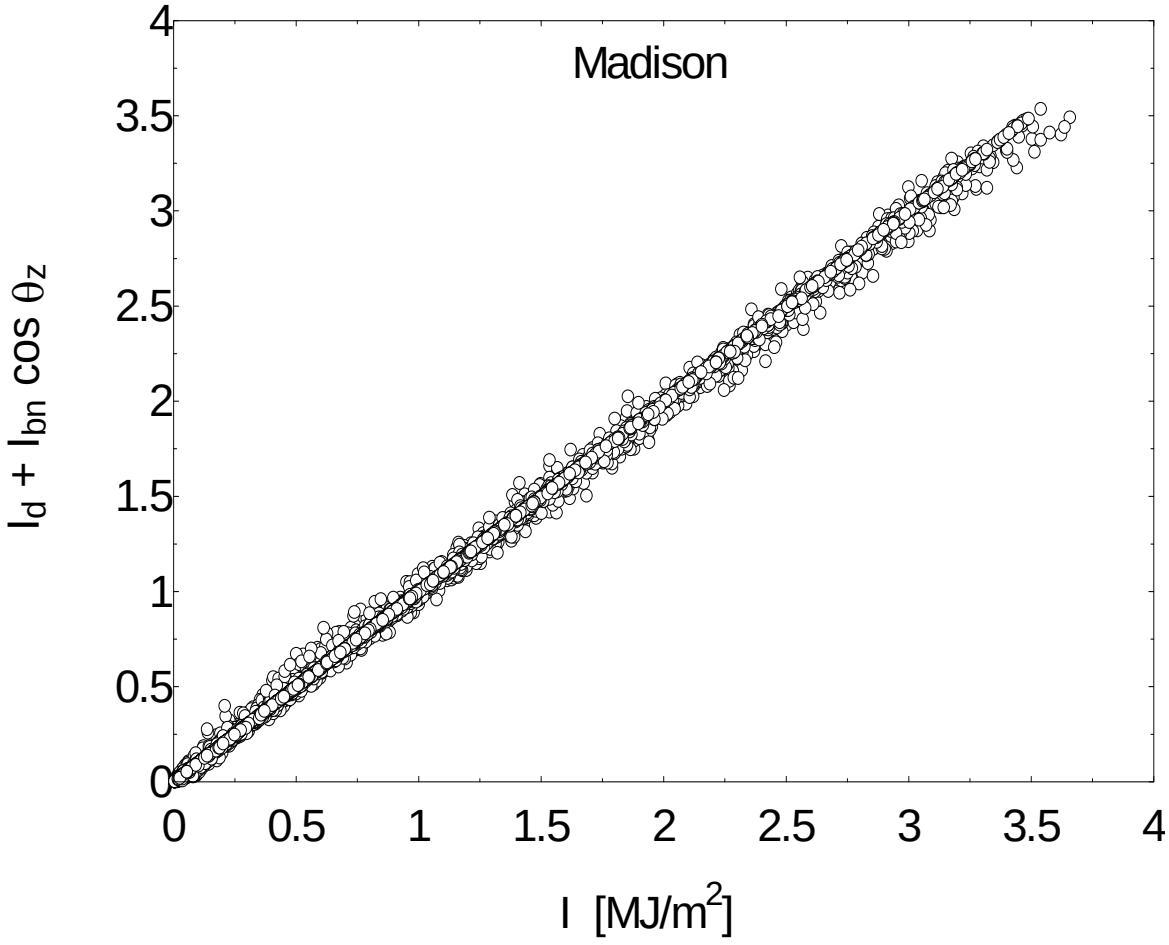

Fig. 2.8: Comparison of TMY2 values of total horizontal radiation to the sum of the components of beam and diffuse on a horizontal surface for Madison, WI.

2.1.4 Data Sources

The inconsistencies in the TMY2 data are surprising considering that approximately 90% of the data are modeled. Further study on the data sources of the reported TMY2 data led to the following results: in Madison, 60.5% of the hourly data for total radiation, I, is measured; 4.3% of the hourly data for beam normal radiation, I_{bn}, is measured; and 0% of the hourly data for diffuse radiation, I_d, is measured. Seattle and Albuquerque are similar with 62%; 37.1%; and 10.3%, for Seattle and 66.1%; 13.6%; and 14.6% for Albuquerque. When both I and I_d are modeled, the diffuse fractions for all three cities never exceed one, as expected. As an example, Figure 2.9 illustrates this behavior for Seattle, where both diffuse and total radiation have been modeled from observed sky cover.

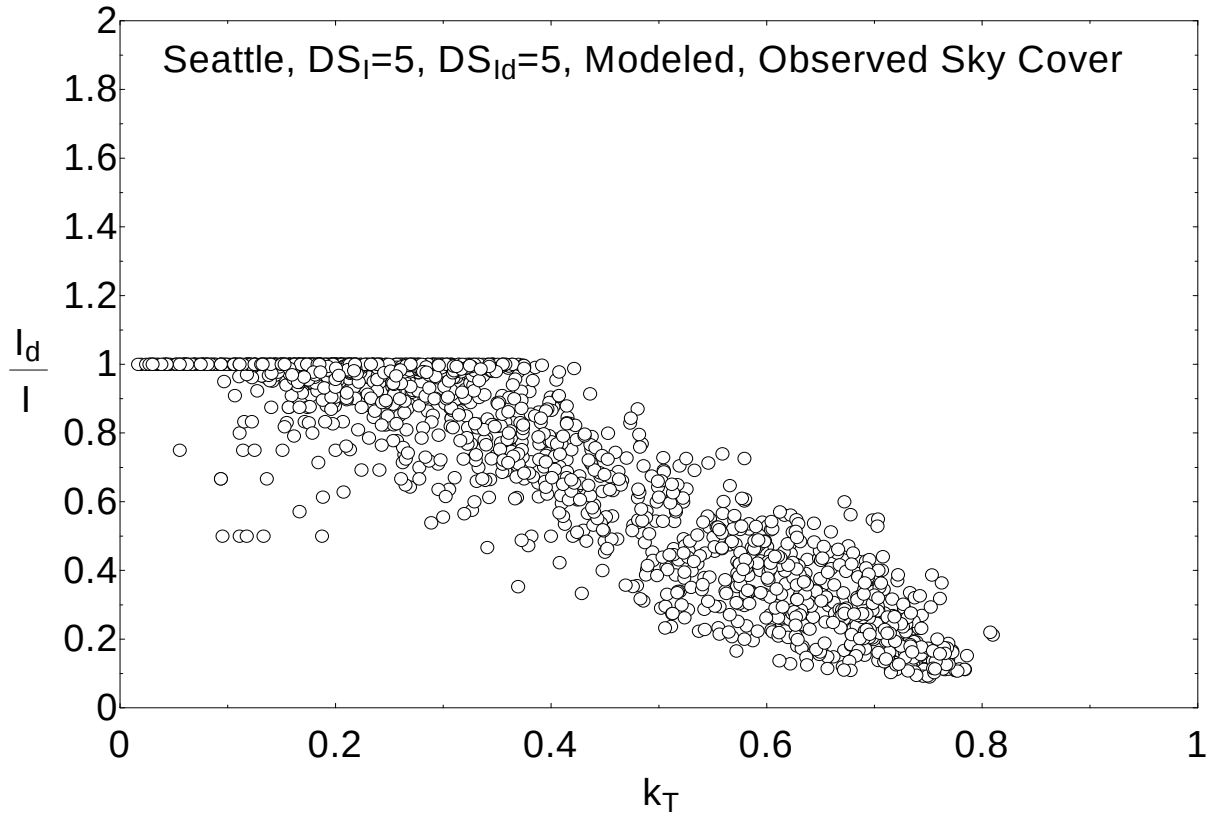

Fig. 2.9: Seattle diffuse fraction; I and I_d modeled from observed sky cover.

When either I or I_d originated from measured data, the diffuse fraction on occasion exceeded one. This was a reasonable error considering that they were independently measured values. However, in some locations, when diffuse radiation was directly derived from measured values of beam normal and total horizontal, using Equation 2.3, the diffuse fraction *still* exceeded one, although the extent of the error was reduced as shown in Fig. 2.10. In this case, it is possible the error resulted from applying a calibration correction to the total radiation data value *after* the diffuse radiation had already been derived.

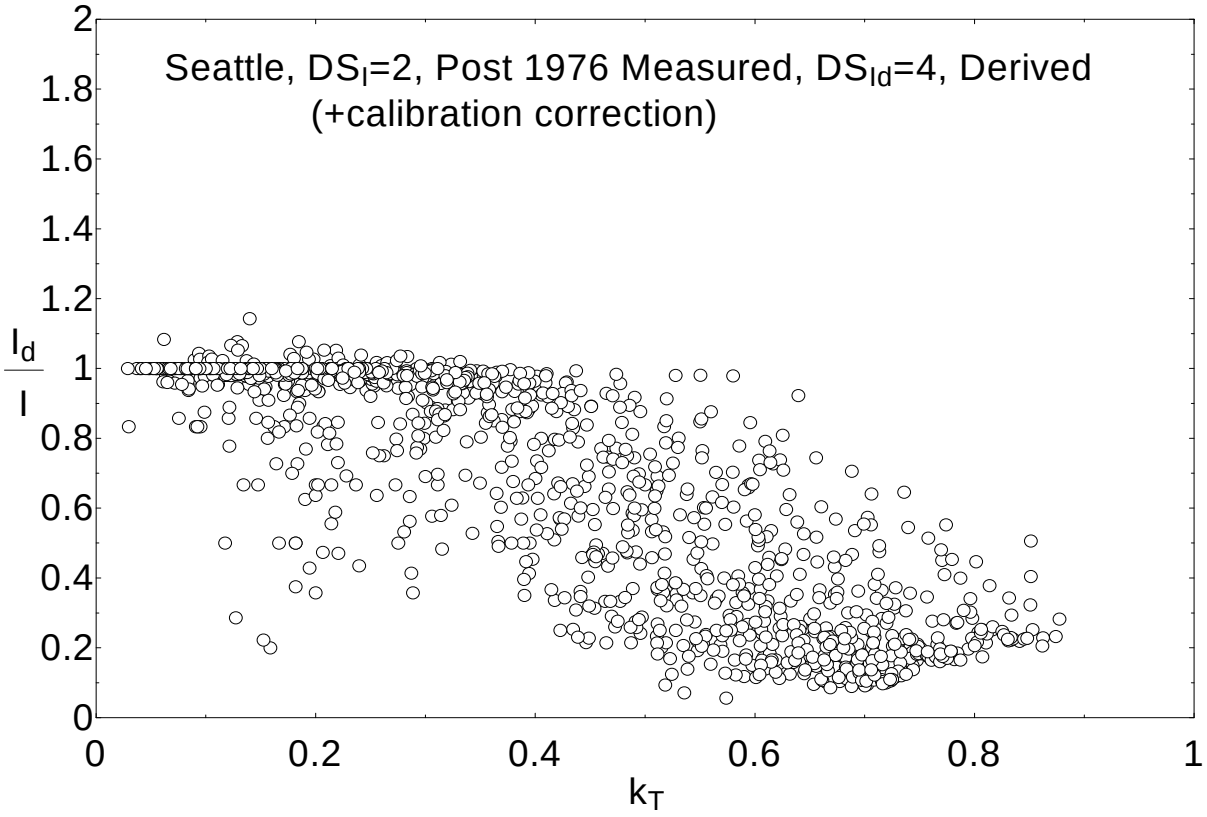

Fig. 2.10: Seattle diffuse fraction; *I* is measured post-1976 with a calibration correction and I_d is derived from *I* and I_{bn}.

2.2 Radiation on a Tilted Surface

Having observed inconsistencies in the TMY2 data, an approach to determine their impact was necessary. Calculation of the hourly radiation on a tilted surface, I_T, allows for an initial estimate of the impact. Radiation on a tilted surface was calculated using Equation 2.4, the Liu and Jordan [1962] method in two scenarios.

$$I_T = I_b \cdot R_b + I_d \cdot \left(\frac{1+\cos\beta}{2}\right) + I \cdot \rho_g \cdot \left(\frac{1-\cos\beta}{2}\right) \tag{2.4}$$

where ρ_g is the ground reflectance and R_b is the ratio of the beam radiation on a tilted surface to that on a horizontal surface defined as

$$R_b = \frac{\cos\theta}{\cos\theta_z} \tag{2.5}$$

The angle of incidence, θ, and the zenith angle, θ_z, are calculated at the midpoint of the hour for which TMY2 data are reported. The first scenario calculated radiation on a tilted surface based on I_{bn} and I_d, which are mostly modeled data. Beam radiation on a horizontal surface, I_b, was determined by Equation 2.6.

$$I_b = I_{bn} \cos\theta_z \tag{2.6}$$

The second scenario used values of I, and applied Erbs' correlation to determine I_b and I_d from k_T. The slope of the south-facing surface, β, was chosen to be equal to the latitude of the location and ρ_g was set to 0.4.

Due to the low levels of radiation and instrument uncertainties, tilted radiation was not calculated for hours that contained sunrise or sunset. Plots similar to Figure 2.11 were generated for each city comparing the two methods of using TMY2 data.

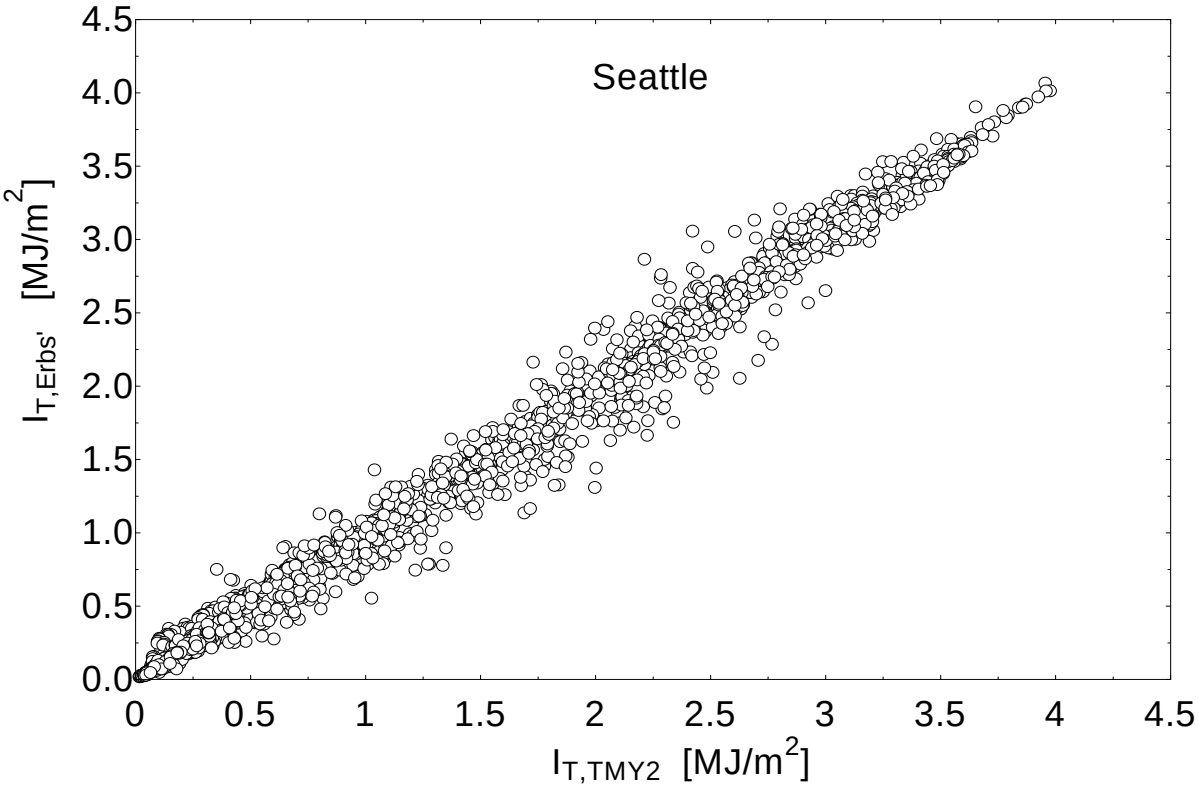

Fig. 2.11: Hourly radiation on a tilted surface calculated using TMY2 beam and diffuse data, compared to using TMY2 total radiation data and Erbs' diffuse fraction, using Liu and Jordan method.

Independently measured data yield similar results for calculated radiation on a surface tilted to its own latitude. Hours exist where one method overestimates radiation on a tilted

surface as compared to the other method. These occurrences, however, cannot be attributed consistently to one particular method as seen in Figure 2.11. Other models for calculating radiation on a tilted surface, such as Perez et al.[1987], or Hay, Davies, Klucher and Reindl (HDKR) [1979], would yield similar results. The HDKR model is represented by Equations 2.7-2.9 and Figure 2.12 show the results for Madison when using the HDKR method for calculating hourly tilted radiation using TMY2 data and data estimated using Erbs' correlation.

$$I_T = (I_b + I_d A_i)R_b + I_d(1 - A_i)(\frac{1+\cos\beta}{2})[1 + f\sin^3(\frac{\beta}{2})] + I\rho_g(\frac{1-\cos\beta}{2}) \quad (2.7)$$

$$A_i = \frac{I_{bn}}{I_{on}} = \frac{I_b}{I_o} \quad (2.8)$$

$$f = \sqrt{\frac{I_b}{I}} \quad (2.9)$$

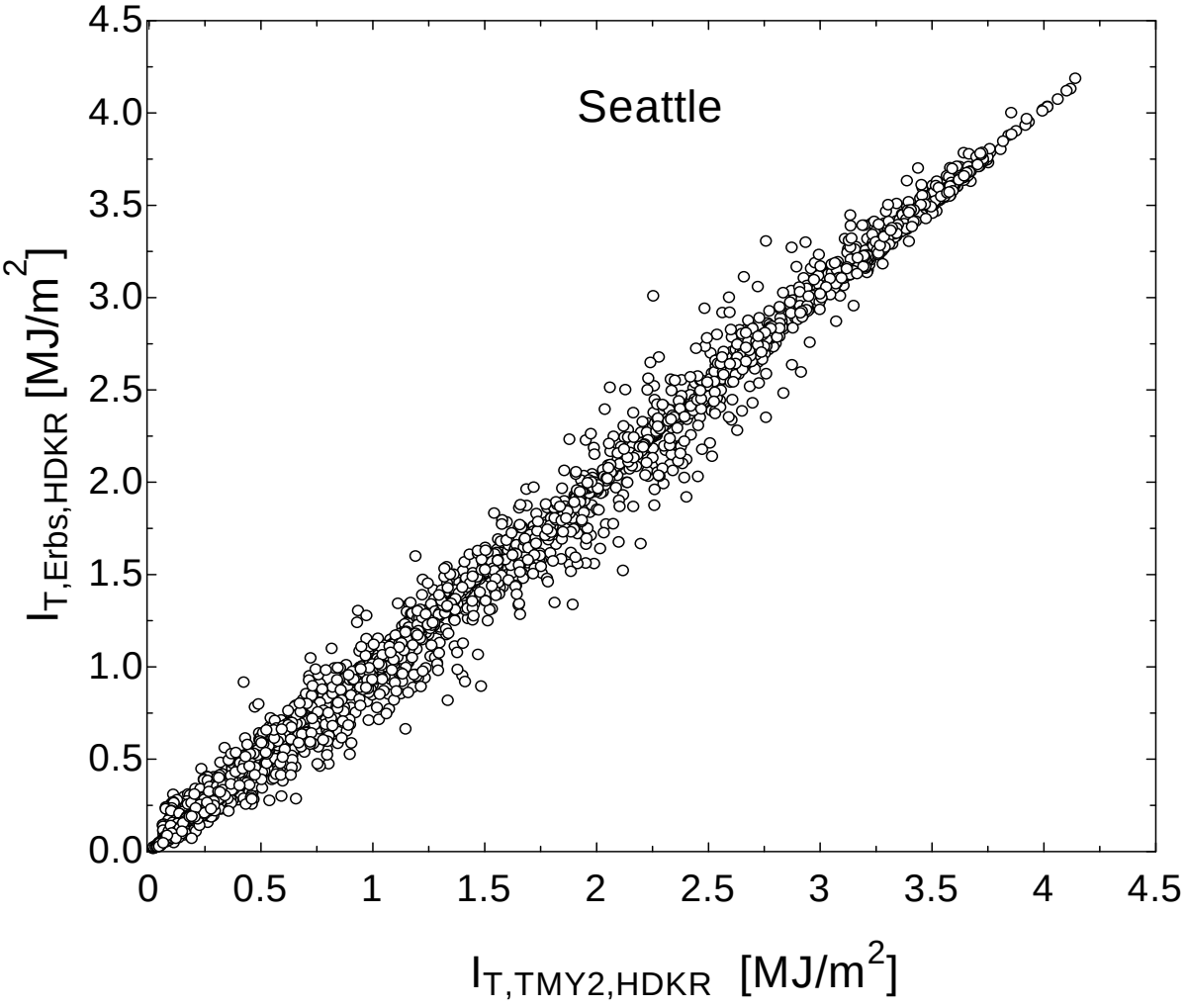

Fig. 2.12: Hourly radiation on a tilted surface calculated using TMY2 beam and diffuse data, compared to using TMY2 total radiation data and Erbs' diffuse fraction, using HDKR method.

2.3 Utilizability

Utilizability is a concept that can be used to evaluate the performance of many types of solar energy systems, from flat-plate solar collectors to photovoltaic systems. It is defined as the fraction of the solar radiation incident on a surface that exceeds a specified threshold or critical level, I_C (Klein & Beckman, [1984]). The monthly average daily utilizability, $\bar{\phi}$, can be calculated if the critical level is assumed constant over all hours of the day. It is then

the fraction of a month's solar radiation incident on a surface between sunrise and sunset that exceeds the critical level.

$$\bar{\phi} = \frac{\sum_{days}\sum_{hours}(I_T - I_C)^+}{\sum_{days}\sum_{hours} I_T} \tag{2.10}$$

Applying this definition, monthly utilizability values were determined based on both TMY2 beam normal and diffuse data and TMY2 total horizontal data combined with Erbs' correlation. Results indicative of poor, average and excellent conformance are shown in Figures 2.13-2.15. Also shown for comparison is the monthly average daily utilizability values resulting from the Klein [1984] correlation.

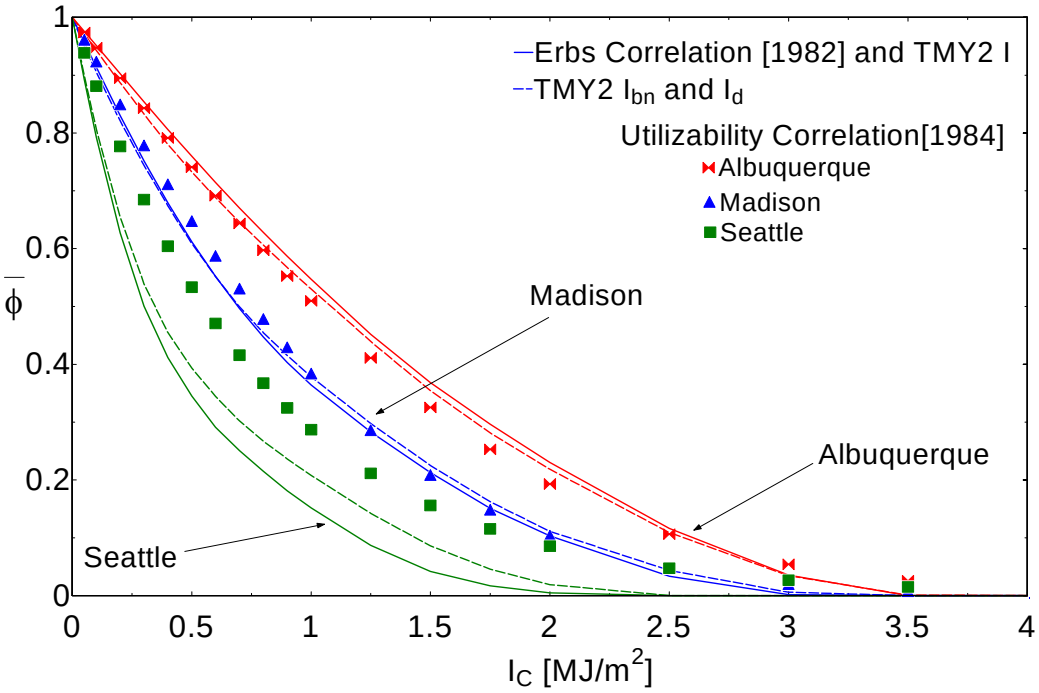

Fig. 2.13: Average daily utilizability for December for critical levels ranging from 0 to 4 MJ/m^2.

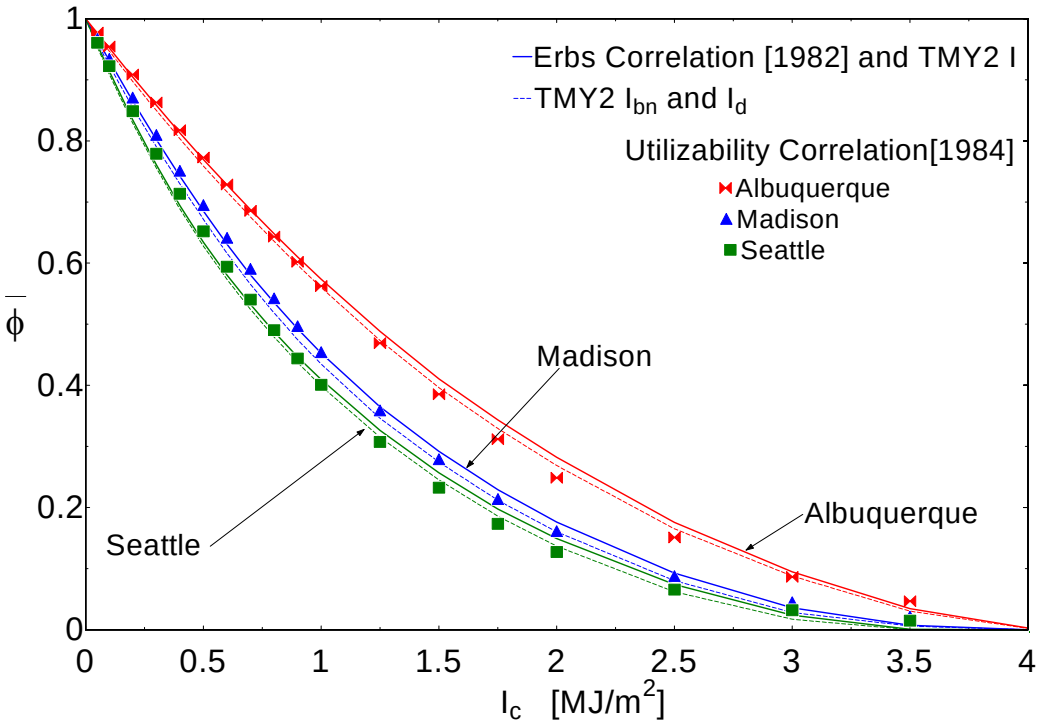

Fig. 2.14: Average daily utilizability for March for critical levels ranging from 0 to 4 MJ/m^2.

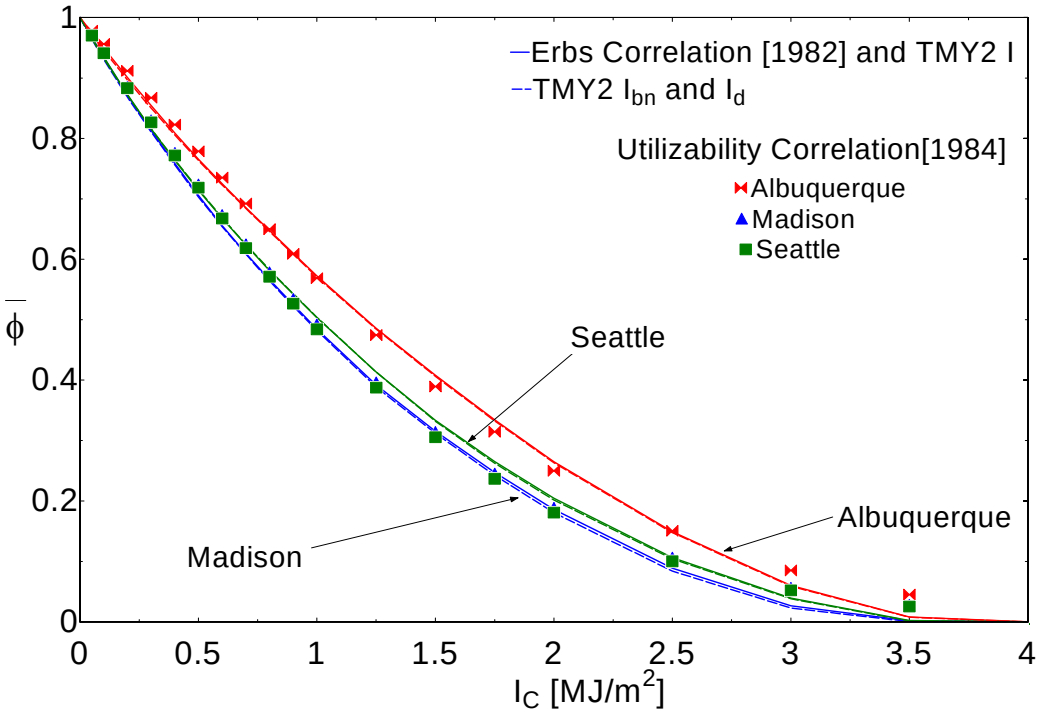

Fig. 2.15: Average daily utilizability for July for critical levels ranging from 0 to 4 MJ/m^2.

Fig 2.16 compares utilizability calculations using the 30 year database to calculations using the TMY2 data. This comparison, for the majority of months and locations, shows good agreement (see Appendix A).

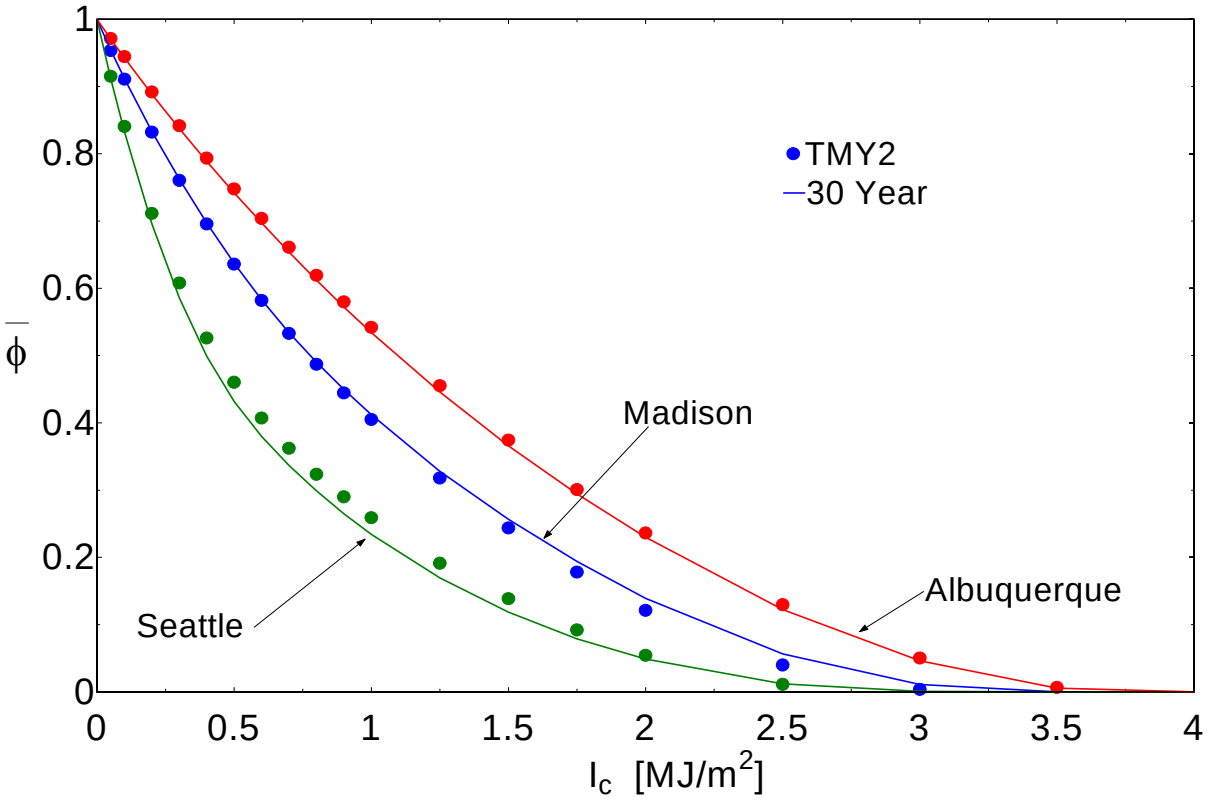

Fig. 2.16: Average daily utilizability for January for critical levels ranging from 0 to 4 MJ/m^2.

Although TMY2 data reasonably represent long-term averages in monthly total radiation and frequency distribution, at certain months and critical levels, calculated values of utilizability can be quite different, depending on which TMY2 data element is used. For example, in December in Seattle (Fig 2.13), in an application like a solar collector, where all elements of radiation are useful, utilizability at a critical level of 1.5 MJ/m^2 can be 50%

lower using TMY2 data for total horizontal radiation as compared to using TMY2 data for beam normal and diffuse. However, for a location like Albuquerque, the greatest percent difference over all months in the year and all critical levels is rarely more than 10%.

2.4 Assessment of Data

This chapter explores the inconsistencies that were found to exist within TMY2 data and the impact they have on studies of solar system performance. TMY2 data were analyzed for six locations and show a range of inconsistencies. However, overall, they agree reasonably well with the long-term average distribution of daily radiation on a monthly basis as well as long-term average monthly radiation.

The concept of utilizability was applied to determine the impact of the inconsistencies on performance of solar energy systems. Energy above a certain threshold that is 'utilizable' is an efficient indicator of performance that can be applied to a range of solar energy systems. This energy is dependent on many factors, including the threshold level of the system and the frequency distribution of daily solar radiation. Depending on threshold level, utilizability can be considerably different simply based on which TMY2 data elements are used in the calculations. Utilizability analyses of the long-term data showed that the distributions of solar radiation represented in the TMY2 database appropriately represented long-term data insofar as their affect on utilizability is concerned.

TMY2 data could be improved by eliminating obvious inconsistencies in reported data, particularly in the diffuse fractions. Based on the results of the six locations considered in this study, however, the TMY2 data provide a reasonably good approximation of long-

term solar radiation data, with respect to long-term averages, frequency distributions, and performance analyses.

CHAPTER 3. 3-Minute Radiation

The analysis of available short-term radiation data is divided into two chapters. This chapter discusses the analysis of 3-minute solar radiation data and their impact on performance analyses for the 8 ISIS network stations (Albuquerque, Seattle, Madison, Sterling, Salt Lake City, Oak Ridge, Hanford and Bismarck). Chapter 4 provides a similar analysis for 1-minute solar radiation data for Madison. One year of ISIS data, from November 2002 to October 2003, were used in both analyses.

3.1 Analysis of Data

When hourly diffuse radiation data are not available, they can be estimated knowing only the total radiation. Studies have shown that the hourly diffuse fraction can be simply correlated to the hourly clearness index. More complicated correlations exist that incorporate the dependence of diffuse fraction on other parameters, like solar altitude angle, temperature, and relative humidity, as shown in Chapter 2. Since existing diffuse fraction correlations were developed based on hourly or daily radiation data, it is not known to what extent these correlations are applicable on shorter time scales. In addition, the frequency distribution of short-term radiation data and its effect on solar system performance have not been conclusively determined. The distributions, and the solar radiation utilizability that depends on them, are investigated in this study.

3.1.1 Diffuse Fraction

Analogous to the hourly diffuse fraction, the short-term diffuse fraction in this chapter is the ratio of diffuse radiation to total radiation in a 3-minute time period. If

correlations are available for short-term data, beam and diffuse components can be estimated from only knowing the short-term total radiation.

Figure 3.1 is a plot of the short-term diffuse fraction as a function of clearness index based on 3-minute data in Madison, WI for December 2002. The diffuse fraction is calculated from ISIS data; the clearness index requires additional knowledge of the extraterrestrial radiation which is calculated from Equation 3.1, where n is the day of the year, and G_{sc} is the solar constant 1367 W/m^2 (Beckman & Duffie, [1991]).

$$G_o = G_{sc}(1 + 0.033 \cdot \cos\frac{360n}{365})\cos\theta_z \tag{3.1}$$

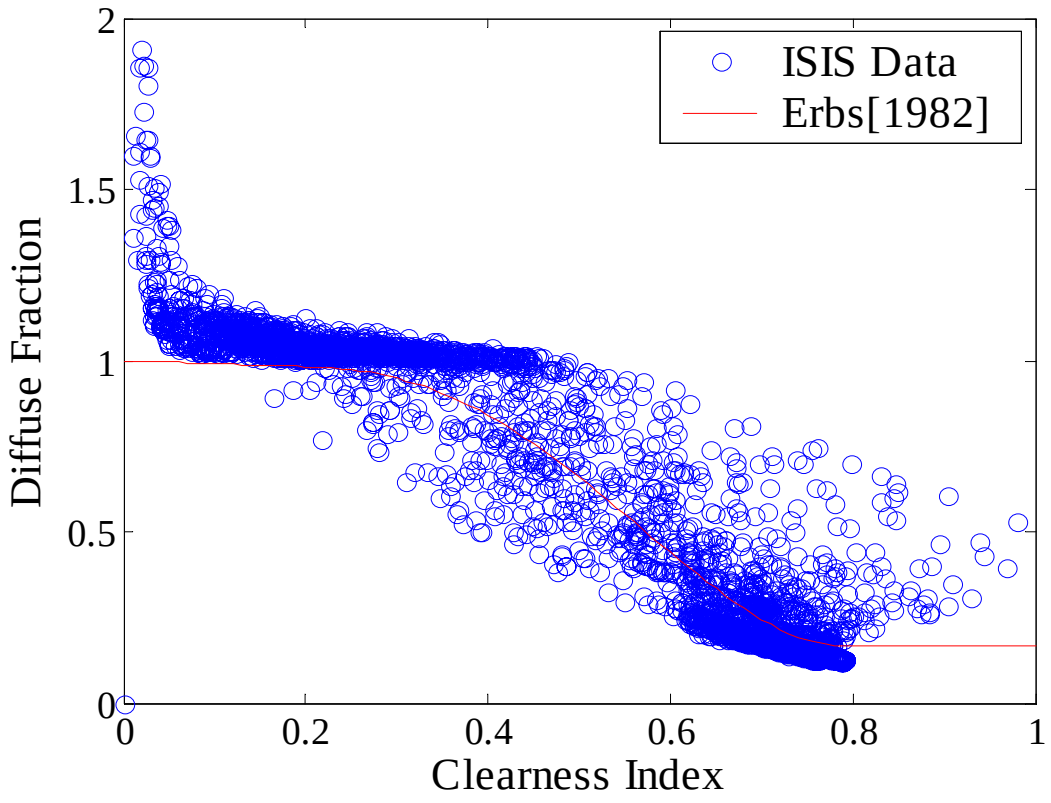

Fig. 3.1: Three minute diffuse fraction as a function of clearness index for December 2002, in Madison, WI.

This plot is similar to those seen in the TMY2 analysis and typical of the short-term diffuse fraction plots observed for the other months and locations in this analysis (see Appendix B). The diffuse fraction should not, in theory, ever be greater than one. However, due to independent instrument measurements and low levels of radiation, values over one are observed for cloudy mornings and evenings. For calculation purposes, the diffuse fraction was corrected to a value of one whenever diffuse exceeded total radiation.

Figure 3.2 shows the same relationship for a single clear day in April in Oak Ridge, representative of clear days in other locations. The diffuse fraction correlation developed by Erbs et al. [1982], based on hourly radiation measurements, is shown on both plots for comparison. Figure 3.2 shows that for a clear day the diffuse radiation is overestimated when applying Erbs' correlation for hourly data to 3-minute data.

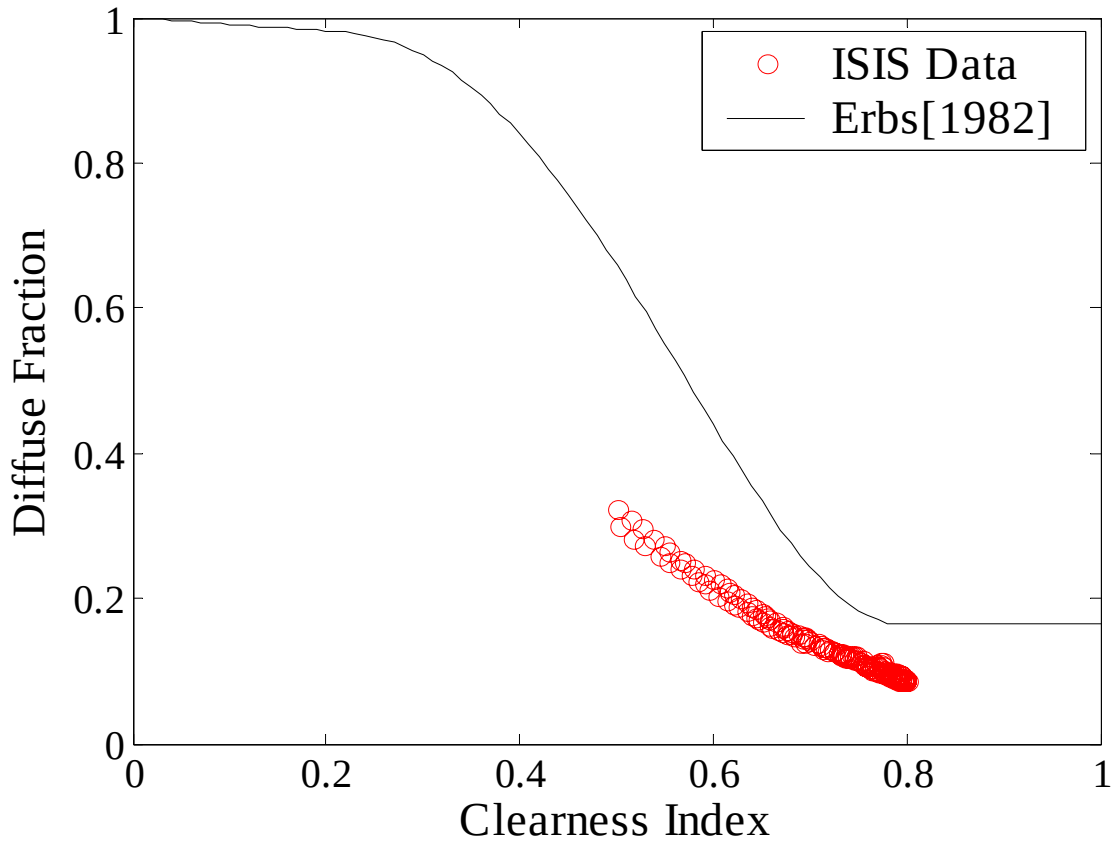

Fig. 3.2: Diffuse fraction as a function of clearness index for a clear April day in Oak Ridge, TN.

Analogous to Reindl's hourly diffuse fraction correlation, Gansler [1993] suggested that the short-term diffuse fraction also depends on other factors such as relative humidity, ambient temperature, and air mass. Air mass, *m*, is defined as

$$m = \frac{1}{\cos\theta_z} \tag{3.2}$$

Temperature and relative humidity data are not available from ISIS. To compare ISIS data to both Erbs' and Reindl's correlation, weather data were obtained from the National Climatic Data Center for a station in Madison, that was relatively close to the ISIS station. The data were available in an hourly format and two clear days, January 26, 2003, and July

18, 2003, were chosen for the comparison. In order to apply Reindl's correlation, in Figures 3.3 and 3.4, all 3-minute ISIS data within an hour are assumed to have the same temperature and relative humidity. In both figures, the correlations overestimate the actual diffuse fraction.

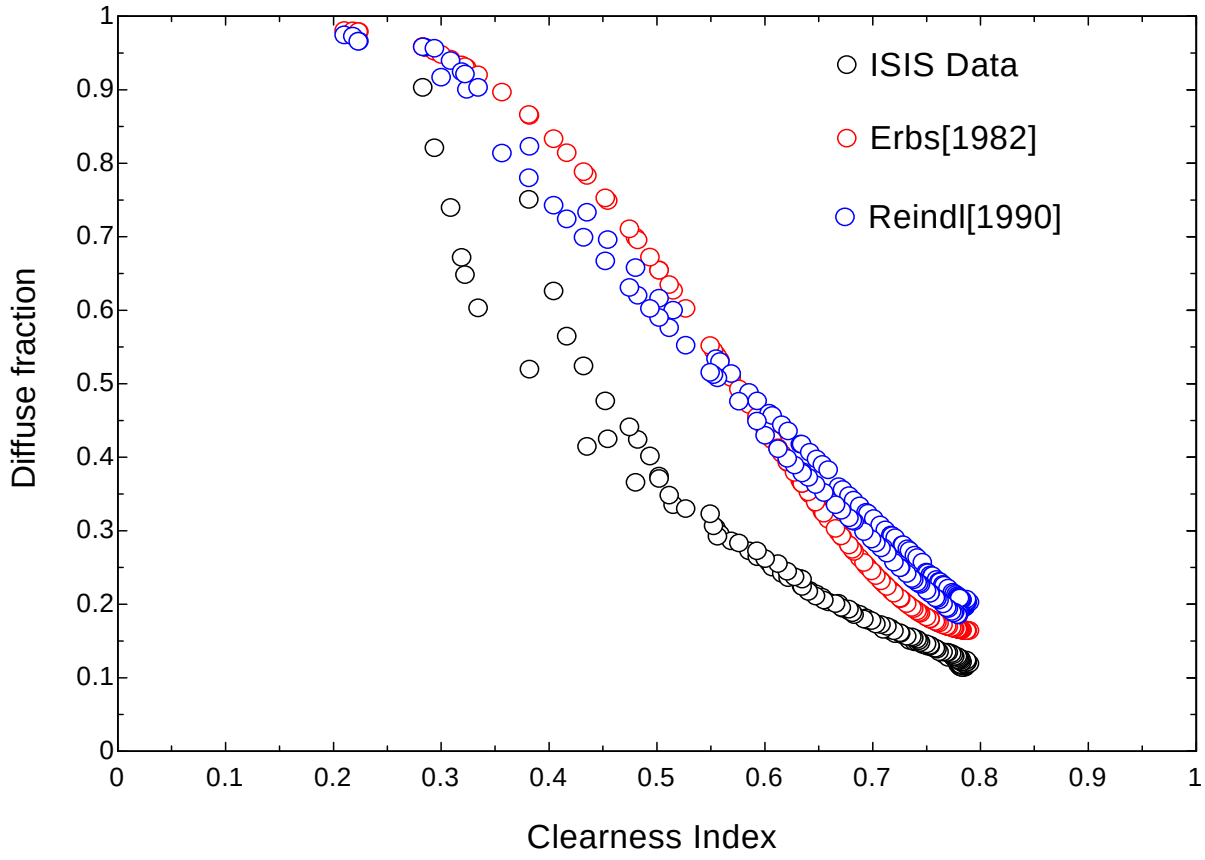

Fig. 3.3: Comparison of diffuse fraction correlations to ISIS data, for January 26, 2003.

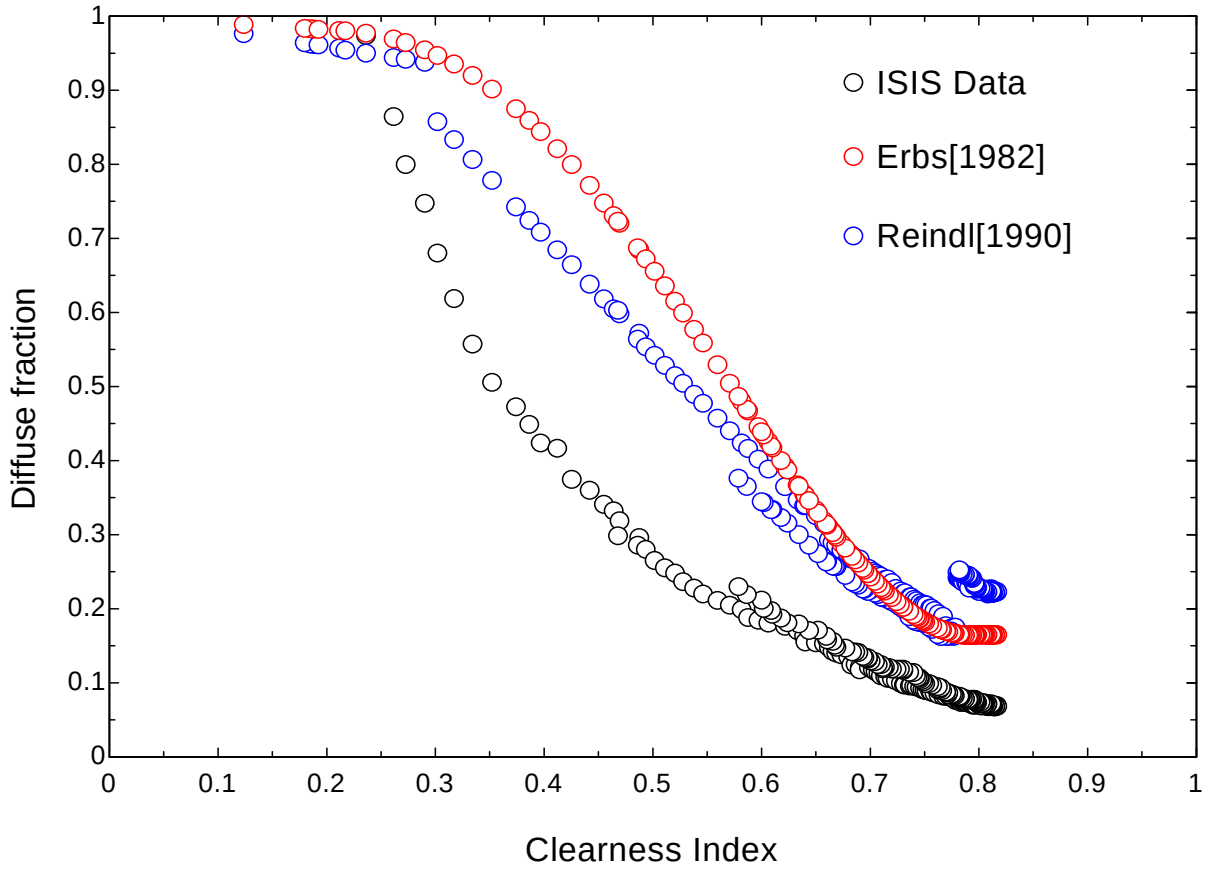

Fig. 3.4: Comparison of diffuse fraction correlations to ISIS data, for July 18, 2003.

Figure 3.5 shows the air mass dependence of diffuse fraction for 3-minute radiation data for June 2002, in Hanford, CA. The dependence on air mass is apparent on clear days, and less so on cloudy and partly cloudy days. This month was selected for its high frequency of perfectly clear days.

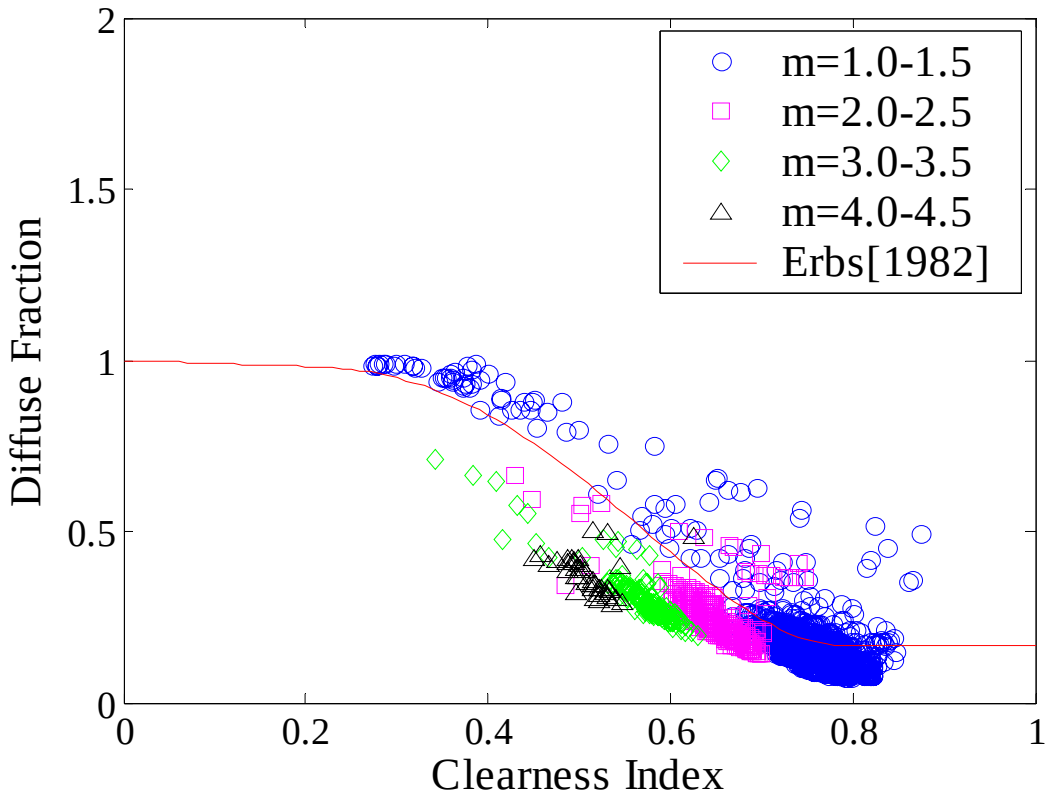

Fig. 3.5: The dependence of diffuse fraction on air mass for June 2002, Hanford, CA.

Another way to demonstrate the influence of air mass on diffuse fraction for clear days is shown in Figures 3.6 and 3.7. Figure 3.6 shows diffuse fraction as a function of air mass for one clear winter day and one clear summer day, for each ISIS station in Albuquerque, Seattle, and Madison. These stations were selected for their varying climates and it appears that the diffuse fraction is affected by the moisture content of the air as well as the ambient temperature as suggested by Gansler and Reindl. Drier climates and winter months appear low in the graph, and wetter climates and warmer months appear higher in the graph.

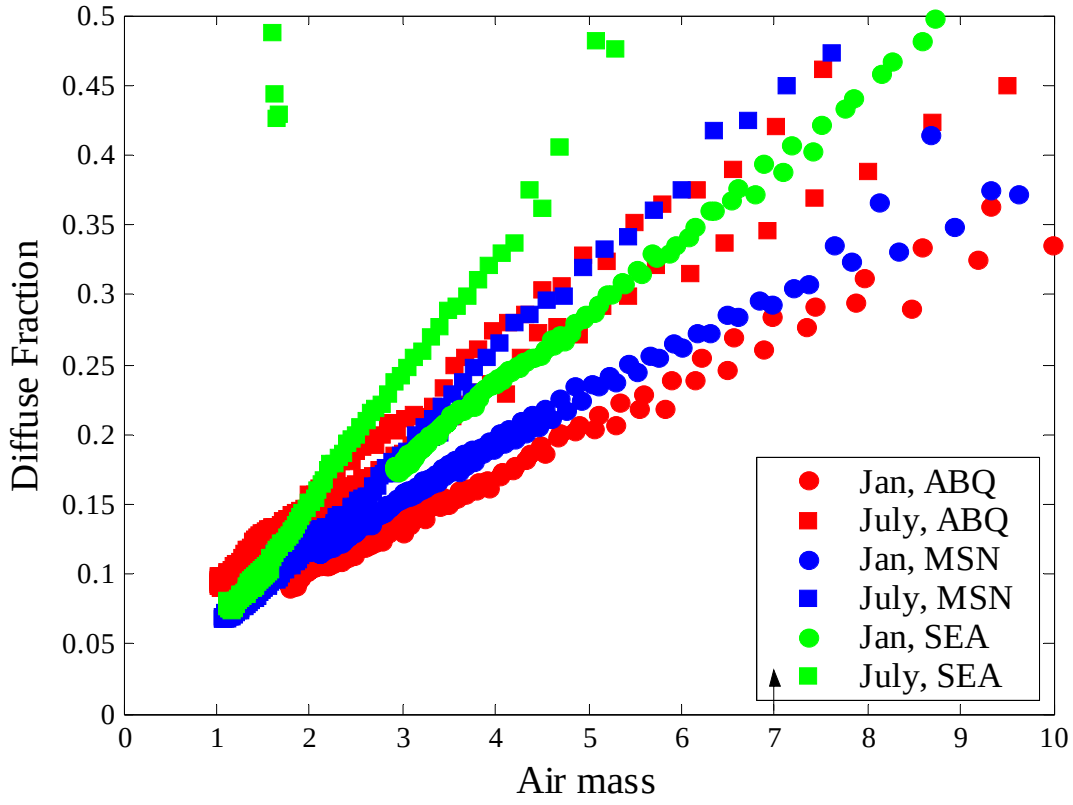

Fig. 3.6: Diffuse fraction as a function of air mass for clear January and July days in Seattle, Albuquerque, and Madison.

Figure 3.7 shows diffuse fraction as a function of air mass for one clear day in September for all eight ISIS stations, noting their latitude. These two figures support the claims that short-term diffuse fraction is dependent on factors other than clearness index. Again, drier locations, such as Albuquerque and Salt Lake City, appear to be less affected by air mass as locations, like Seattle, that have higher relative humidity.

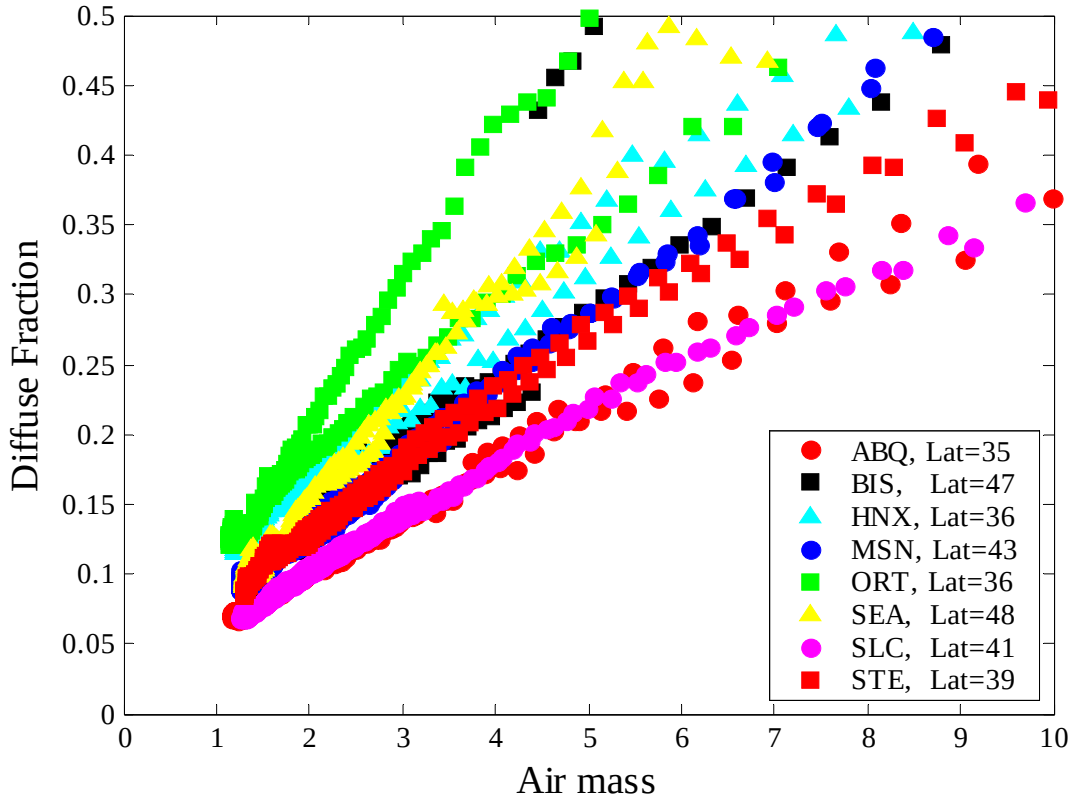

Fig. 3.7: Diffuse fraction as a function of air mass for clear September days in eight ISIS stations.

3.1.2 Distribution of Short-term Solar Radiation

The definition of frequency distributions for short-term radiation is similar to the definition of daily distributions. It is the relative number of cloudy, average and sunny time periods in an hour that together form the hourly average. This distribution is very important in determining the performance of solar energy systems. The distribution can similarly be represented in a non-dimensional manner in terms of the fractional time of occurrence of the 3-minute clearness index, c_T, the ratio of the total radiation to the extraterrestrial radiation for a particular 3-minute time period. The curves developed by Bendt et al. that represent the Liu and Jordan equations for the long-term average distribution of daily clearness index

values as unique functions of $\bar{K}_T$, the monthly daily average clearness index are again used for comparison.

The results from Suehrcke's analysis of 1-minute data in Perth, Australia, showed a strong bimodal distribution that differed greatly from the Bendt et al. distributions. Gansler's results from a similar analysis of 1-minute data in San Antonio, Albany, and Atlanta, also showed significant differences from the Bendt et al. distributions, but not the strong bimodal shape as observed by Suehrcke.

Figure 3.8 shows the cumulative frequency distribution of 3-minute clearness indices for Sterling, VA, for a one year time period. Clearness indices were grouped according to their hourly clearness index for comparison to the Bendt et al. correlation.

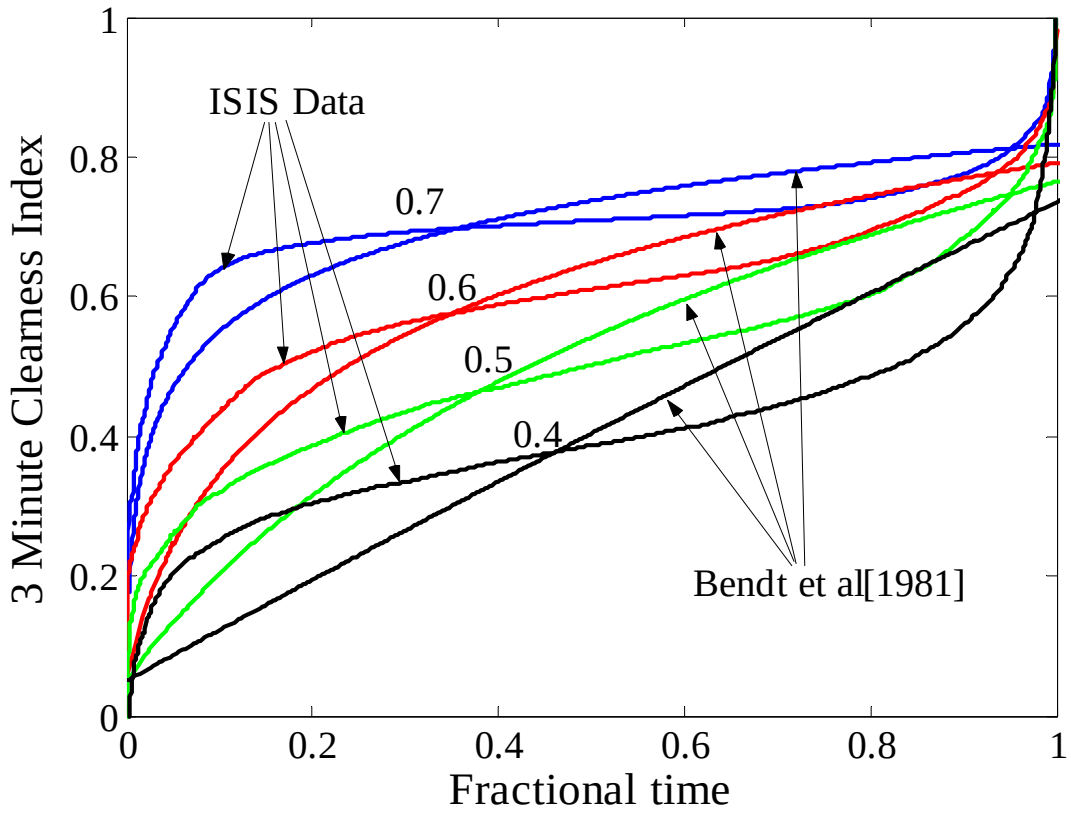

Fig. 3.8: Frequency distribution of 3-minute clearness indices in Sterling, VA, grouped by hourly average.

The behavior seen in Suehrcke's research was not observed in the 8 locations used in this study; however the distributions did vary significantly from Bendt et al. Although the Bendt correlations were developed for daily clearness indices, it had been shown previously by Whillier [1956] that the frequency distribution of hourly clearness indices in a day were a unique function of the daily clearness index, similar to the daily clearness indices being a unique function of the monthly average daily clearness index. Figure 3.9 shows that the equations representing the Bendt et al. distribution of daily clearness indices can be

accurately used with hourly clearness indices. Figure 3.8 shows that these equations do not represent clearness indices based on 3-minute data quite as well.

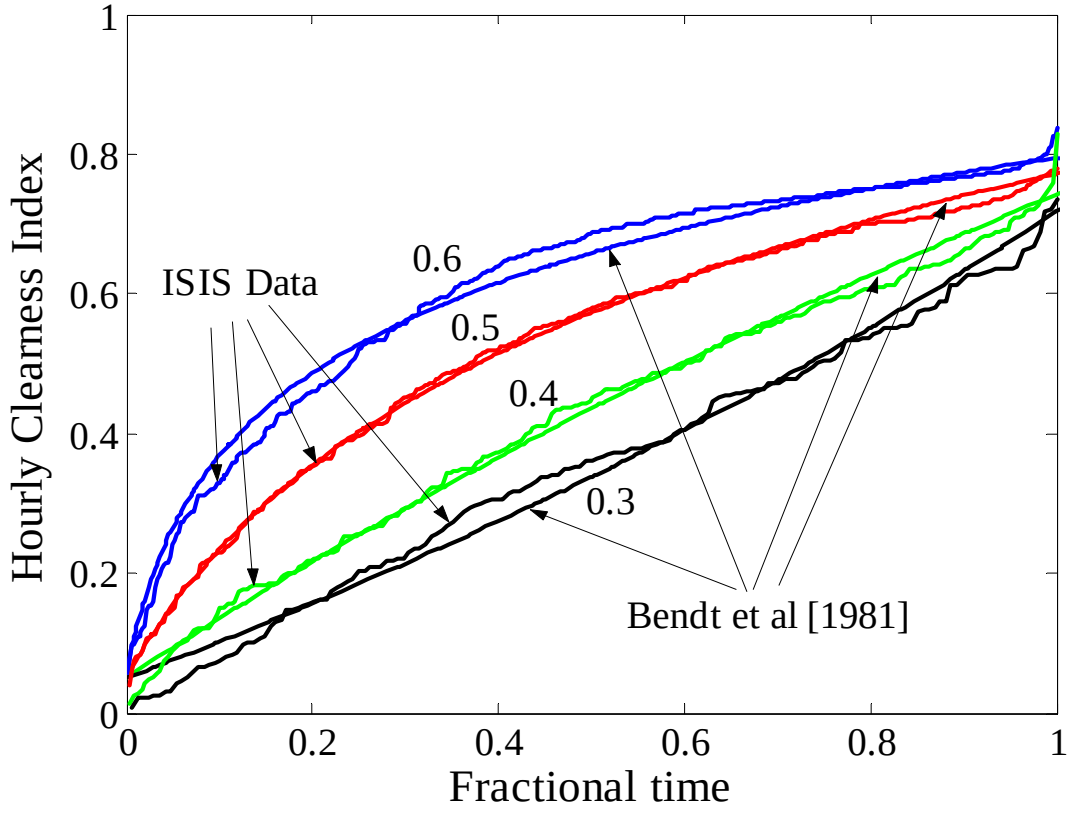

Fig. 3.9: Frequency distribution of hourly clearness indices in Sterling, VA, grouped by daily average.

The air mass dependence of the short-term distribution of solar radiation was also investigated. Figure 3.10 shows the frequency distribution of 3-minute clearness indices for Albuquerque, grouped by hourly clearness index and by air mass.

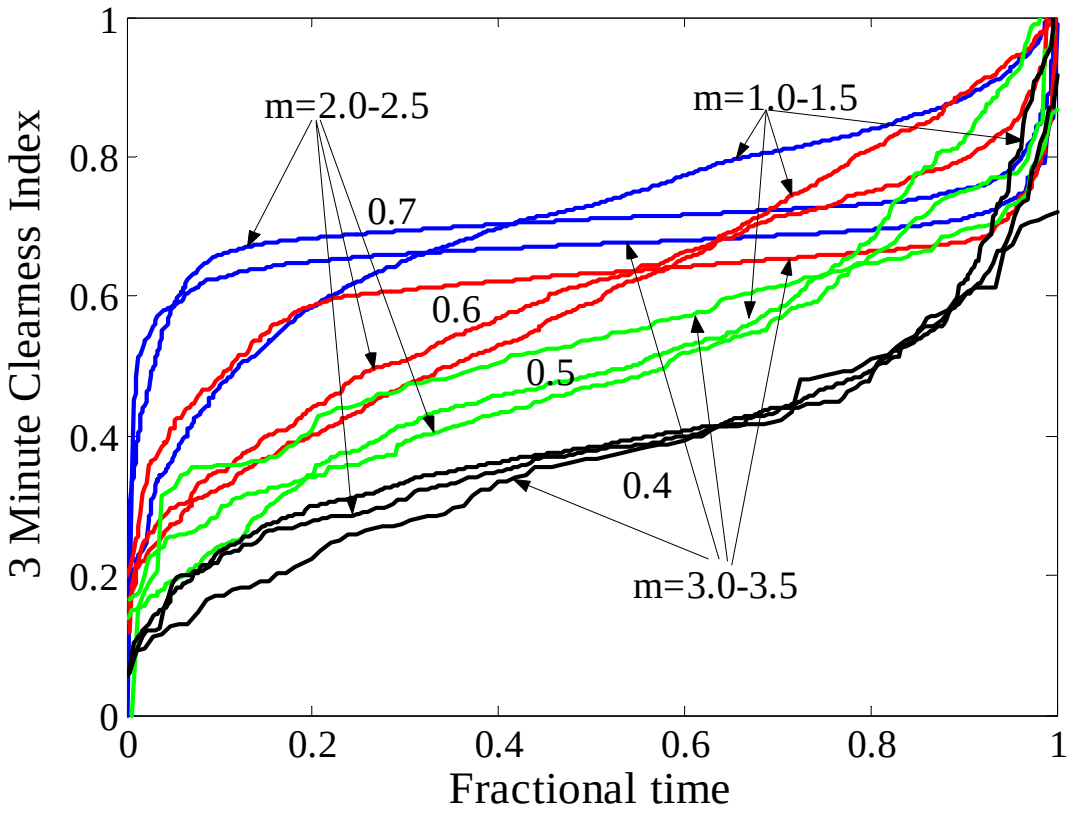

Fig. 3.10: Frequency distribution of 3-minute clearness indices in Albuquerque, NM, grouped by hourly average and air mass, *m*.

The strong air mass dependence, particularly at high air mass values, was observed in all 8 locations and supports Gansler's conclusion that frequency distribution correlations for short-term radiation data should be developed as functions of air mass and hourly clearness index. The development of such correlations would allow locations where short-term data is unavailable to use available hourly averages to predict the distribution of short-term clearness indices. If a diffuse fraction correlation were also developed for short-term data, the diffuse and beam components of the total radiation could also be estimated. If it were not computationally prohibitive, these short-term data could then be used in calculations and

performance analyses. Attempts at such correlations have been made by Gansler [1993], Skartveit and Olseth [1992], and Tovar, Olmo, and Alados-Arboledas [1998]. 3-minute data on ambient temperature and relative humidity would need to be obtained for the ISIS stations in order to accurately develop a correlation for the data in this research.

3.2 Radiation on a Tilted Surface

Calculation of the hourly radiation on a tilted surface, I_T, allows for a quantitative estimate of the impact of using short-term data rather than hourly data. Radiation data on a tilted surface were calculated using the Liu and Jordan [1962] model from Chapter 2 with four methods.

The first two methods apply Equation 2.4 to available 3-minute radiation data to calculate 3-minute radiation on a tilted surface. These tilted radiation values were then summed to create hourly tilted radiation values. The difference between the first two methods is the method of calculation of the beam radiation that is a variable (I_b) in Equation 2.4. M is used here to denote short-term radiation whereas I denotes hourly radiation.

In the first method, beam radiation on the horizontal surface is determined from the available beam normal radiation measurements using geometric relationships (Eqn. 2.6).

Method 1:

$$M_T = (M_{bn} \cdot \cos\theta_z) \cdot R_b + M_d \cdot (\frac{1+\cos\beta}{2}) + M \cdot \rho \cdot (\frac{1-\cos\beta}{2}) \tag{3.3}$$

$$I_T = \sum^{60} M_T \tag{3.4}$$

In the second method, beam radiation on the horizontal surface is calculated as the difference between the measurements of total and diffuse radiation.

Method 2:

$$M_T = (M - M_d) \cdot R_b + M_d \cdot (\frac{1+\cos\beta}{2}) + M \cdot \rho \cdot (\frac{1-\cos\beta}{2}) \quad (3.5)$$

$$I_T = \sum^{60} M_T \quad (3.6)$$

The third method sums the 3-minute total radiation for an hour and then applies the Erbs hourly correlation to the summed hourly values to determine the hourly beam and diffuse components. The Erbs correlation was originally intended to be used in this manner. These values are then used in Equation 2.4 to determine the hourly radiation on the tilted surface.

Method 3:

$$I = \sum^{60} M \quad (3.7)$$

$$\frac{I_{d,Erb}}{I} = f(\frac{I}{I_o}) \quad (3.8)$$

$$I - I_{d,Erb} = I_{b,Erb} \quad (3.9)$$

$$I_T = I_{b,Erb} \cdot R_b + I_{d,Erb} \cdot (\frac{1+\cos\beta}{2}) + I \cdot \rho \cdot (\frac{1-\cos\beta}{2}) \quad (3.10)$$

The final method applies Erbs' hourly correlation directly to the 3-minute radiation data to calculate 3-minute diffuse and beam components. Liu and Jordan's model is then

used to calculate 3-minute radiation on a tilted surface. These 3-minute values are then summed to create hourly tilted radiation values.

Method 4:

$$\frac{M_{d,Erb}}{M} = f(\frac{M}{M_o}) \tag{3.11}$$

$$M - M_{d,Erb} = M_{b,Erb} \tag{3.12}$$

$$M_T = M_{b,Erb} \cdot R_b + M_{d,Erb} \cdot (\frac{1+\cos\beta}{2}) + M \cdot \rho \cdot (\frac{1-\cos\beta}{2}) \tag{3.13}$$

$$I_T = \sum^{60} M_T \tag{3.14}$$

The differences in the results of the four methods are small, although there is a trend that on clear days the available 3-minute data used in the first two methods result in higher values than the Erbs data (Fig. 3.11), and on cloudy days this trend is reversed (Fig. 3.12). Also, the Erbs diffuse correlation appears to work equally well when applied to 3-minute data as when applied to hourly data, as seen in the similarities between methods 3 and 4 in Figures 3.11 and 3.12. Results from the other locations show similar behavior (see Appendix B).

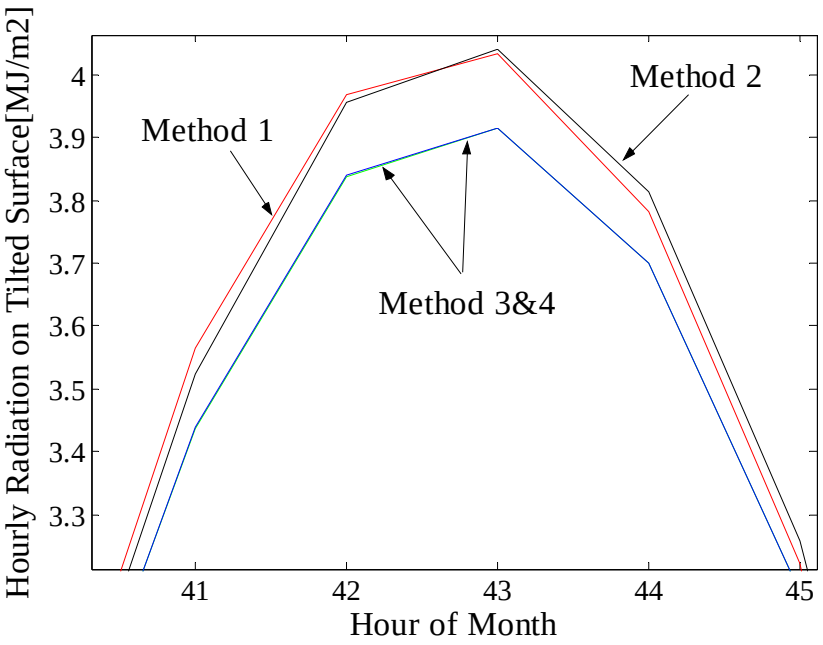

Fig. 3.11: Comparison of 4 methods of calculating hourly tilted radiation for a clear March day in Madison, WI.

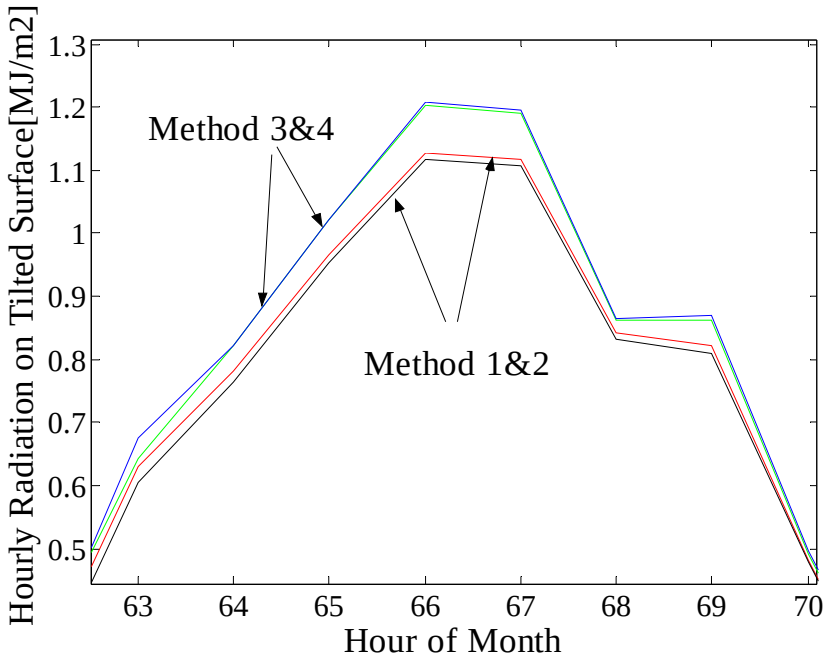

Fig. 3.12: Comparison of 4 methods of calculating hourly tilted radiation for a cloudy March day in Madison, WI.

To quantify this observation, the daily average tilted radiation, $\overline{H_T}$, was calculated for each month and location. Figure 3.13 shows the results using 3-minute data from Madison, WI and Seattle, WA. Some months were not used in the study due to missing data. The results for the other ISIS stations are located in Appendix B. Calculation of the relative difference between the four methods for each month and location does not show one method to consistently exceed any other method in the calculation of radiation on a tilted surface. Of the 42 months studied, Method 2 showed less than ±5% difference from Method 1 in 34 of the months; Method 3 showed less than ±5% difference from Method 1 in 33 of the months; and Method 4 showed less than ±5% difference from Method 1 in 32 of the months.

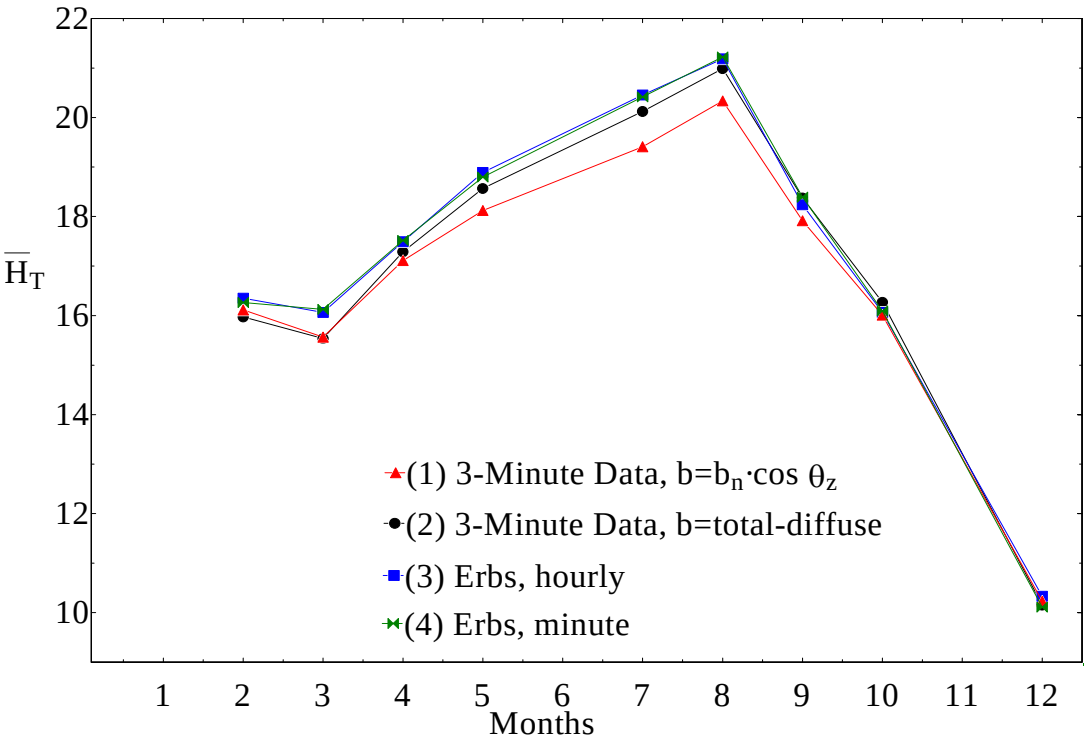

Fig. 3.13a: Comparing 4 methods of calculating monthly average daily tilted radiation from 3-minute data in Madison, WI. Note expanded scale.

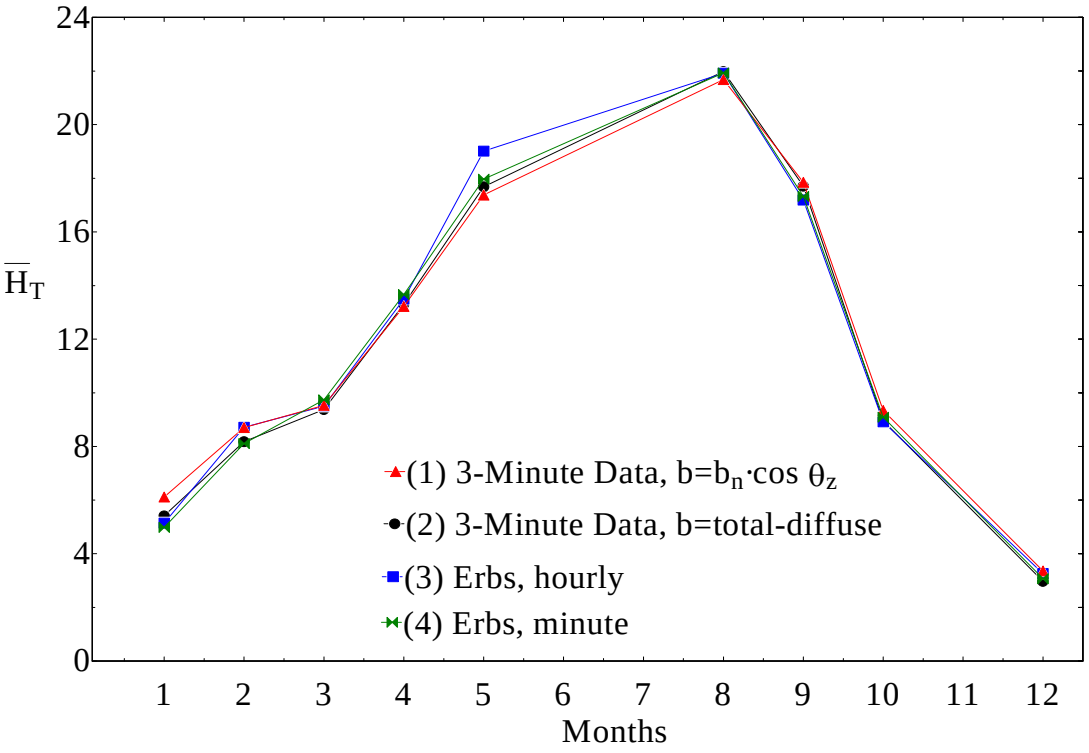

Fig. 3.13b: Comparing 4 methods of calculating monthly average daily tilted radiation from 3-minute data in Seattle, WA.

Because there are so many variables that influence the calculation of radiation on a tilted surface, it becomes difficult to identify the specific impact of using short-term data over hourly data or to make comparisons between using real data and correlated data. In order to simplify the comparison, a utilizability analysis was performed based only on beam normal data to eliminate dependence on other variables.

3.3 Utilizability

The utilizability concept introduced in Chapter 2 can be used to evaluate the performance of many types of solar energy systems, including active, passive and photovoltaic systems. It is defined as the fraction of the solar radiation incident on a surface that exceeds a specified threshold or critical level, I_C. The monthly average daily

utilizability, $\bar{\phi}$, can be calculated if the critical level is assumed constant over all time periods of the day. It is then the fraction of the total solar radiation during a month that exceeds the critical level.

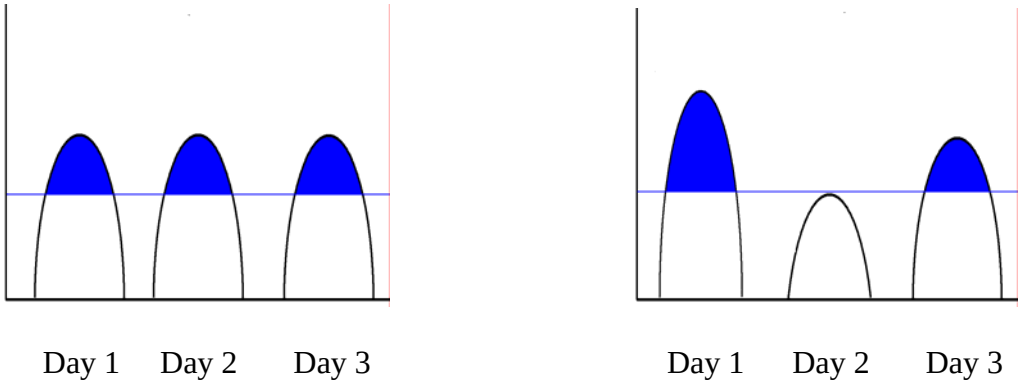

Fig. 3.14: Graphical representation of utilizability.

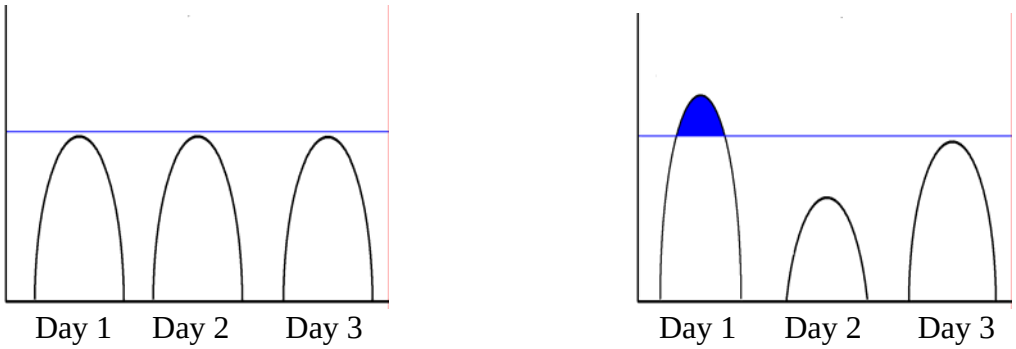

Fig. 3.15: Graphical representation of utilizability with a raised critical level.

The mathematical representation of utilizability is provided in Equation 2.7. An additional summation is required to apply use the 3-minute data to provide utilizability. The graphical representation shows the great influence the distribution of solar radiation has on utilizability. In Figure 3.14, there are two series of days with identical total radiation, but

different distributions. The critical level is represented by the horizontal line. If the critical level is raised, as in Figure 3.15, the utilizability, or the fraction of the shaded area to the whole, decreases. For the first series of days, utilizability drops to zero, whereas the series with variability still has some utilizable energy. This analysis is the same when considering shorter time periods, such as 3-minute intervals. More variability within an hour should result in greater utilizability for the same total radiation.

Utilizability was determined for a range of critical levels by applying critical levels to 3-minute and hourly beam normal radiation values. 3-minute beam normal utilizability was calculated from both measurements of beam normal and from the difference between total and diffuse radiation. In this latter case, both diffuse radiation measurements and the Erbs correlation were used to determine the diffuse fraction and thus the beam normal radiation used in Figure 3.16. Utilizability analyses for these short-term beam normal data were compared to the ISIS 3-minute beam normal data, as shown in Figures 3.16 and 3.17.

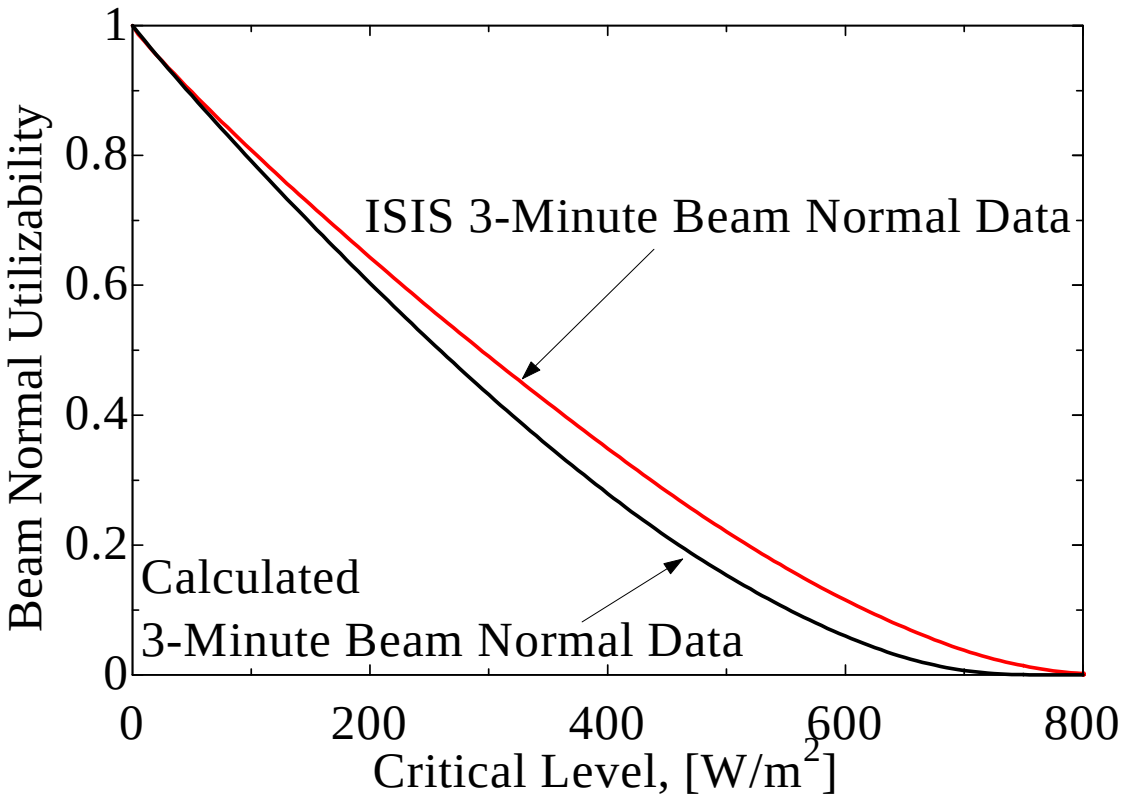

Fig. 3.16: Comparison of average daily beam normal utilizability for January in Seattle for calculated and actual short-term data.

Figure 3.16 shows the discrepancy between using measurements of beam normal and using values calculated from other available data. This difference results from the measurements being taken with independent instruments. The magnitude of this difference varies by location, and months where the calculated data results in greater utilizability were also observed.

Currently, performance analyses in locations where limited data are available use hourly diffuse fraction correlations to determine diffuse and beam radiation from the available total. Figure 3.14 and 3.15 show how such analyses can greatly underestimate the true performance of a system.

Applying the Erbs diffuse correlation to 3-minute data for this month and location significantly underestimates utilizability, as seen in Figure 3.14 for January in Seattle.

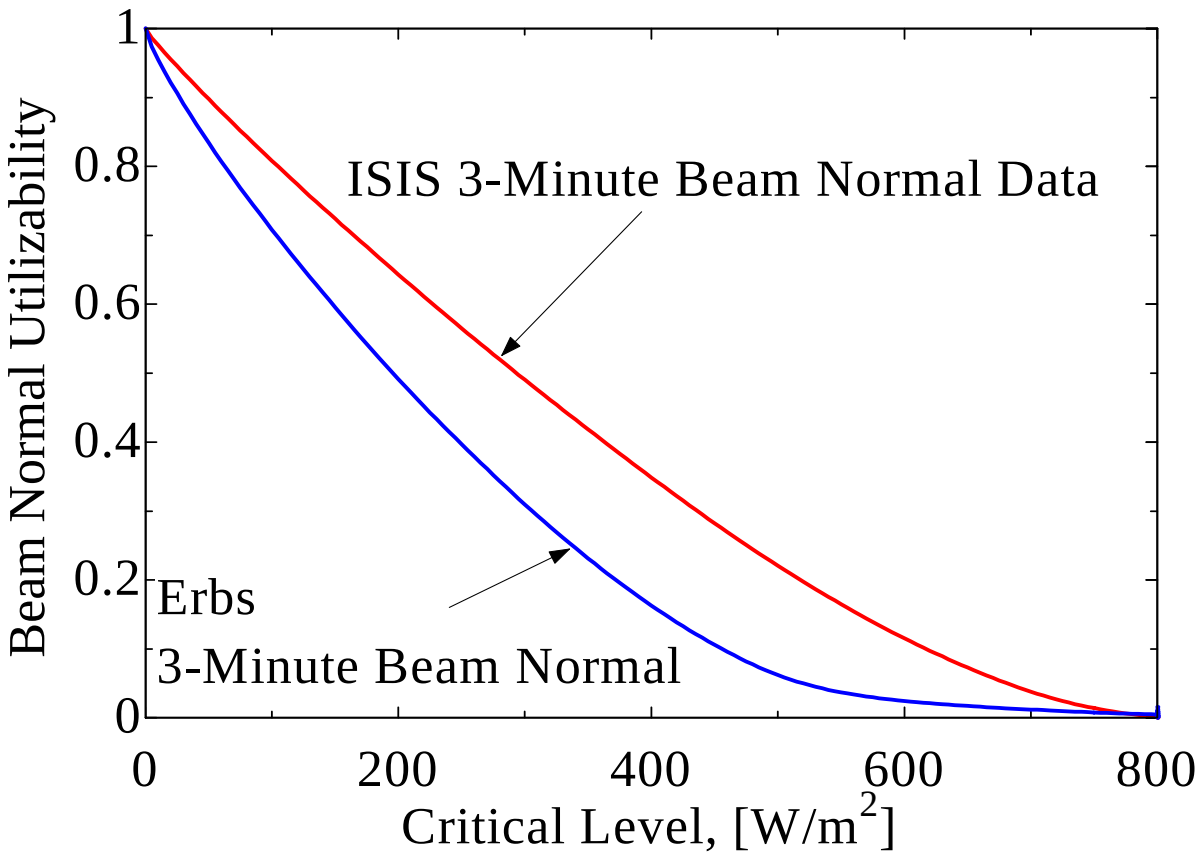

Fig. 3.17: Comparison of average daily beam normal utilizability for January in Seattle for actual and correlated short-term data.

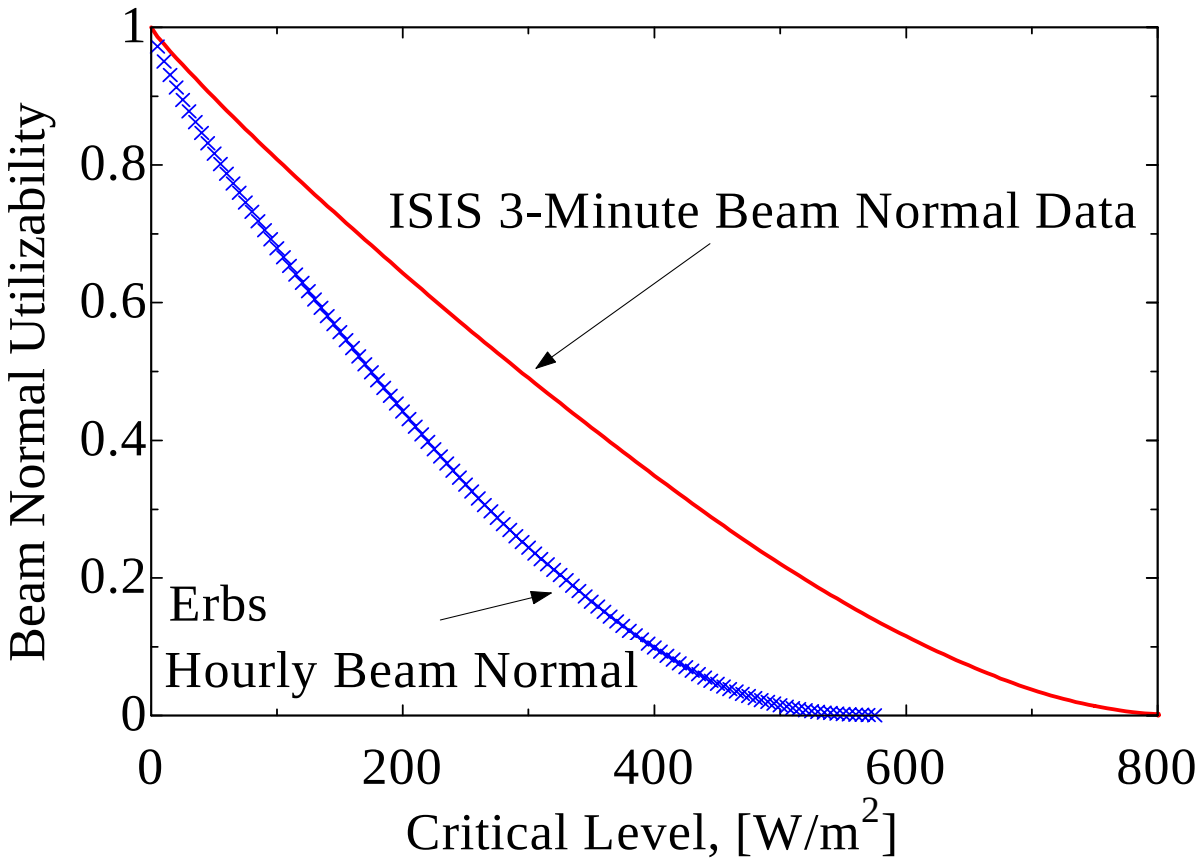

Fig. 3.18: Comparison of average daily beam normal utilizability for January in Seattle for actual short-term data and hourly correlated data.

In Figure 3.18 the Erbs correlation is applied to hourly data, as is more commonly done. This option also usually resulted in an underestimate of utilizability but there were months and locations where the Erbs correlation resulted in an overestimate of the utilizability. Over and under estimation of utilizability occurs because the Erbs correlation can both underestimate and overestimate the amount of beam radiation, depending on the type of day, as seen in Figure 3.1. The distribution of days, therefore, greatly influences the results of the utilizability analyses.

The argument for using short-term radiation data rather than hourly data is apparent in Figure 3.19. Variations in beam normal radiation during an hour can lead to greater utilizability than would be indicated in an analysis using hourly data. This result was found consistently among all months and all locations, although the magnitude of the underestimation varied from 1% to 50% depending on the location and critical level (see Appendix B for beam normal utilizability analyses from other ISIS stations).

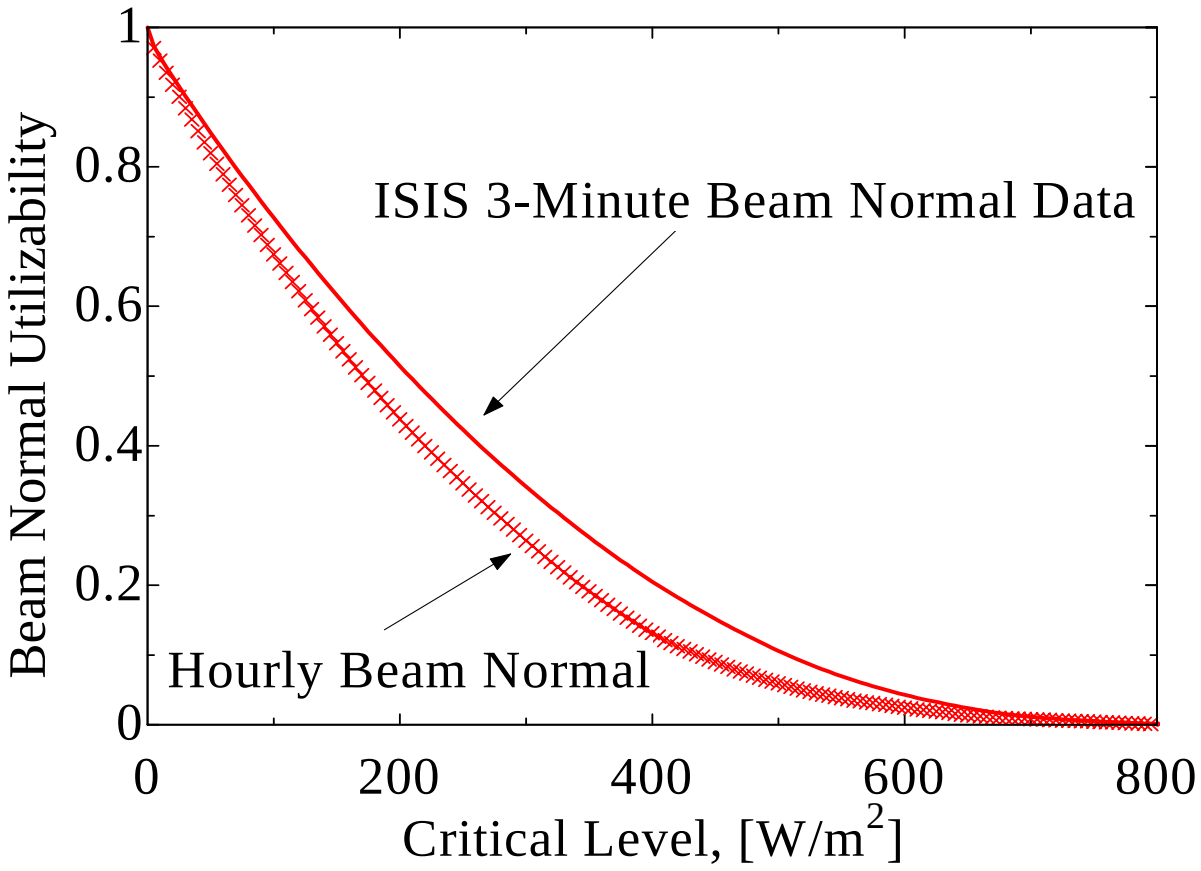

Fig. 3.19: Comparison of average daily beam normal utilizability for January in Hanford for short-term data and hourly data.

CHAPTER 4. 1-Minute Radiation

The previous chapter provided an analysis of short-term solar radiation data on the order of 3-minute intervals. 1-minute solar radiation data for one ISIS station (Madison, WI) were made available to us for the research in this Chapter.

Fig. 4.1: ISIS instruments in Madison, WI.

4.1 Analysis of Data

Similar to the analysis in Chapter 3, the diffuse fraction and frequency distribution of the ISIS 1-minute data were investigated. Similar relationships were observed when comparing either interval of short-term radiation data to hourly data.

4.1.1 Diffuse Fraction

Similar to Figure 3.1, Figure 4.2 shows the diffuse fraction for a single month in Madison, now based upon 1-minute diffuse fractions as functions of 1-minute clearness indices. Figure 4.3 shows how this data would collapse into an hourly diffuse fraction as a function of hourly clearness indices, similar to those seen in Chapter 2.

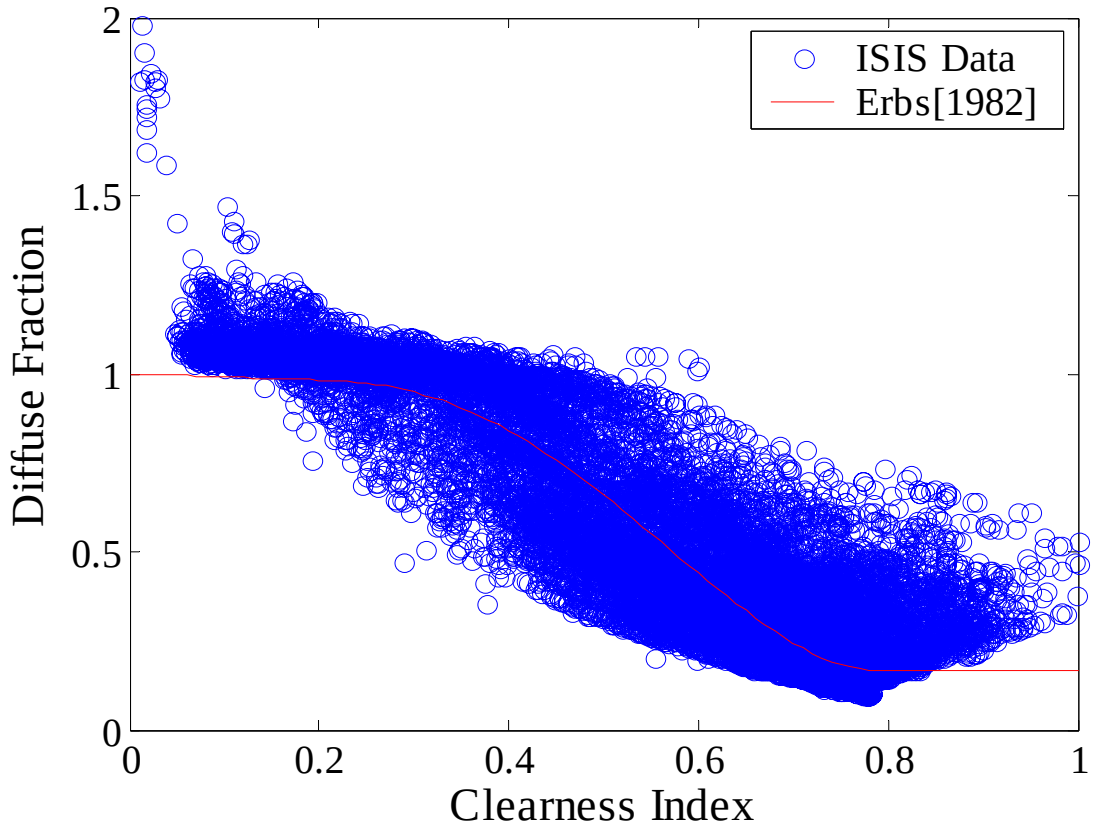

Fig. 4.2: One minute diffuse fraction as a function of clearness index for August 2003, in Madison, WI.

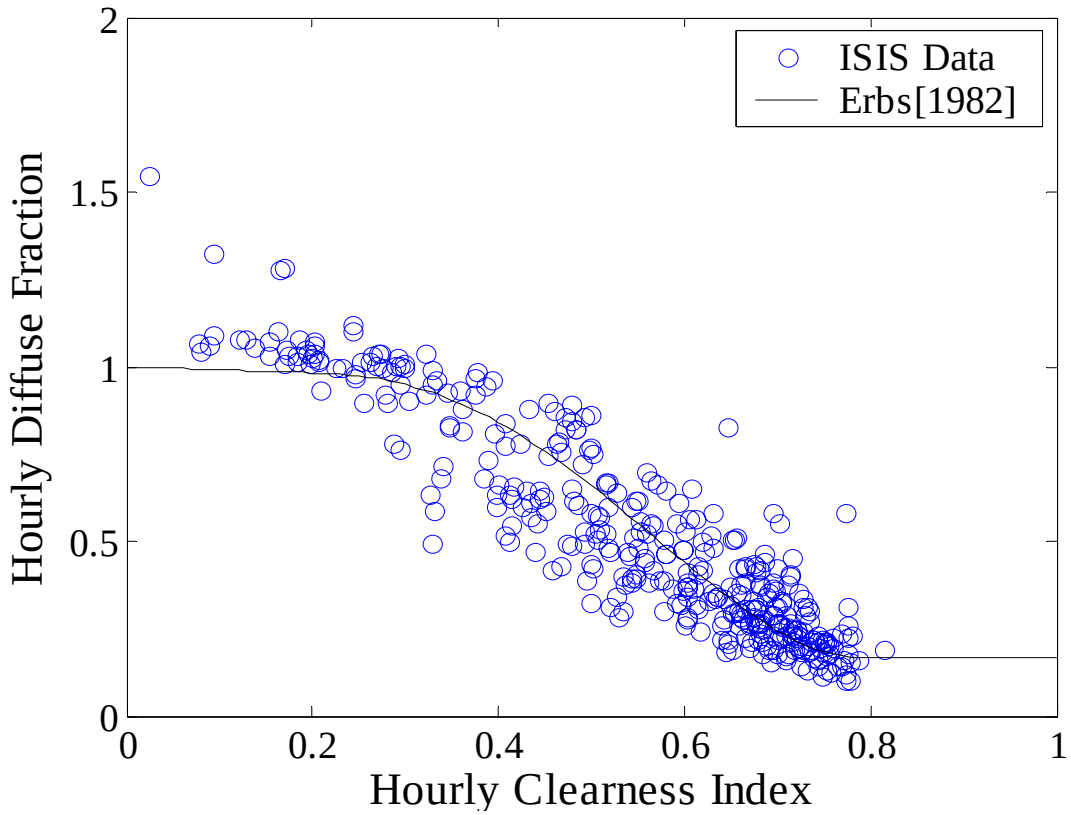

Fig. 4.3: Hourly diffuse fraction as a function of clearness index for August 2003, in Madison, WI.

Figure 4.4 shows for a series of days in April in Madison, ISIS 1-minute data for total, diffuse and beam normal radiation. The three days respectively represent a cloudy, partly cloudy and clear day. On a cloudy day, total solar radiation is low and diffuse and total measurements are approximately equal. Beam normal radiation is non-existent. On a clear day, diffuse radiation is low, and beam normal can exceed the total radiation. The partly cloudy day consists of fully cloudy morning hours, followed by partly cloudy hours, followed by perfectly clear afternoon hours.

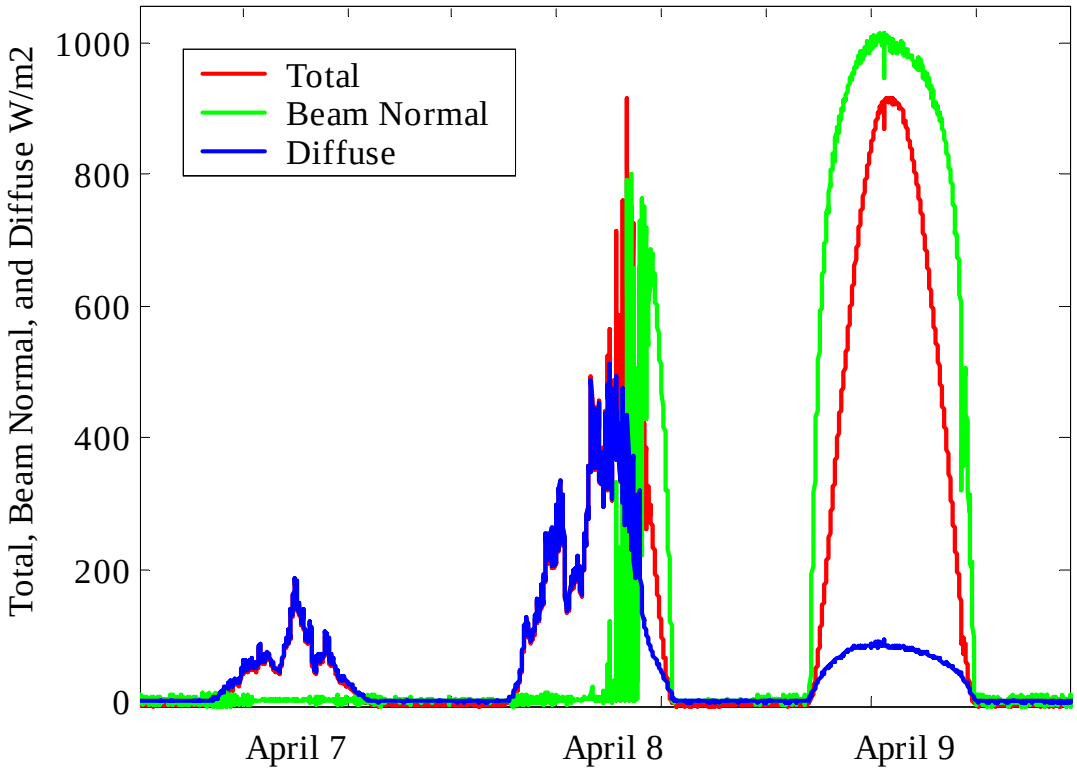

Fig. 4.4: ISIS data for consecutive April days, representative of a cloudy, partly cloudy, and clear day.

The diffuse fraction for this series of days in April in Madison is shown in Figure 4.5. As expected, cloudy time periods are consistently shown to result in low clearness indices and high diffuse fractions, and clear time periods are shown to result in higher clearness indices and lower diffuse fractions. During the hours of mixed sunshine and clouds, the diffuse fraction shows significant scattering, with behavior that is markedly different from perfectly clear or cloudy time periods.

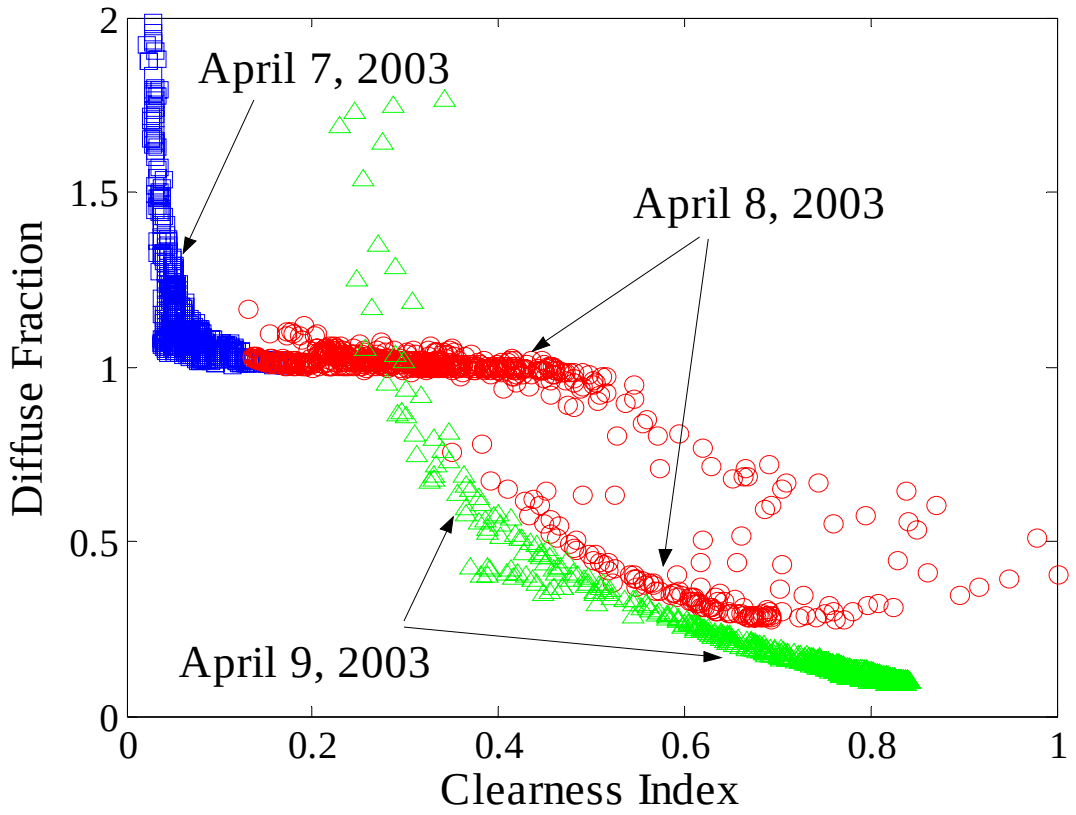

Fig. 4.5: One-minute diffuse fraction as a function of one-minute clearness indices for the three consecutive days in April shown in Figure 4.4.

Closer inspection of the cloudy day shows that the erroneous values where diffuse fraction exceeds one are during early morning and late evening (Fig. 4.6). Similar to the TMY2 analysis in Chapter 2, this can be reasonably attributed to independent measurements and instrument error at these times. Figure 4.7 shows the time dependence of the minute diffuse fraction for a perfectly clear day, which is similar to the relationship observed in Chapter 3 with the 3-minute data. Plots for other months are located in Appendix C.

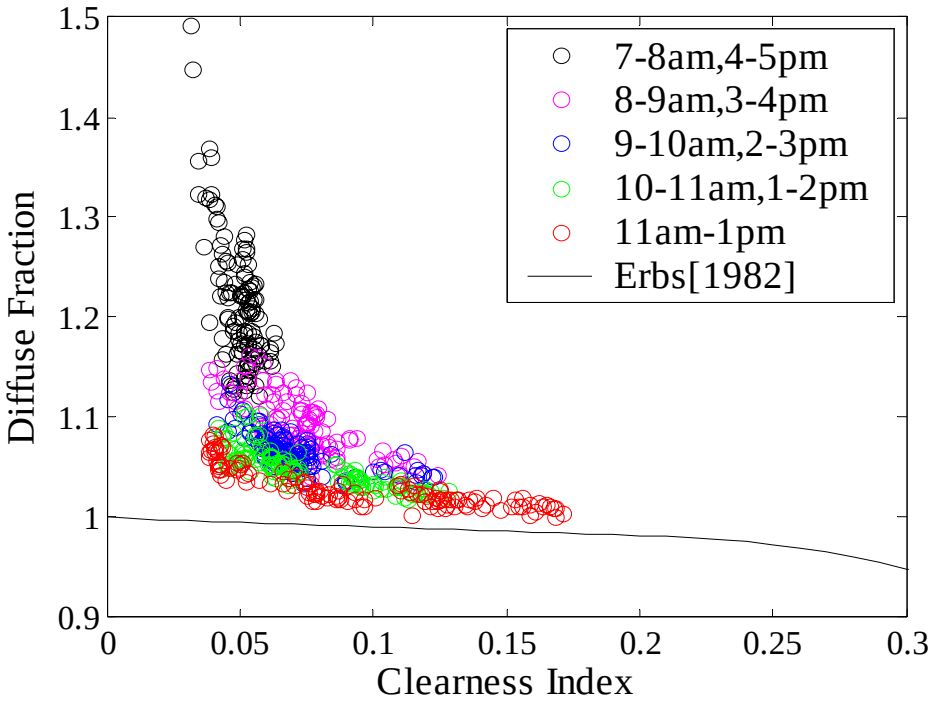

Fig. 4.6: One-minute diffuse fraction as a function of one-minute clearness indices for a cloudy April day. Note expanded scale.

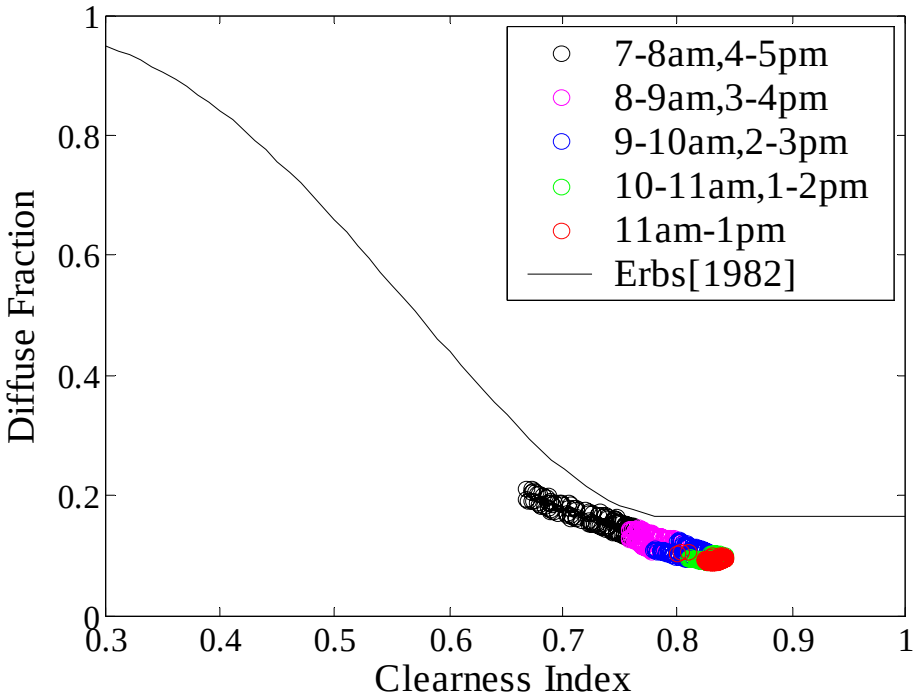

Fig. 4.7: One-minute diffuse fraction as a function of one-minute clearness indices for a clear April day.

The dependence of diffuse fraction on air mass is related to its time dependence. High zenith angles indicate early morning or late evening hours. High zenith angles also correlate to a high air mass. Figure 3.3 is similar to Figure 4.7 in the way that clearness index increases with decreasing air mass and decreasing zenith angle (approaching noon).

4.1.2 Distribution of Short-term Solar Radiation

Figure 4.8 shows the cumulative frequency distribution of 1-minute clearness indices for Madison for a one month time period. The monthly average minute clearness index was calculated in order to compare the real frequency distribution to the Bendt et al. distribution.

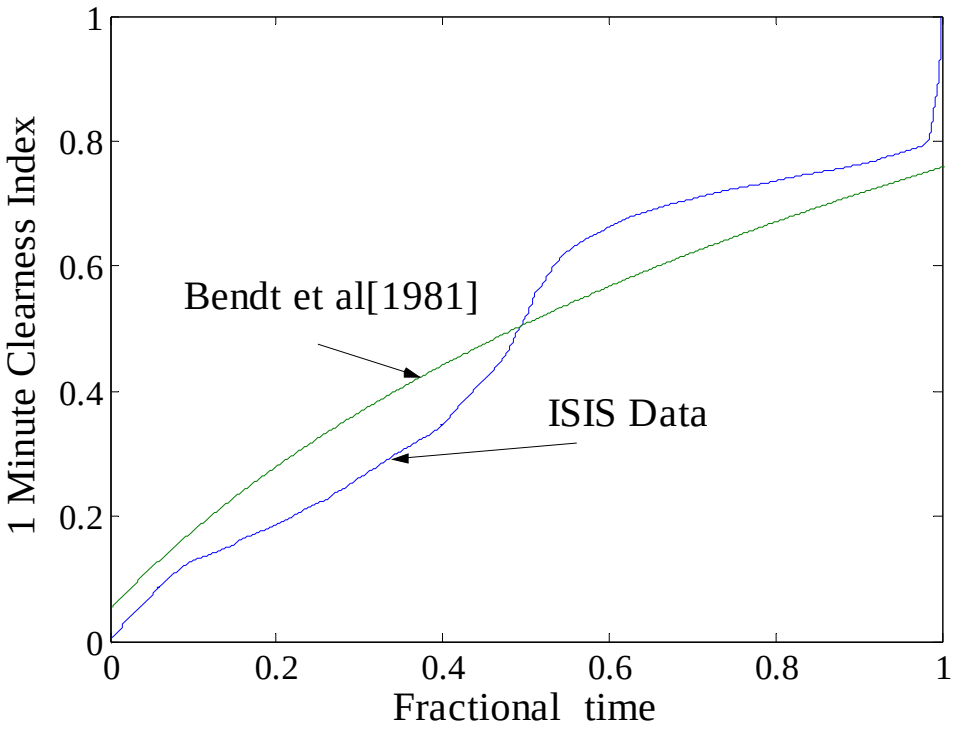

Fig. 4.8: Frequency distribution of 1-minute clearness indices in December in Madison, WI.

Similar to the results from Chapter 3, given the same monthly average as the ISIS data, the Bendt et al. equations cannot accurately predict the distribution of cloudy and clear minutes

within a month. The ISIS data does look similar to the data used in Suehrcke's [1988] research of 1-minute radiation in Perth, Australia, reaffirming that short-term radiation has a markedly different frequency distribution than hourly or daily radiation.

4.2 Radiation on a Tilted Surface

Hourly radiation on a tilted surface, I_T, is again calculated to obtain a quantitative estimate of the impact of using 1-minute data rather than hourly data. Application of the Liu and Jordan model in the four methods described in Chapter 3 is repeated here for 1-minute data. Table 4.1 shows the results using 1-minute data from Madison. Due to problems in the data, certain months were not used in this analysis.

TABLE 4.1: MONTHLY AVERAGE DAILY TILTED RADIATION $\overline{H}_T$

Month	Madison			
	Method 1	Method 2	Method 3	Method 4
January	11.6	11.6	11.8	11.9
February	15.8	16.1	16.5	16.6
March	15.3	15.6	16.1	16.3
April	17.0	17.3	17.5	17.6
May	N/A	N/A	N/A	N/A
June	18.4	20.3	20.6	20.6
July	19.4	20.1	20.4	20.4
August	20.3	20.9	21.0	21.2
September	17.7	18.3	18.1	18.4
October	N/A	N/A	N/A	N/A
November	10.1	10.2	10.4	10.7
December	10.2	10.2	10.2	10.2

Large differences are not observed between the four methods; however, Method 4 does consistently appear to result in the highest monthly average for radiation on a tilted surface. Method 4 used Erbs' correlation to predict 1-minute values of beam and diffuse, given only the total radiation for one minute.

By calculating radiation on a tilted surface, various factors, such as location, slope, ground reflectance, and model selection (Liu and Jordan, Hay and Davies, etc), were being introduced that were perhaps clouding the comparison. In order to simplify the comparison between using actual data and using correlated data, calculations of just the hourly beam normal value were made.

The available 1-minute data were summed for an hour and compared to the hourly beam normal data that were predicted by applying Erbs' correlation to hourly totals. Figure 4.9 shows the comparison for the month of April in Madison. The small 'x' data points represent morning hours, while the round 'o' data points represent afternoon hours. The comparison for one month of data does not provide much information on how well the correlation works.

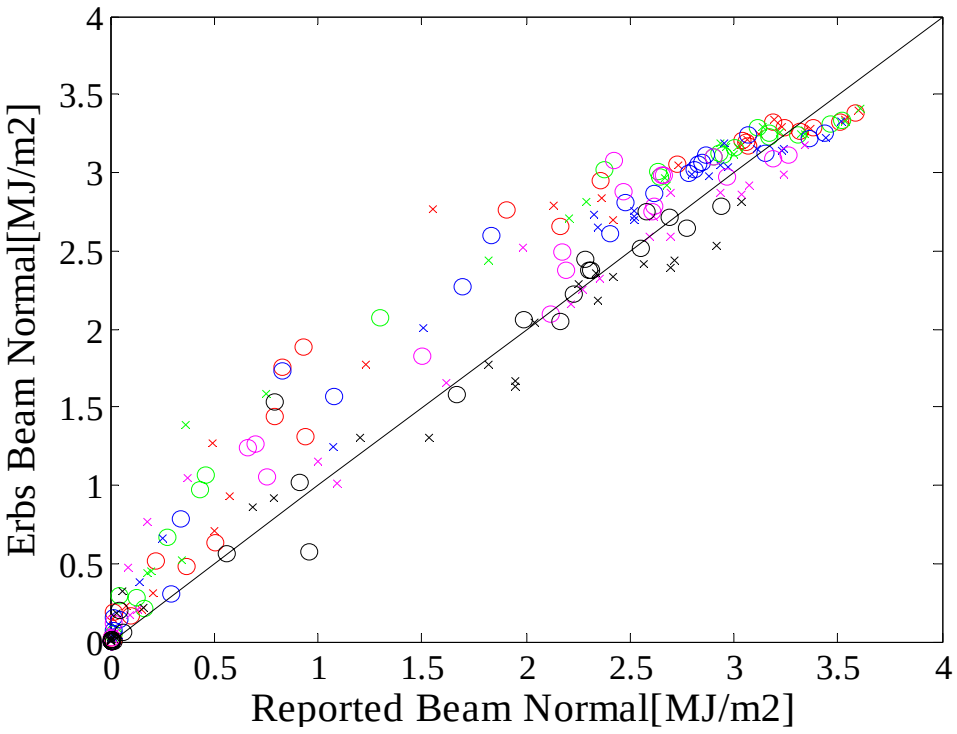

Fig. 4.9: Hourly comparison of ISIS beam normal data to estimated beam normal data using Erbs' correlation for the month of April.

From Figure 4.9 alone, it is hard to determine the impact of using the diffuse fraction correlation to calculate beam normal data. In a one-month period, consisting of clear days, cloudy days and days of variable cloudiness, beam normal values can be overestimated or underestimated by using Erbs' hourly correlation. Figure 4.10 shows the comparison for a clear day in April. In this figure, in addition to applying Erbs' correlation to hourly totals, Erbs' correlation has been applied to minute data and those values were then summed to create hours of beam normal data. These data points are represented by the small '•' and '+' data points. It is clear that beam normal data is consistently underestimated when using Erbs' correlation to predict the components of total radiation. This conclusion will certainly affect the predicted performance of solar energy systems that require tracking devices that only utilize the beam normal component of radiation.

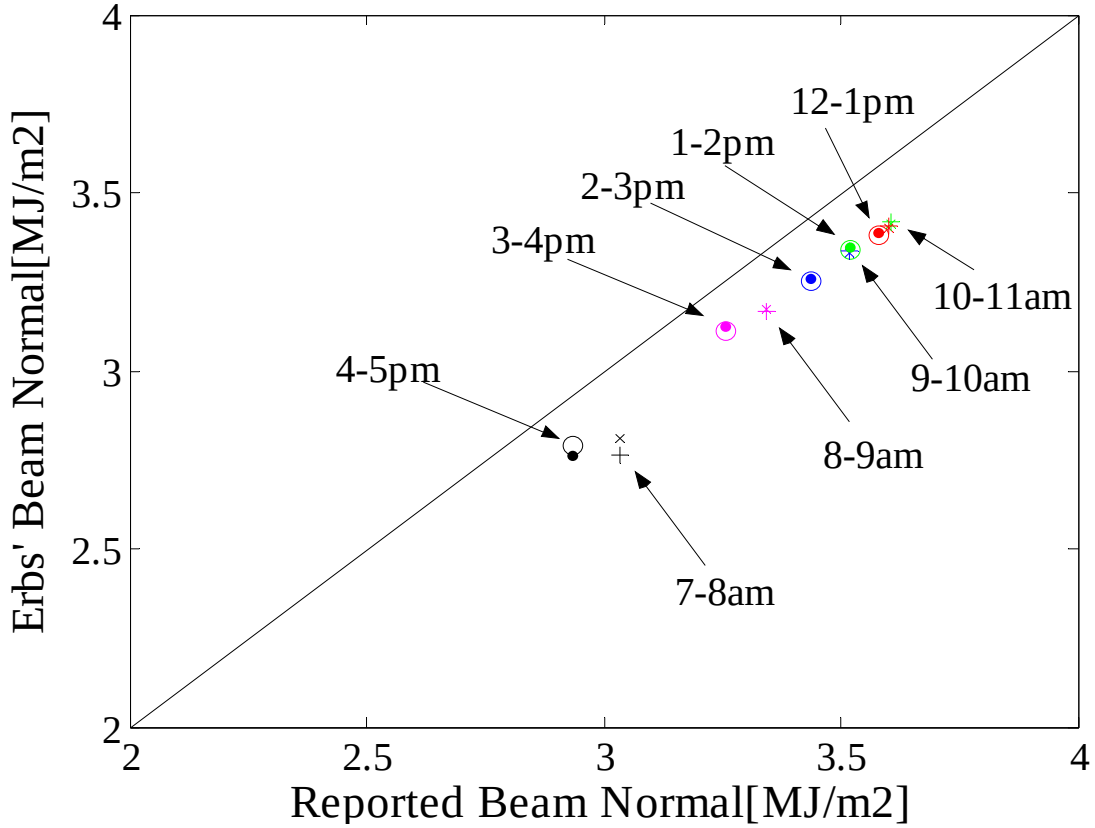

Fig. 4.10: Hourly comparison of ISIS beam normal data to estimated beam normal data using Erbs' correlation for a clear day in April.

4.3 Utilizability

Two important comparisons are being made regarding estimated performance of solar energy systems. The first comparison is whether existing diffuse fraction correlations can be used in conjunction with available data to provide accurate results. The second comparison is between using 1-minute or short-term data instead of the traditional hourly data sets. Figure 4.11 shows the comparison between using correlated data and available data for a beam normal utilizability analysis in September in Madison. If all the days in September had been perfectly clear, the magnitude of the underestimation of utilizability by using the

correlation would have been more pronounced. However, since there are other cloudy and partly cloudy days during the month where Erbs' correlation will overestimate utilizability, the difference is diminished. There are months where using Erbs hourly data results in higher utilizability than when using actual data.

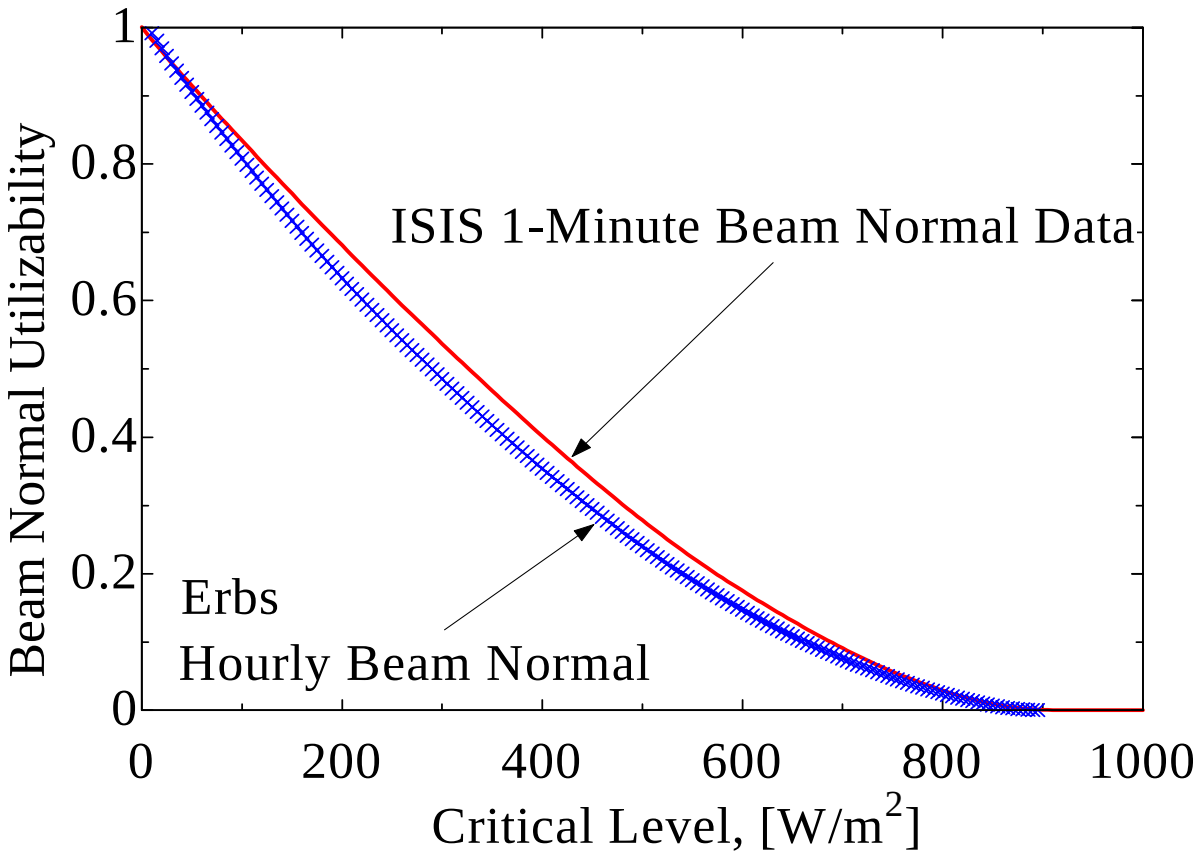

Fig. 4.11: Comparison of average daily beam normal utilizability for September in Madison for actual 1-minute data and hourly correlated data.

The one comparison that can be demonstrated very clearly is the underestimation of utilizability when using hourly data instead of 1-minute data. Because the distribution of radiation within an hour can vary, assuming a constant value for the entire hour underestimates the utilizable energy, as shown in Figure 4.12. Assume that the average radiation over the hour is exactly equal to the critical level shown and that the sum of the

minute radiation yields the same as the hourly radiation. Since utilizability is the fraction of energy above a constant critical level, using short-term data takes advantage of the variations within an hour and consistently results in greater utilizability than using the hourly data (Fig. 4.13).

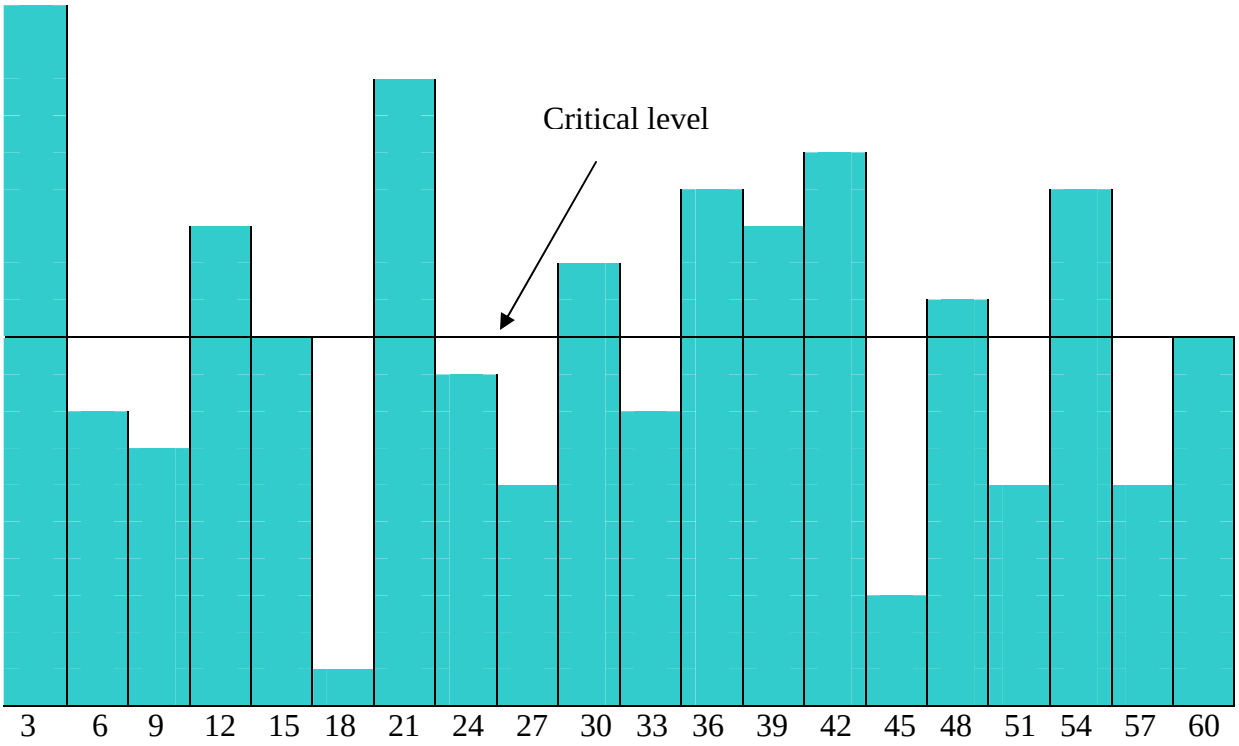

Fig. 4.12: Distribution of 3-minute solar radiation.

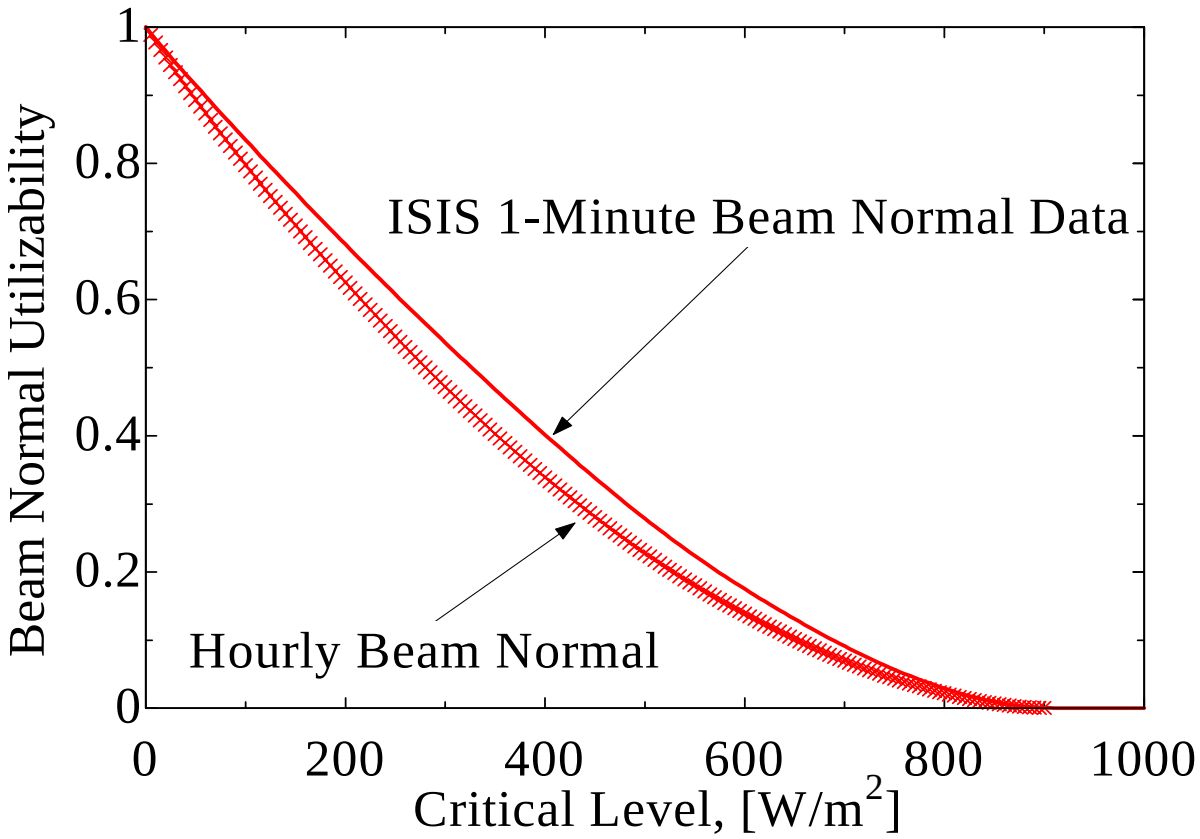

Fig. 4.13: Comparison of average daily beam normal utilizability for September in Madison for 1-minute data and hourly data.

4.4 Assessment of Short-term Radiation Data

The system-independent analyses presented here confirm that the variations in solar radiation within an hour cannot be ignored when conducting performance analyses of solar energy systems. The distribution of 1-minute and 3-minute radiation are not described well by current correlations and the use of short-term data results in greater utilizability, if the minute data vary significantly from each other as during partly cloudy periods. On a clear day when the variation within the hour is minimal, the magnitude of the difference decreases.

CHAPTER 5. Conclusions

Chapter 2 explores the inconsistencies that were found to exist within TMY2 data and the impact they have on studies of solar system performance. TMY2 data were analyzed for six locations and showed inconsistencies such as diffuse fractions that exceeded one for modeled data and during hours unaffected by sunrise or sunset, calibration errors, and discrepancies between instrument measurements. However, overall, they agree reasonably well with the long-term average distribution of daily radiation on a monthly basis as well as long-term average monthly radiation.

The concept of utilizability was applied to determine the impact of the inconsistencies on performance of solar energy systems. Energy above a certain threshold that is 'utilizable' is an efficient indicator of performance that can be applied to a range of solar energy systems. Utilizability is dependent on many factors, including the threshold level of the system and the frequency distribution of daily solar radiation. Depending on threshold level, utilizability can be considerably different simply based on which TMY2 data elements are used in the calculations.

TMY2 data could be improved by eliminating obvious inconsistencies in reported data, particularly in the diffuse fractions. However, TMY2 data showed reasonably good correlation with Bendt generalized distribution for daily solar radiation and an analysis of long-term data demonstrated that the distributions of solar radiation represented in the TMY2 database appropriately represented the actual long-term distribution. Based on the results of the six locations considered in this study, the TMY2 data provide a reasonably good approximation of long-term data.

The analyses presented in Chapters 3 and 4 demonstrate that existing diffuse fraction correlations and frequency distribution curves may not adequately describe short-term radiation. The diffuse fraction on clear days when the radiation incident on a solar collector is most significant is overestimated by using Erbs' and Reindl's correlation and the distribution of short-term solar radiation does not agree with the Bendt distribution curves commonly used for hourly and daily data.

The analyses in these chapters also confirm that the short-term variations in solar radiation cannot be considered negligible when estimating the performance of solar energy systems. The distribution of short-term radiation within an hour consistently results in greater utilizability than when the radiation is assumed to be constant throughout the hour. On a clear day when the variation within the hour is minimal, the magnitude of the difference decreases. On a partly cloudy day when large variations exist within the hour, hourly analyses will underestimate the true performance of a system.

It is inadequate to apply existing correlations developed for hourly and daily data to short-term data. When available and practical to use, actual short-term radiation data should be used in simulation studies. If hourly or short-term diffuse or beam data are unavailable and correlations are needed to generate them, diffuse fraction correlations, such as Reindl's, that incorporate a dependence on temperature, solar altitude, and relative humidity should be used rather than those based solely on clearness index. If only hourly radiation data is available, the Skartveith and Olseth model could be used to generate short-term distributions until better correlations are developed.

Future work should include the development of new diffuse fraction correlations and frequency distributions of short-term data as functions of air mass, ambient temperature,

relative humidity and other influential, yet available, parameters. There has been some research recently in the development of these types of correlations as noted in Chapter 1. However, the data available for this development is limited. The Skartveit and Olseth [1992] model is based only on data from 3 stations and does not include dependence on meteorological elements. The functions developed by Tovar, Olmo, and Alados-Arboledas [1998] are conditioned to air mass, but are based on data from just one station in southeastern Spain. An adequate number of stations representing both temperate and tropical climates that provide reliable records of short-term solar radiation and meteorological data are needed for the proper and accurate development of these correlations. The ISIS stations represent different North American climates, however exclude a tropical climate and do not provide the relevant short-term meteorological data needed to develop a correlation from the data used in this research.

If developed, they would allow users the ability to accurately generate short-term data from commonly available hourly averages. These short-term data could then be used in simulations and performance analyses of solar energy systems, if it is not computationally prohibitive to do so.

Appendix A:TMY2 Data (see CD for complete figures from all six stations studied)

I. Distribution of Daily Solar Radiation(72 figures, by month and by location)
II. TMY2 Diffuse Fraction(6 figures, a typical year's data, by location)
III. Monthly Average Daily Utilizability, TMY2 vs 30 yr(24 figures, by month)
IV. Monthly Average Daily Utilizability, TMY2 vs Erbs(24 figures, by month)

I. Distribution of Daily Solar Radiation

A.1: TMY2 Frequency Distribution for January, Madison, WI
A.2: TMY2 Frequency Distribution for January, Seattle, WA
A.3: TMY2 Frequency Distribution for January, Albuquerque, NM
A.4: TMY2 Frequency Distribution for January, Miami, FL
A.5: TMY2 Frequency Distribution for January, Boston, MA
A.6: TMY2 Frequency Distribution for January, Atlanta, GA
A.7: TMY2 Frequency Distribution for February, Madison, WI
A.8: TMY2 Frequency Distribution for February, Seattle, WA
A.9: TMY2 Frequency Distribution for February, Albuquerque, NM
A.10: TMY2 Frequency Distribution for February, Miami, FL
A.11: TMY2 Frequency Distribution for February, Boston, MA
A.12: TMY2 Frequency Distribution for February, Atlanta, GA
A.13: TMY2 Frequency Distribution for March, Madison, WI
A.14: TMY2 Frequency Distribution for March, Seattle, WA
A.15: TMY2 Frequency Distribution for March, Albuquerque, NM
A.16: TMY2 Frequency Distribution for March, Miami, FL
A.17: TMY2 Frequency Distribution for March, Boston, MA
A.18: TMY2 Frequency Distribution for March, Atlanta, GA
A.19: TMY2 Frequency Distribution for April, Madison, WI
A.20: TMY2 Frequency Distribution for April, Seattle, WA
A.21: TMY2 Frequency Distribution for April, Albuquerque, NM
A.22: TMY2 Frequency Distribution for April, Miami, FL
A.23: TMY2 Frequency Distribution for April, Boston, MA
A.24: TMY2 Frequency Distribution for April, Atlanta, GA
A.25: TMY2 Frequency Distribution for May, Madison, WI
A.26: TMY2 Frequency Distribution for May, Seattle, WA
A.27: TMY2 Frequency Distribution for May, Albuquerque, NM
A.28: TMY2 Frequency Distribution for May, Miami, FL
A.29: TMY2 Frequency Distribution for May, Boston, MA
A.30: TMY2 Frequency Distribution for May, Atlanta, GA
A.31: TMY2 Frequency Distribution for June, Madison, WI
A.32: TMY2 Frequency Distribution for June, Seattle, WA
A.33: TMY2 Frequency Distribution for June, Albuquerque, NM
A.34: TMY2 Frequency Distribution for June, Miami, FL
A.35: TMY2 Frequency Distribution for June, Boston, MA
A.36: TMY2 Frequency Distribution for June, Atlanta, GA
A.37: TMY2 Frequency Distribution for July, Madison, WI

A.38: TMY2 Frequency Distribution for July, Seattle, WA
A.39: TMY2 Frequency Distribution for July, Albuquerque, NM
A.40: TMY2 Frequency Distribution for July, Miami, FL
A.41: TMY2 Frequency Distribution for July, Boston, MA
A.42: TMY2 Frequency Distribution for July, Atlanta, GA
A.43: TMY2 Frequency Distribution for August, Madison, WI
A.44: TMY2 Frequency Distribution for August, Seattle, WA
A.45: TMY2 Frequency Distribution for August, Albuquerque, NM
A.46: TMY2 Frequency Distribution for August, Miami, FL
A.47: TMY2 Frequency Distribution for August, Boston, MA
A.48: TMY2 Frequency Distribution for August, Atlanta, GA
A.49: TMY2 Frequency Distribution for September, Madison, WI
A.50: TMY2 Frequency Distribution for September, Seattle, WA
A.51: TMY2 Frequency Distribution for September, Albuquerque, NM
A.52: TMY2 Frequency Distribution for September, Miami, FL
A.53: TMY2 Frequency Distribution for September, Boston, MA
A.54: TMY2 Frequency Distribution for September, Atlanta, GA
A.55: TMY2 Frequency Distribution for October, Madison, WI
A.56: TMY2 Frequency Distribution for October, Seattle, WA
A.57: TMY2 Frequency Distribution for October, Albuquerque, NM
A.58: TMY2 Frequency Distribution for October, Miami, FL
A.59: TMY2 Frequency Distribution for October, Boston, MA
A.60: TMY2 Frequency Distribution for October, Atlanta, GA
A.61: TMY2 Frequency Distribution for November, Madison, WI
A.62: TMY2 Frequency Distribution for November, Seattle, WA
A.63: TMY2 Frequency Distribution for November, Albuquerque, NM
A.64: TMY2 Frequency Distribution for November, Miami, FL
A.65: TMY2 Frequency Distribution for November, Boston, MA
A.66: TMY2 Frequency Distribution for November, Atlanta, GA
A.67: TMY2 Frequency Distribution for December, Madison, WI
A.68: TMY2 Frequency Distribution for December, Seattle, WA
A.69: TMY2 Frequency Distribution for December, Albuquerque, NM
A.70: TMY2 Frequency Distribution for December, Miami, FL
A.71: TMY2 Frequency Distribution for December, Boston, MA
A.72: TMY2 Frequency Distribution for December, Atlanta, GA

II. TMY2 Diffuse Fraction

A.1: TMY2 Diffuse Fraction, Madison, WI
A.2: TMY2 Diffuse Fraction, Albuquerque, NM
A.3: TMY2 Diffuse Fraction, Seattle, WA
A.4: TMY2 Diffuse Fraction, Miami, FL
A.5: TMY2 Diffuse Fraction, Atlanta, GA
A.6: TMY2 Diffuse Fraction, Boston, MA

III. Monthly Average Daily Utilizability, TMY2 vs 30 yr

A.1: January Average Daily Utilizability: Madison, Albuquerque, Seattle
A.2: January Average Daily Utilizability: Miami, Boston, Atlanta
A.3: February Average Daily Utilizability : Madison, Albuquerque, Seattle
A.4: February Average Daily Utilizability: Miami, Boston, Atlanta
A.5: March Average Daily Utilizability: Madison, Albuquerque, Seattle
A.6: March Average Daily Utilizability: Miami, Boston, Atlanta
A.7: April Average Daily Utilizability: Madison, Albuquerque, Seattle
A.8: April Average Daily Utilizability: Miami, Boston, Atlanta
A.9: May Average Daily Utilizability: Madison, Albuquerque, Seattle
A.10: May Average Daily Utilizability: Miami, Boston, Atlanta
A.11: June Average Daily Utilizability: Madison, Albuquerque, Seattle
A.12: June Average Daily Utilizability: Miami, Boston, Atlanta
A.13: July Average Daily Utilizability: Madison, Albuquerque, Seattle
A.14: July Average Daily Utilizability: Miami, Boston, Atlanta
A.15: August Average Daily Utilizability: Madison, Albuquerque, Seattle
A.16: August Average Daily Utilizability: Miami, Boston, Atlanta
A.17: September Average Daily Utilizability: Madison, Albuquerque, Seattle
A.18: September Average Daily Utilizability: Miami, Boston, Atlanta
A.19: October Average Daily Utilizability: Madison, Albuquerque, Seattle
A.20: October Average Daily Utilizability: Miami, Boston, Atlanta
A.21: November Average Daily Utilizability: Madison, Albuquerque, Seattle
A.22: November Average Daily Utilizability: Miami, Boston, Atlanta
A.23: December Average Daily Utilizability: Madison, Albuquerque, Seattle
A.24: December Average Daily Utilizability: Miami, Boston, Atlanta

IV. Monthly Average Daily Utilizability, TMY2 vs Erbs

A.1: January Average Daily Utilizability: Madison, Albuquerque, Seattle
A.2: January Average Daily Utilizability: Miami, Boston, Atlanta
A.3: February Average Daily Utilizability : Madison, Albuquerque, Seattle
A.4: February Average Daily Utilizability: Miami, Boston, Atlanta
A.5: March Average Daily Utilizability: Madison, Albuquerque, Seattle
A.6: March Average Daily Utilizability: Miami, Boston, Atlanta
A.7: April Average Daily Utilizability: Madison, Albuquerque, Seattle
A.8: April Average Daily Utilizability: Miami, Boston, Atlanta
A.9: May Average Daily Utilizability: Madison, Albuquerque, Seattle
A.10: May Average Daily Utilizability: Miami, Boston, Atlanta
A.11: June Average Daily Utilizability: Madison, Albuquerque, Seattle
A.12: June Average Daily Utilizability: Miami, Boston, Atlanta
A.13: July Average Daily Utilizability: Madison, Albuquerque, Seattle
A.14: July Average Daily Utilizability: Miami, Boston, Atlanta
A.15: August Average Daily Utilizability: Madison, Albuquerque, Seattle
A.16: August Average Daily Utilizability: Miami, Boston, Atlanta
A.17: September Average Daily Utilizability: Madison, Albuquerque, Seattle
A.18: September Average Daily Utilizability: Miami, Boston, Atlanta

A.19: October Average Daily Utilizability: Madison, Albuquerque, Seattle
A.20: October Average Daily Utilizability: Miami, Boston, Atlanta
A.21: November Average Daily Utilizability: Madison, Albuquerque, Seattle
A.22: November Average Daily Utilizability: Miami, Boston, Atlanta
A.23: December Average Daily Utilizability: Madison, Albuquerque, Seattle
A.24: December Average Daily Utilizability: Miami, Boston, Atlanta

Appendix B: 3-Minute Data (see CD for complete figures from all ISIS stations)

I. Diffuse Fraction, by month (42 figures, by location, no missing data)
II. Diffuse Fraction, by airmass (42 figures, by location, no missing data)
III. Diffuse Fraction, Clear Days (91 figures, by month and by location)
IV. Diffuse Fraction, Cloudy Days (86 figures, by month and by location)
V. Monthly Daily Average Tilted Radiation (6 figures, by location)
VI. Beam Normal Utilizability (42 figures, by month and location)
VII. Cumulative Frequency Distribution (24 figures, by location and by airmass)

I. Diffuse Fraction, by month

B.1: 3-minute Diffuse fraction, January 2003, Albuquerque, NM
B.2: 3-minute Diffuse fraction, January 2003, Hanford, CA
B.3: 3-minute Diffuse fraction, January 2003, Seattle, WA
B.4: 3-minute Diffuse fraction, January 2003, Salt Lake City, UT
B.5: 3-minute Diffuse fraction, January 2003, Sterling, VA
B.6: 3-minute Diffuse fraction, February 2003, Albuquerque, NM
B.7: 3-minute Diffuse fraction, February 2003, Hanford, CA
B.8: 3-minute Diffuse fraction, February 2003, Madison, WI
B.9: 3-minute Diffuse fraction, February 2003, Seattle, WA
B.10: 3-minute Diffuse fraction, February 2003, Salt Lake City, UT
B.11: 3-minute Diffuse fraction, February 2003, Sterling, VA
B.12: 3-minute Diffuse fraction, March 2003, Hanford, CA
B.13: 3-minute Diffuse fraction, March 2003, Madison, WI
B.14: 3-minute Diffuse fraction, March 2003, Oak Ridge, TN
B.15: 3-minute Diffuse fraction, March 2003, Seattle, WA
B.16: 3-minute Diffuse fraction, March 2003, Salt Lake City, UT
B.17: 3-minute Diffuse fraction, March 2003, Sterling, VA
B.18: 3-minute Diffuse fraction, April 2003, Madison, WI
B.19: 3-minute Diffuse fraction, April 2003, Seattle, WA
B.20: 3-minute Diffuse fraction, May 2003, Madison, WI
B.21: 3-minute Diffuse fraction, May 2003, Seattle, WA
B.22: 3-minute Diffuse fraction, May 2003, Sterling, VA
B.23: 3-minute Diffuse fraction, July 2003, Albuquerque, NM
B.24: 3-minute Diffuse fraction, July 2003, Madison, WI
B.25: 3-minute Diffuse fraction, July 2003, Sterling, VA
B.26: 3-minute Diffuse fraction, August 2003, Madison, WI
B.27: 3-minute Diffuse fraction, August 2003, Seattle, WA
B.28: 3-minute Diffuse fraction, September 2003, Bismarck, ND
B.29: 3-minute Diffuse fraction, September 2003, Madison, WI
B.30: 3-minute Diffuse fraction, September 2003, Seattle, WA
B.31: 3-minute Diffuse fraction, October 2003, Albuquerque, NM
B.32: 3-minute Diffuse fraction, October 2003, Madison, WI
B.33: 3-minute Diffuse fraction, October 2003, Seattle, WA
B.34: 3-minute Diffuse fraction, October 2003, Sterling, VA

B.35: 3-minute Diffuse fraction, November 2002, Hanford, CA
B.36: 3-minute Diffuse fraction, November 2002, Salt Lake City, UT
B.37: 3-minute Diffuse fraction, December 2002, Albuquerque, NM
B.38: 3-minute Diffuse fraction, December 2002, Hanford, CA
B.39: 3-minute Diffuse fraction, December 2002, Madison, WI
B.40: 3-minute Diffuse fraction, December 2002, Seattle, WA
B.41: 3-minute Diffuse fraction, December 2002, Salt Lake City, UT
B.42: 3-minute Diffuse fraction, December 2002, Sterling, VA

II. Diffuse Fraction, by air mass

B.1: Air mass Diffuse fraction, January 2003, Albuquerque, NM
B.2: Air mass Diffuse fraction, January 2003, Hanford, CA
B.3: Air mass Diffuse fraction, January 2003, Seattle, WA
B.4: Air mass Diffuse fraction, January 2003, Salt Lake City, UT
B.5: Air mass Diffuse fraction, January 2003, Sterling, VA
B.6: Air mass Diffuse fraction, February 2003, Albuquerque, NM
B.7: Air mass Diffuse fraction, February 2003, Hanford, CA
B.8: Air mass Diffuse fraction, February 2003, Madison, WI
B.9: Air mass Diffuse fraction, February 2003, Seattle, WA
B.10: Air mass Diffuse fraction, February 2003, Salt Lake City, UT
B.11: Air mass Diffuse fraction, February 2003, Sterling, VA
B.12: Air mass Diffuse fraction, March 2003, Hanford, CA
B.13: Air mass Diffuse fraction, March 2003, Madison, WI
B.14: Air mass Diffuse fraction, March 2003, Oak Ridge, TN
B.15: Air mass Diffuse fraction, March 2003, Seattle, WA
B.16: Air mass Diffuse fraction, March 2003, Salt Lake City, UT
B.17: Air mass Diffuse fraction, March 2003, Sterling, VA
B.18: Air mass Diffuse fraction, April 2003, Madison, WI
B.19: Air mass Diffuse fraction, April 2003, Seattle, WA
B.20: Air mass Diffuse fraction, May 2003, Madison, WI
B.21: Air mass Diffuse fraction, May 2003, Seattle, WA
B.22: Air mass Diffuse fraction, May 2003, Sterling, VA
B.23: Air mass Diffuse fraction, July 2003, Albuquerque, NM
B.24: Air mass Diffuse fraction, July 2003, Madison, WI
B.25: Air mass Diffuse fraction, July 2003, Sterling, VA
B.26: Air mass Diffuse fraction, August 2003, Madison, WI
B.27: Air mass Diffuse fraction, August 2003, Seattle, WA
B.28: Air mass Diffuse fraction, September 2003, Bismarck, ND
B.29: Air mass Diffuse fraction, September 2003, Madison, WI
B.30: Air mass Diffuse fraction, September 2003, Seattle, WA
B.31: Air mass Diffuse fraction, October 2003, Albuquerque, NM
B.32: Air mass Diffuse fraction, October 2003, Madison, WI
B.33: Air mass Diffuse fraction, October 2003, Seattle, WA
B.34: Air mass Diffuse fraction, October 2003, Sterling, VA
B.35: Air mass Diffuse fraction, November 2002, Hanford, CA

B.36: Air mass Diffuse fraction, November 2002, Salt Lake City, UT
B.37: Air mass Diffuse fraction, December 2002, Albuquerque, NM
B.38: Air mass Diffuse fraction, December 2002, Hanford, CA
B.39: Air mass Diffuse fraction, December 2002, Madison, WI
B.40: Air mass Diffuse fraction, December 2002, Seattle, WA
B.41: Air mass Diffuse fraction, December 2002, Salt Lake City, UT
B.42: Air mass Diffuse fraction, December 2002, Sterling, VA

III. Diffuse Fraction, Clear Days

B.1: Clear Day Diffuse fraction, January 2003, Albuquerque, NM
B.2: Clear Day Diffuse fraction, January 2003, Bismarck, ND
B.3: Clear Day Diffuse fraction, January 2003, Madison, WI
B.4: Clear Day Diffuse fraction, January 2003, Oak Ridge, TN
B.5: Clear Day Diffuse fraction, January 2003, Seattle, WA
B.6: Clear Day Diffuse fraction, January 2003, Salt Lake City, UT
B.7: Clear Day Diffuse fraction, January 2003, Sterling, VA
B.8: Clear Day Diffuse fraction, February 2003, Albuquerque, NM
B.9: Clear Day Diffuse fraction, February 2003, Bismarck, ND
B.10: Clear Day Diffuse fraction, February 2003, Hanford, CA
B.11: Clear Day Diffuse fraction, February 2003, Madison, WI
B.12: Clear Day Diffuse fraction, February 2003, Oak Ridge, TN
B.13: Clear Day Diffuse fraction, February 2003, Seattle, WA
B.14: Clear Day Diffuse fraction, February 2003, Salt Lake City, UT
B.15: Clear Day Diffuse fraction, February 2003, Sterling, VA
B.16: Clear Day Diffuse fraction, March 2003, Albuquerque, NM
B.17: Clear Day Diffuse fraction, March 2003, Bismarck, ND
B.18: Clear Day Diffuse fraction, March 2003, Hanford, CA
B.19: Clear Day Diffuse fraction, March 2003, Madison, WI
B.20: Clear Day Diffuse fraction, March 2003, Oak Ridge, TN
B.21: Clear Day Diffuse fraction, March 2003, Salt Lake City, UT
B.22: Clear Day Diffuse fraction, March 2003, Sterling, VA
B.23: Clear Day Diffuse fraction, April 2003, Albuquerque, NM
B.24: Clear Day Diffuse fraction, April 2003, Bismarck, ND
B.25: Clear Day Diffuse fraction, April 2003, Hanford, CA
B.26: Clear Day Diffuse fraction, April 2003, Madison, WI
B.27: Clear Day Diffuse fraction, April 2003, Oak Ridge, TN
B.28: Clear Day Diffuse fraction, April 2003, Salt Lake City, UT
B.29: Clear Day Diffuse fraction, April 2003, Sterling, VA
B.30: Clear Day Diffuse fraction, May 2003, Albuquerque, NM
B.31: Clear Day Diffuse fraction, May 2003, Bismarck, ND
B.32: Clear Day Diffuse fraction, May 2003, Hanford, CA
B.33: Clear Day Diffuse fraction, May 2003, Madison, WI
B.34: Clear Day Diffuse fraction, May 2003, Oak Ridge, TN
B.35: Clear Day Diffuse fraction, May 2003, Seattle, WA
B.36: Clear Day Diffuse fraction, May 2003, Salt Lake City, UT

B.37: Clear Day Diffuse fraction, May 2003, Sterling, VA
B.38: Clear Day Diffuse fraction, June 2003, Albuquerque, NM
B.39: Clear Day Diffuse fraction, June 2003, Bismarck, ND
B.40: Clear Day Diffuse fraction, June 2003, Hanford, CA
B.41: Clear Day Diffuse fraction, June 2003, Oak Ridge, TN
B.42: Clear Day Diffuse fraction, June 2003, Seattle, WA
B.43: Clear Day Diffuse fraction, June 2003, Salt Lake City, UT
B.44: Clear Day Diffuse fraction, June 2003, Sterling, VA
B.45: Clear Day Diffuse fraction, July 2003, Albuquerque, NM
B.46: Clear Day Diffuse fraction, July 2003, Bismarck, ND
B.47: Clear Day Diffuse fraction, July 2003, Hanford, CA
B.48: Clear Day Diffuse fraction, July 2003, Madison, WI
B.49: Clear Day Diffuse fraction, July 2003, Oak Ridge, TN
B.50: Clear Day Diffuse fraction, July 2003, Seattle, WA
B.51: Clear Day Diffuse fraction, July 2003, Salt Lake City, UT
B.52: Clear Day Diffuse fraction, July 2003, Sterling, VA
B.53: Clear Day Diffuse fraction, August 2003, Albuquerque, NM
B.54: Clear Day Diffuse fraction, August 2003, Bismarck, ND
B.55: Clear Day Diffuse fraction, August 2003, Hanford, CA
B.56: Clear Day Diffuse fraction, August 2003, Madison, WI
B.57: Clear Day Diffuse fraction, August 2003, Seattle, WA
B.58: Clear Day Diffuse fraction, August 2003, Salt Lake City, UT
B.59: Clear Day Diffuse fraction, August 2003, Sterling, VA
B.60: Clear Day Diffuse fraction, September 2003, Albuquerque, NM
B.61: Clear Day Diffuse fraction, September 2003, Bismarck, ND
B.62: Clear Day Diffuse fraction, September 2003, Hanford, CA
B.63: Clear Day Diffuse fraction, September 2003, Madison, WI
B.64: Clear Day Diffuse fraction, September 2003, Oak Ridge, TN
B.65: Clear Day Diffuse fraction, September 2003, Seattle, WA
B.66: Clear Day Diffuse fraction, September 2003, Salt Lake City, UT
B.67: Clear Day Diffuse fraction, September 2003, Sterling, VA
B.68: Clear Day Diffuse fraction, October 2003, Albuquerque, NM
B.69: Clear Day Diffuse fraction, October 2003, Bismarck, ND
B.70: Clear Day Diffuse fraction, October 2003, Hanford, CA
B.71: Clear Day Diffuse fraction, October 2003, Madison, WI
B.72: Clear Day Diffuse fraction, October 2003, Oak Ridge, TN
B.73: Clear Day Diffuse fraction, October 2003, Seattle, WA
B.74: Clear Day Diffuse fraction, October 2003, Salt Lake City, UT
B.75: Clear Day Diffuse fraction, October 2003, Sterling, VA
B.76: Clear Day Diffuse fraction, November 2002, Albuquerque, NM
B.77: Clear Day Diffuse fraction, November 2002, Bismarck, ND
B.78: Clear Day Diffuse fraction, November 2002, Hanford, CA
B.79: Clear Day Diffuse fraction, November 2002, Madison, WI
B.80: Clear Day Diffuse fraction, November 2002, Oak Ridge, TN
B.81: Clear Day Diffuse fraction, November 2002, Seattle, WA

B.82: Clear Day Diffuse fraction, November 2002, Salt Lake City, UT
B.83: Clear Day Diffuse fraction, November 2002, Sterling, VA
B.84: Clear Day Diffuse fraction, December 2002, Albuquerque, NM
B.85: Clear Day Diffuse fraction, December 2002, Bismarck, ND
B.86: Clear Day Diffuse fraction, December 2002, Hanford, CA
B.87: Clear Day Diffuse fraction, December 2002, Madison, WI
B.88: Clear Day Diffuse fraction, December 2002, Oak Ridge, TN
B.89: Clear Day Diffuse fraction, December 2002, Seattle, WA
B.90: Clear Day Diffuse fraction, December 2002, Salt Lake City, UT
B.91: Clear Day Diffuse fraction, December 2002, Sterling, VA

IV. Diffuse Fraction, Cloudy Days

B.1: Cloudy Day Diffuse fraction, January 2003, Albuquerque, NM
B.2: Cloudy Day Diffuse fraction, January 2003, Bismarck, ND
B.3: Cloudy Day Diffuse fraction, January 2003, Hanford, CA
B.4: Cloudy Day Diffuse fraction, January 2003, Madison, WI
B.5: Cloudy Day Diffuse fraction, January 2003, Oak Ridge, TN
B.6: Cloudy Day Diffuse fraction, January 2003, Seattle, WA
B.7: Cloudy Day Diffuse fraction, January 2003, Salt Lake City, UT
B.8: Cloudy Day Diffuse fraction, January 2003, Sterling, VA
B.9: Cloudy Day Diffuse fraction, February 2003, Albuquerque, NM
B.10: Cloudy Day Diffuse fraction, February 2003, Hanford, CA
B.11: Cloudy Day Diffuse fraction, February 2003, Madison, WI
B.12: Cloudy Day Diffuse fraction, February 2003, Oak Ridge, TN
B.13: Cloudy Day Diffuse fraction, February 2003, Seattle, WA
B.14: Cloudy Day Diffuse fraction, February 2003, Salt Lake City, UT
B.15: Cloudy Day Diffuse fraction, February 2003, Sterling, VA
B.16: Cloudy Day Diffuse fraction, March 2003, Albuquerque, NM
B.17: Cloudy Day Diffuse fraction, March 2003, Hanford, CA
B.18: Cloudy Day Diffuse fraction, March 2003, Madison, WI
B.19: Cloudy Day Diffuse fraction, March 2003, Oak Ridge, TN
B.20: Cloudy Day Diffuse fraction, March 2003, Seattle, WA
B.21: Cloudy Day Diffuse fraction, March 2003, Salt Lake City, UT
B.22: Cloudy Day Diffuse fraction, March 2003, Sterling, VA
B.23: Cloudy Day Diffuse fraction, April 2003, Albuquerque, NM
B.24: Cloudy Day Diffuse fraction, April 2003, Bismarck, ND
B.25: Cloudy Day Diffuse fraction, April 2003, Hanford, CA
B.26: Cloudy Day Diffuse fraction, April 2003, Madison, WI
B.27: Cloudy Day Diffuse fraction, April 2003, Oak Ridge, TN
B.28: Cloudy Day Diffuse fraction, April 2003, Seattle, WA
B.29: Cloudy Day Diffuse fraction, April 2003, Salt Lake City, UT
B.30: Cloudy Day Diffuse fraction, April 2003, Sterling, VA
B.31: Cloudy Day Diffuse fraction, May 2003, Albuquerque, NM
B.32: Cloudy Day Diffuse fraction, May 2003, Bismarck, ND
B.33: Cloudy Day Diffuse fraction, May 2003, Hanford, CA

B.34: Cloudy Day Diffuse fraction, May 2003, Madison, WI
B.35: Cloudy Day Diffuse fraction, May 2003, Oak Ridge, TN
B.36: Cloudy Day Diffuse fraction, May 2003, Seattle, WA
B.37: Cloudy Day Diffuse fraction, May 2003, Salt Lake City, UT
B.38: Cloudy Day Diffuse fraction, May 2003, Sterling, VA
B.39: Cloudy Day Diffuse fraction, June 2003, Albuquerque, NM
B.40: Cloudy Day Diffuse fraction, June 2003, Bismarck, ND
B.41: Cloudy Day Diffuse fraction, June 2003, Madison, WI
B.42: Cloudy Day Diffuse fraction, June 2003, Oak Ridge, TN
B.43: Cloudy Day Diffuse fraction, June 2003, Seattle, WA
B.44: Cloudy Day Diffuse fraction, June 2003, Salt Lake City, UT
B.45: Cloudy Day Diffuse fraction, June 2003, Sterling, VA
B.46: Cloudy Day Diffuse fraction, July 2003, Albuquerque, NM
B.47: Cloudy Day Diffuse fraction, July 2003, Bismarck, ND
B.48: Cloudy Day Diffuse fraction, July 2003, Hanford, CA
B.49: Cloudy Day Diffuse fraction, July 2003, Madison, WI
B.50: Cloudy Day Diffuse fraction, July 2003, Oak Ridge, TN
B.51: Cloudy Day Diffuse fraction, July 2003, Seattle, WA
B.52: Cloudy Day Diffuse fraction, July 2003, Sterling, VA
B.53: Cloudy Day Diffuse fraction, August 2003, Bismarck, ND
B.54: Cloudy Day Diffuse fraction, August 2003, Madison, WI
B.55: Cloudy Day Diffuse fraction, August 2003, Salt Lake City, UT
B.56: Cloudy Day Diffuse fraction, August 2003, Sterling, VA
B.57: Cloudy Day Diffuse fraction, September 2003, Albuquerque, NM
B.58: Cloudy Day Diffuse fraction, September 2003, Bismarck, ND
B.59: Cloudy Day Diffuse fraction, September 2003, Madison, WI
B.60: Cloudy Day Diffuse fraction, September 2003, Oak Ridge, TN
B.61: Cloudy Day Diffuse fraction, September 2003, Seattle, WA
B.62: Cloudy Day Diffuse fraction, September 2003, Salt Lake City, UT
B.63: Cloudy Day Diffuse fraction, September 2003, Sterling, VA
B.64: Cloudy Day Diffuse fraction, October 2003, Albuquerque, NM
B.65: Cloudy Day Diffuse fraction, October 2003, Bismarck, ND
B.66: Cloudy Day Diffuse fraction, October 2003, Hanford, CA
B.67: Cloudy Day Diffuse fraction, October 2003, Madison, WI
B.68: Cloudy Day Diffuse fraction, October 2003, Oak Ridge, TN
B.69: Cloudy Day Diffuse fraction, October 2003, Seattle, WA
B.70: Cloudy Day Diffuse fraction, October 2003, Salt Lake City, UT
B.71: Cloudy Day Diffuse fraction, October 2003, Sterling, VA
B.72: Cloudy Day Diffuse fraction, November 2002, Albuquerque, NM
B.73: Cloudy Day Diffuse fraction, November 2002, Bismarck, ND
B.74: Cloudy Day Diffuse fraction, November 2002, Hanford, CA
B.75: Cloudy Day Diffuse fraction, November 2002, Madison, WI
B.76: Cloudy Day Diffuse fraction, November 2002, Oak Ridge, TN
B.77: Cloudy Day Diffuse fraction, November 2002, Seattle, WA
B.78: Cloudy Day Diffuse fraction, November 2002, Salt Lake City, UT

B.79: Cloudy Day Diffuse fraction, December 2002, Albuquerque, NM
B.80: Cloudy Day Diffuse fraction, December 2002, Bismarck, ND
B.81: Cloudy Day Diffuse fraction, December 2002, Hanford, CA
B.82: Cloudy Day Diffuse fraction, December 2002, Madison, WI
B.83: Cloudy Day Diffuse fraction, December 2002, Oak Ridge, TN
B.84: Cloudy Day Diffuse fraction, December 2002, Seattle, WA
B.85: Cloudy Day Diffuse fraction, December 2002, Salt Lake City, UT
B.86: Cloudy Day Diffuse fraction, December 2002, Sterling, VA

V. Monthly Daily Average Tilted Radiation

B.1: Monthly Daily Average Tilted Radiation, Albuquerque, NM
B.2: Monthly Daily Average Tilted Radiation, Hanford, CA
B.3: Monthly Daily Average Tilted Radiation, Madison, WI
B.4: Monthly Daily Average Tilted Radiation, Seattle, WA
B.5: Monthly Daily Average Tilted Radiation, Salt Lake City, UT
B.6: Monthly Daily Average Tilted Radiation, Sterling, VA

VI. Beam Normal Utilizability

B.1: Beam Normal Utilizability, January 2003, Albuquerque, NM
B.2: Beam Normal Utilizability, January 2003, Hanford, CA
B.3: Beam Normal Utilizability, January 2003, Seattle, WA
B.4: Beam Normal Utilizability, January 2003, Salt Lake City, UT
B.5: Beam Normal Utilizability, January 2003, Sterling, VA
B.6: Beam Normal Utilizability, February 2003, Albuquerque, NM
B.7: Beam Normal Utilizability, February 2003, Hanford, CA
B.8: Beam Normal Utilizability, February 2003, Madison, WI
B.9: Beam Normal Utilizability, February 2003, Seattle, WA
B.10: Beam Normal Utilizability, February 2003, Salt Lake City, UT
B.11: Beam Normal Utilizability, February 2003, Sterling, VA
B.12: Beam Normal Utilizability, March 2003, Hanford, CA
B.13: Beam Normal Utilizability, March 2003, Madison, WI
B.14: Beam Normal Utilizability, March 2003, Oak Ridge, TN
B.15: Beam Normal Utilizability, March 2003, Seattle, WA
B.16: Beam Normal Utilizability, March 2003, Salt Lake City, UT
B.17: Beam Normal Utilizability, March 2003, Sterling, VA
B.18: Beam Normal Utilizability, April 2003, Madison, WI
B.19: Beam Normal Utilizability, April 2003, Seattle, WA
B.20: Beam Normal Utilizability, May 2003, Madison, WI
B.21: Beam Normal Utilizability, May 2003, Seattle, WA
B.22: Beam Normal Utilizability, May 2003, Sterling, VA
B.23: Beam Normal Utilizability, July 2003, Albuquerque, NM
B.24: Beam Normal Utilizability, July 2003, Madison, WI
B.25: Beam Normal Utilizability, July 2003, Sterling, VA
B.26: Beam Normal Utilizability, August 2003, Madison, WI
B.27: Beam Normal Utilizability, August 2003, Seattle, WA

B.28: Beam Normal Utilizability, September 2003, Bismarck, ND
B.29: Beam Normal Utilizability, September 2003, Madison, WI
B.30: Beam Normal Utilizability, September 2003, Seattle, WA
B.31: Beam Normal Utilizability, October 2003, Albuquerque, NM
B.32: Beam Normal Utilizability, October 2003, Madison, WI
B.33: Beam Normal Utilizability, October 2003, Seattle, WA
B.34: Beam Normal Utilizability, October 2003, Sterling, VA
B.35: Beam Normal Utilizability, November 2002, Hanford, CA
B.36: Beam Normal Utilizability, November 2002, Salt Lake City, UT
B.37: Beam Normal Utilizability, December 2002, Albuquerque, NM
B.38: Beam Normal Utilizability, December 2002, Hanford, CA
B.39: Beam Normal Utilizability, December 2002, Madison, WI
B.40: Beam Normal Utilizability, December 2002, Seattle, WA
B.41: Beam Normal Utilizability, December 2002, Salt Lake City, UT
B.42: Beam Normal Utilizability, December 2002, Sterling, VA

VII. Cumulative Frequency Distributions

B.1: Frequency Distribution, by air mass, Albuquerque, NM (1 year of data)
B.2: Frequency Distribution, Albuquerque, NM (1 year of 3-minute data)
B.3: Frequency Distribution, Albuquerque, NM (1 year of hourly data)
B.4: Frequency Distribution, by air mass, Bismarck, ND (1 year of data)
B.5: Frequency Distribution, Bismarck, ND (1 year of 3-minute data)
B.6: Frequency Distribution, Bismarck, ND (1 year of hourly data)
B.7: Frequency Distribution, by air mass, Hanford, CA (1 year of data)
B.8: Frequency Distribution, Hanford, CA (1 year of 3-minute data)
B.9: Frequency Distribution, Hanford, CA (1 year of hourly data)
B.10: Frequency Distribution, by air mass, Madison, WI (1 year of data)
B.11: Frequency Distribution, Madison, WI (1 year of 3-minute data)
B.12: Frequency Distribution, Madison, WI (1 year of hourly data)
B.13: Frequency Distribution, by air mass, Oak Ridge, TN (1 year of data)
B.14: Frequency Distribution, Oak Ridge, TN (1 year of 3-minute data)
B.15: Frequency Distribution, Oak Ridge, TN (1 year of hourly data)
B.16: Frequency Distribution, by air mass, Seattle, WA (1 year of data)
B.17: Frequency Distribution, Seattle, WA (1 year of 3-minute data)
B.18: Frequency Distribution, Seattle, WA (1 year of hourly data)
B.19: Frequency Distribution, by air mass, Salt Lake City, UT (1 year of data)
B.20: Frequency Distribution, Salt Lake City, UT (1 year of 3-minute data)
B.21: Frequency Distribution, Salt Lake City, UT (1 year of hourly data)
B.22: Frequency Distribution, by air mass, Sterling, VA (1 year of data)
B.23: Frequency Distribution, Sterling, VA (1 year of 3-minute data)
B.24: Frequency Distribution, Sterling, VA (1 year of hourly data)

Appendix C: 1-Minute Data (see CD for complete figures from Madison, WI)

- **I. Diffuse Fraction, by month (20 figures, 1-minute and hourly data)**
- **II. Diffuse Fraction, Clear Days (10 figures, by month)**
- **III. Diffuse Fraction, Cloudy Days (10 figures, by month)**
- **IV. Cumulative Frequency Distributions (10 figures, by month)**
- **V. Monthly Average Daily Beam Normal Utilizability (10 figures, by month)**

I. Diffuse Fraction, by month

C.1: 1-minute Diffuse Fraction, January 2003, Madison, WI
C.2: Hourly Diffuse Fraction, January 2003, Madison, WI
C.3: 1-minute Diffuse Fraction, February 2003, Madison, WI
C.4: Hourly Diffuse Fraction, February 2003, Madison, WI
C.5: 1-minute Diffuse Fraction, March 2003, Madison, WI
C.6: Hourly Diffuse Fraction, March 2003, Madison, WI
C.7: 1-minute Diffuse Fraction, April 2003, Madison, WI
C.8: Hourly Diffuse Fraction, April 2003, Madison, WI
C.9: 1-minute Diffuse Fraction, June 2003, Madison, WI
C.10: Hourly Diffuse Fraction, June 2003, Madison, WI
C.11: 1-minute Diffuse Fraction, July 2003, Madison, WI
C.12: Hourly Diffuse Fraction, July 2003, Madison, WI
C.13: 1-minute Diffuse Fraction, August 2003, Madison, WI
C.14: Hourly Diffuse Fraction, August 2003, Madison, WI
C.15: 1-minute Diffuse Fraction, September 2003, Madison, WI
C.16: Hourly Diffuse Fraction, September 2003, Madison, WI
C.17: 1-minute Diffuse Fraction, November 2002, Madison, WI
C.18: Hourly Diffuse Fraction, November 2002, Madison, WI
C.19: 1-minute Diffuse Fraction, December 2002, Madison, WI
C.20: Hourly Diffuse Fraction, December 2002, Madison, WI

II. Diffuse Fraction, Clear Days

C.1: Clear Day Diffuse fraction, January 2003, Madison, WI
C.2: Clear Day Diffuse fraction, February 2003, Madison, WI
C.3: Clear Day Diffuse fraction, March 2003, Madison, WI
C.4: Clear Day Diffuse fraction, April 2003, Madison, WI
C.5: Clear Day Diffuse fraction, June 2003, Madison, WI
C.6: Clear Day Diffuse fraction, July 2003, Madison, WI
C.7: Clear Day Diffuse fraction, August 2003, Madison, WI
C.8: Clear Day Diffuse fraction, September 2003, Madison, WI
C.9: Clear Day Diffuse fraction, November 2002, Madison, WI
C.10: Clear Day Diffuse fraction, December 2002, Madison, WI

III. Diffuse Fraction, Cloudy Days

C.1: Cloudy Day Diffuse fraction, January 2003, Madison, WI
C.2: Cloudy Day Diffuse fraction, February 2003, Madison, WI
C.3: Cloudy Day Diffuse fraction, March 2003, Madison, WI
C.4: Cloudy Day Diffuse fraction, April 2003, Madison, WI
C.5: Cloudy Day Diffuse fraction, June 2003, Madison, WI
C.6: Cloudy Day Diffuse fraction, July 2003, Madison, WI
C.7: Cloudy Day Diffuse fraction, August 2003, Madison, WI
C.8: Cloudy Day Diffuse fraction, September 2003, Madison, WI
C.9: Cloudy Day Diffuse fraction, November 2002, Madison, WI
C.10: Cloudy Day Diffuse fraction, December 2002, Madison, WI

IV. Cumulative Frequency Distributions

C.1: 1-Minute Frequency Distribution, January 2003, Madison, WI
C.2: 1-Minute Frequency Distribution, February 2003, Madison, WI
C.3: 1-Minute Frequency Distribution, March 2003, Madison, WI
C.4: 1-Minute Frequency Distribution, April 2003, Madison, WI
C.5: 1-Minute Frequency Distribution, June 2003, Madison, WI
C.6: 1-Minute Frequency Distribution, July 2003, Madison, WI
C.7: 1-Minute Frequency Distribution, August 2003, Madison, WI
C.8: 1-Minute Frequency Distribution, September 2003, Madison, WI
C.9: 1-Minute Frequency Distribution, November 2002, Madison, WI
C.10 1-Minute Frequency Distribution, December 2002, Madison, WI

V. Monthly Average Daily Beam Normal Utilizability

C.1: January 2003, Average Daily Beam Normal Utilizability, Madison, WI
C.2: February 2003, Average Daily Beam Normal Utilizability, Madison, WI
C.3: March 2003, Average Daily Beam Normal Utilizability, Madison, WI
C.4: April 2003, Average Daily Beam Normal Utilizability, Madison, WI
C.5: June 2003, Average Daily Beam Normal Utilizability, Madison, WI
C.6: July 2003, Average Daily Beam Normal Utilizability, Madison, WI
C.7: August 2003, Average Daily Beam Normal Utilizability, Madison, WI
C.8: September 2003, Average Daily Beam Normal Utilizability, Madison, WI
C.9: November 2002, Average Daily Beam Normal Utilizability, Madison, WI
C.10: December 2002, Average Daily Beam Normal Utilizability, Madison, WI

Appendix D: Computer Programs (see CD for computer codes, TMY2 and ISIS data)

Matlab code

- **3 Minute data**
- **Minute data**

EES code

- **TMY2 Data**
- **3-Minute Data**

References

Babu, K.S., and Satyamurty, V.V., "Frequency Distribution of Daily Clearness Indices through Generalized Parameters," *Solar Energy*, Vol. 70, 2001, p. 35.

Bendt, P., Collares-Pereira, M., and Rabl, A., "The Frequency Distribution of Daily Radiation Values," *Solar Energy*, Vol. 27, 1981, p.1.

Duffie, J.A., and Beckman, W.A., *Solar Engineering of Thermal Processes, 2nd ed.*, John Wiley & Sons, New York, 1991.

Erbs, D.G., Klein, S.A., and Duffie, J.A., "Estimation of the Diffuse Radiation Fraction for Hourly, Daily, and Monthly-Average Global Radiation," *Solar Energy*, Vol. 28, 1982, p.13.

Feuillard, T., and Abillon, J.M., and Martias, C., "The Probability Density Function of the Clearness Index: A New Approach," *Solar Energy*, Vol.43, 1989, p.363.

Gansler, R., Klein, S.A., and Beckman, W.A., "Investigation of minute solar radiation data," *Solar Energy*, Vol. 55, 1995, p.21-27.

Gansler, R., Assessment of generated meteorological data for use in solar energy simulations. M.S.Thesis, Mechanical Engineering Deparment, Univ. of Wisconsin-Madison, Madison(1993).

Gonzalez, Josep-abel, and Calbo, Josep, "Influence of the Global Radiation Variability on the hourly diffuse fraction correlations," *Solar Energy,* Vol. 65, 1999, p.119-131.

Integrated Surface Irradiance Study (ISIS) network, http://www.srrb.noaa.gov/isis/ Last accessed 3/10/04.

Klein, S.A., and Beckman, W.A., "Review of Solar Radiation Utilizability," *Journal of Solar Energy Engineering,* Vol.106, 1984, p.393.

Klucher, T.M., "Evaluating Models to Predict Insolation on Tilted Surfaces," *Solar Energy*, Vol. 23, 1979, p.111.

Liu, B.Y.H., and Jordan, R.C., "The Interrelationship and Characteristic Distribution of Direct, Diffuse and Total Solar Radiation," *Solar Energy*, Vol. 4, 1960, p.1.

Liu, B.Y.H. and Jordan, R.C., "Daily Insolation on Surfaces Tilted Toward the Equator," *ASHRAE Journal*, Vol. 3, 1962, p.53.

Marion, W. and Urban, K., User's Manual for TMY2's, National Renewable Energy Laboratory, 1995.

National Solar Radiation Data Base Home Page, 1992, http://rredc.nrel.gov/solar/pubs/NSRDB/ Last accessed 3/9/03.

Perez, R., Seals, R., Ineichen, P., Stewart, R., and Menicucci, D., "A New Simplified Version of the Perez Diffuse Irradiance Model for Tilted Surfaces," *Solar Energy*, Vol. 39, 1987, p.221.

Reindl, D.T, Beckman, W.A., and Duffie J.A., "Diffuse Fraction Correlations, " *Solar Energy*, Vol. 45, 1990, p. 1.

Saunier, G.Y., Reddy, T.A., and Kumar, S., "A Monthly Probability Distribution Function of Daily Global Irradiation Values Appropriate for Both Tropical and Temperate Locations," *Solar Energy,* Vol.38, 1987, p.169.

Skartveit, A. and Olseth, J.A., "The Probability Density and Autocorrelation of Short-Term Global and Beam Irradiance," *Solar Energy*, Vol. 49, 1992, p.477-487.

Suehrcke, H. and McCormick, P.G., "The diffuse fraction of instantaneous insolation values," *Solar Energy*, Vol. 40, 1988, p.423-430.

Theilacker, J.C., “An Investigation of Monthly-Average Utilizability for Flat-Plate solar collectors,” University of Wisconsin-Madison, M.S. thesis, 1980.

Tovar, J., Olmo, F.J., and Alados-Arboledas, L., “One-Minute Global Irradiance Probability Density Distributions Conditioned to the Optical Air mass,” *Solar Energy,* Vol. 62, 1998, p.387-393.

Tovar, J., Olmo, F.J., Batlles, F.J., and Alados-Arboledas, L., “One-Minute k_b and k_d Probability Density Distributions Conditioned to the Optical Air mass,” *Solar Energy,* Vol. 65, 1999, p.297-304.

Walkenhorst, O., Luther, J., Reinhart, C. and Timmer, J., “Dynamic annual daylight simulations based on one-hour and one-minute means of irradiance data,” *Solar Energy*, Vol. 72, 2002, p.167-175.

Whillier, A., “The Determination of Hourly Values of Total Radiation from Daily Summations,” *Arch. Met. Geoph. Biokl.* Series B, Vol.7, 1956, p.197 .